2014

APPLICATION OF THE KALMAN FILTER ON FULL TENSOR GRAVITY GRADIOMETRY DATA AROUND THE VINTON SALT DOME, LOUISIANA

Mahnaz Sepehrmanesh
University of Kentucky, mahnaz.sepehrmanesh@uky.edu

STUDENT AGREEMENT:

I represent that my thesis or dissertation and abstract are my original work. Proper attribution has been given to all outside sources. I understand that I am solely responsible for obtaining any needed copyright permissions. I have obtained needed written permission statement(s) from the owner(s) of each third-party copyrighted matter to be included in my work, allowing electronic distribution (if such use is not permitted by the fair use doctrine) which will be submitted to UKnowledge as Additional File.

I hereby grant to The University of Kentucky and its agents the irrevocable, non-exclusive, and royalty-free license to archive and make accessible my work in whole or in part in all forms of media, now or hereafter known. I agree that the document mentioned above may be made available immediately for worldwide access unless an embargo applies.

I retain all other ownership rights to the copyright of my work. I also retain the right to use in future works (such as articles or books) all or part of my work. I understand that I am free to register the copyright to my work.

REVIEW, APPROVAL AND ACCEPTANCE

The document mentioned above has been reviewed and accepted by the student's advisor, on behalf of the advisory committee, and by the Director of Graduate Studies (DGS), on behalf of the program; we verify that this is the final, approved version of the student's thesis including all changes required by the advisory committee. The undersigned agree to abide by the statements above.

Mahnaz Sepehrmanesh, Student

Dr. Edward Woolery, Major Professor

Dr. Edward Woolery, Director of Graduate Studies

APPLICATION OF THE KALMAN FILTER ON FULL TENSOR GRAVITY GRADIOMETRY DATA AROUND THE VINTON SALT DOME, LOUISIANA

THESIS

A thesis submitted in partial fulfillment of the requirements for the degree of Master of Science in the College of Arts and Sciences at the University of Kentucky

By
Mahnaz Sepehrmanesh
Lexington, Kentucky
Director: Dr. Edward W. Woolery, Professor of Geophysics
Lexington, Kentucky
2014

ABSTRACT OF THESIS

APPLICATION OF THE KALMAN FILTER ON FULL TENSOR GRAVITY DATA AROUND THE VINTON SALT DOME, LOUISIANA

Full tensor gravity (FTG) data are known for their high resolution but also for higher noise in its components due to the dynamic nature of the platform used for data acquisition. Although a review of the literature suggests steady increase in the success of gravity gradiometry, we still cannot take advantage of the full potential of the method, mostly because of the noise with the same amplitude and wavenumber characteristics as the signal that affects these data. Smoothing from common low pass filters removes small wavelength features and makes it difficult to detect structural features and other density variations of interest to exploration. In Kalman filtering the components of the FTG are continuously updated to calculate the best estimation of the state. The most important advantage of the Kalman filter is that it can be applied on gravity gradiometry components simultaneously. In addition, one can incorporate constraints. We use the Laplace's equation that is the most meaningful constraint for potential field data to extract signal from noise and improve the detection and continuity of density variations. We apply the Kalman filter on the FTG data acquired by Bell Geospace over the Vinton salt dome in southwest Louisiana.

KEYWORDS: Full Tenser Gradiometry, FTG, Kalman filter, Constrained Kalman filter, Vinton Salt Dome.

Mahnaz Sepehrmanesh

November 16, 2014

APPLICATION OF THE KALMAN FILTER ON FULL TENSOR GRAVITY DATA AROUND THE VINTON SALT DOME, LOUISIANA

By

Mahnaz Sepehrmanesh

Edward W. Woolery

Director of Thesis and Director of Graduate Studies

ACKNOWLEDGMENTS

I want to thank Dr. Edward Woolery for giving me advice in putting together this study. Thanks to my thesis committee member, Dr. Zhenming Wang, for his instructive comments directing me to keep in the right track. Thanks also to my other thesis committee member, Dr. Dave Moecher, for his kind support and help. I also want to acknowledge Prof. D. Ravat, UK EES since this project was initiated based on his suggestion and he provided considerable guidance throughout most of the thesis research and preparation. Prof. Ravat also provided financial support during part of my graduate career at UK. I want to thank Dr. Dan Simon for his useful book and MATLAB codes; this work could not have been carried out without the insights of his book. I am very grateful to Bell Geospace Inc. for providing the Full Tensor Gradiometry data this study focuses on. I want to thank Geosoft Inc. for providing the license to the Montaj software used in this study. I'm thankful to Chris Ennen for giving me the data bases that I used in interpretation.

In addition to the academic support mentioned above, I wish to thank my husband, Mehdi, who has always encouraged me to pursue academic studies and for watching our daughter while I was working on this thesis. I wish to thank my best friend, Ghazaleh who warmed my heart with her love and has been always there to help and support me.

TABLE OF CONTENTS

LIST OF TABLES

LIST OF FIGURES

CHAPTER 1. INTRODUCTION

For over a century, the Gulf Coast region of the United States has been an active producer of oil and gas. Salt dome flanks are one of the most important features in the area since they are one of the best known traps of reservoirs in the area (Harrison et al., 1970; Branson, 1991). The first hydrocarbon exploration started with drilling a well at any location that exhibited evidence of a salt dome, such as a depression in the landscape or any kind of hydrocarbon seepage at the surface (Owen, 1975). Later, in the 1950's, the exploration method converted to seismic reflection surveys which made subsurface imaging possible (Fails, 1995). However, like any other method, seismic exploration has some limitations. The issue is that near salt domes due to the steeply dipping salt flanks that scatter or absorb seismic energy, imaging becomes difficult (Coburn, 2002).

Salt domes in the Gulf Coast can continue to produce hydrocarbons. Based on the United States Geological Survey estimation, more than 9 billion cubic feet of gas have not been recovered from the region (Swanson and Karlsen, 2009). But exploration of these reservoirs requires more sophisticated geophysical techniques, such as Vertical Seismic Profiling (VSP) (Constance et al., 1999; Kisin, 2003), well log data (Coker, 2006), conventional gravity (Eti, 2004), and gravity gradiometry (Prutzman, 1998; O'Brien et al., 2005).

Airborne Full Tensor Gravity (FTG) has been proved to be the "preferred technology" in both mineral and petroleum exploration projects (Dransfield et al., 2010). It is used in hydrocarbon exploration by detecting salt domes, fault blocks or structural closures (Murphy and Dickson, 2009). The FTG data collected by Bell Geospace over the Vinton Salt dome was as an attempt to measure the gravity field for use at the reservoir level (Ennen, 2012).

Vinton Salt Dome

The Vinton salt dome has characteristics that made it a typical Gulf Coast salt dome so its results can be extended to previously unmapped areas. It is one of the eleven domes in the Gulf Coast Region that have salt overhangs (Judson and Stamey, 1933). So if applying the Kalman filter on gravity gradiometry over the Vinton dome can be used to image reservoirs, then it can be a good sign that the filter can be used on other domes as

well. It means that extending field life in the area would be possible (Cossey and Jacobs, 1992; Hoeve and Borowski, 1988). Detecting Faults and fractures in the Vinton dome is considered critical because formations adjacent to the dome have been fractured through faulting and are the focuses of companies trying to find resources to produce in the region. On the other, it has been investigated by different geophysical techniques. So, the result of filtered FTG can be compared with the previous techniques.

Full Tensor Gradiometry (FTG) Method

A review of literature suggests steady increase in the success of gravity gradiometry and the method is now accepted as an exploration tool (DiFrancesco et al., 2009). While Gravity potential can be represented in terms of its components G_x, G_y and G_z (Stasinowsky, 2010), gradiometers measure the spatial rate of change in these components in all three directions and, the term, tensor refers to the elements of the rate of the change of the gravity field or gradients of the components. With this explanation, it can be easily concluded that gravity gradiometry samples all nine components of the gradient for the gravity field (Bell et al., 1997). As the tensor of full gradiometry is symmetric, just six components out of nine are unique. Also, considering Laplace's equation, only five of the components are independent.

The Kalman filter

The Kalman filter which is introduced by R.E. Kalman and was first published in a mechanical engineering journal has been used for five decades. Navigating the Apollo spacecraft, predicting short-term stock market fluctuations, and estimating location with relatively inexpensive hand-held receivers (global positioning systems) are some of the broad applications of the filter. It is recognized as the best performing filter in many disciplines. The Kalman filter is believed by some to be the second most important algorithm technique ever conceived after the Fast Fourier Transform (Zarchan and Musoff, 2000); some even consider it as the greatest discovery of the twentieth century (Haykin, 2001).

This well-known recursive data processing technique attempts to minimize the mean of the squared error between the observations and estimations, not depending on wavenumber-based separation of signal and noise. (Maybeck, 1979).

In this study, the components of the FTG data are processed with the standard and extensions of the Kalman filter. All six components will be processed except in constrained Kalman filter that the five independent ones are filtered.

Objective of Study

The focus of this thesis is to understand how the Kalman filter works, how to find the best parameters of the Kalman filter that can reduce the noise, the advantage of Kalman filter variations and then implement the filter to improve the signal-to-noise ratio of components of Full Tensor Gradiometry (FTG) data of Vinton dome area.

The other target of this study is to detect and map possible faults and fractures near the flanks of the Vinton salt dome using gravity gradiometry data. Mapping these features may provide a better understanding of the Vinton salt dome system, and can be applied to other salt domes in the Gulf Coast Region.

CHAPTER 2. STUDY AREA

Study area

Vinton dome is located 5 kilometers southwest of Vinton in Calcasieu Parish, Louisiana. The morphology of the dome is a minor depression within a raised mound filled by Gray Lake (Barton, 1933). Vinton salt dome has accumulated hydrocarbons in different types of reservoirs that can be associated with salt domes. It has trapped oil and gas in caprock, fault blocks, steeply dipping salt flanks as well as beneath salt overhangs (Owen, 1975). Discussion about its occurrence still is unfinished. Some geologists believe that it is an attached offshoot of the Louann salt (Coker, 2006) while others assume it was emplaced in the Eocene and is not attached to the Louann salt (Eti, 2004). The dome is cut by a fault system.

Early clues that implied the evidence of the salt dome and the probable hydrocarbon resources were Oil seepages, sour water and the topographic depression (Thompson and Echelberger, 1928, Paine et al., 1968).

Miocene Fleming and Oligocene Vicksburg formations are the major productive formations in the dome. 10 million cubic feet of gas from a depth of 1,060 meters was excavated from the one of the largest gas wells in 1911 (Thompson and Eichelberger, 1928).

Figure 2-1: Survey location, Vinton dome location, Northwest Golf of Mexico and Southwest of Louisiana.

History of the studies

Over a century, the Gulf Coast region of the United States has been an important area in producing oil and gas. Salt dome flanks, are one of the traps that lots of reservoirs in the area are accumulated in (Harrison et al., 1970; Branson, 1991). Exploration in the area started by drilling wells wherever a hint of a dome was recognized, it could be any kind of hydrocarbon seepage at the surface or a depression in the landscape (Owen, 1975).

The Vinton salt dome, located in Calcasieu Parish, Louisiana, is a typical dome of the Gulf Coast area. It is considered important because of its oil and natural gas reservoir. Due to its size and form, as well as gas and sour water discharge, it always has been recognized as the most likely locality for oil exploration in the area (Harris, 1910). W.B. Sharp and E. Prather started their explorations by drilling on the dome in 1902 and oil was reported in Vinton dome that year (Harris, 1910). Efforts for extraction of oil on Vinton dome continued in the following years by Fenneman from 1902 to 1904 (Fenneman, 1906) and Wilkins, Zeigler and Rowson (Harris, 1910). Study of the Vinton dome continued, and research done by Thompson and Eichelberger (1928), Seni and Jackson (1983), Breard et al. (1996), Constance et al. (1999), Galloway et al. (2000) and Zhou (2006) best illustrate the structure of the Vinton dome.

Exploration in the 1950's started with seismic and reflection surveys which were the only exploration method to image the subsurface for decades (Fails, 1995), but it has its own limitations near salt domes. One limitation is the difficulty in imaging which results from steeply dipping salt flanks that scatter or absorb seismic energy (Coburn, 2002).

Eventually most of the hydrocarbon resources in the Vinton dome were extracted. Therefore the United States Geological Survey (USGS) studies proposed still 9 billion cubic feet of gas remaines in the region (Swanson and Karlsen, 2009). Most of these resources are accumulated in unconventional reservoirs such as the Eocene Jackson Shale or formations deeper than 3 km (Swanson and Karlsen, 2009). To recover the remaining resources and extend field life, new geophysical techniques are needed.

Vertical Seismic Profiling (VSP) (Constance et al., 1999; Kisin, 2003), well logging (Coker, 2006), conventional gravity (Eti, 2004), and gravity gradiometry (Prutzman, 1998; O'Brien et al., 2005) are some of the approaches that have been applied to explore

possible available resources in the Gulf Coast region. A Full Tensor Gradiometry (FTG) survey done by Bell Geospace in July 2008 is one of the attempts to measure the gravity field for use at the reservoir level.

Structure

The dome has three main structural sections: caprock, dome, and faults (Figure 2-2)

Caprock: limestone, gypsum, and anhydrite form the caprock, which has a thickness of 60 m to 210 m. It is believed that it is formed by either precipitation in place or solution of impure salt rock at the top of the dome (Ingram, 1991).

Dome: it is 3.8 km in height (Eti, 2400). It extends 1,280 meters from north to south and 1,520 meters from east to west. It has caused a -26.5 mGal residual gravity anomaly in the center (Wilson and Noel, 1983). There is still an argument whether it is attached to autochthonous salt. Some models of the gravity of the dome suggest that the salt is not as deep as 8 km so it would not be autochthonous (Eti, 2004), while seismic studies does not show any subsalt reflection, leads to the interpretation the the dome is attached to the Louann salt (Coker, 2006).

Faults: a counter-regional fault downthrown to the northwest, along with three sets of peripheral faults is the main and characteristic fault of the Vinton dome area (Coker, 2006). It also has an extensive fault-line scarp system radiating from it. This system is unique to Vinton in that it is not part of the regional east-west trend in Louisiana. This fault-line scarp is considered an indication of salt flowage at depth associated with domes (Heinrich, 2005).

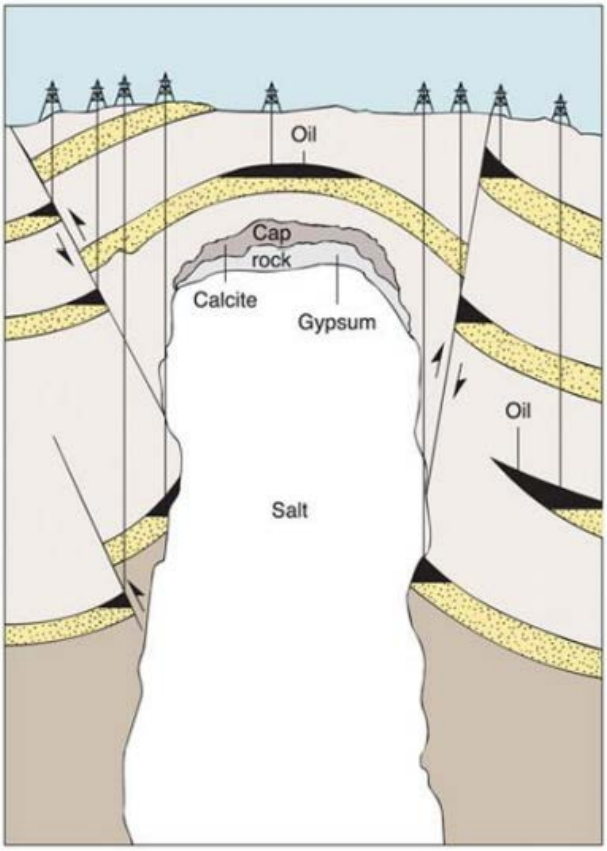

Figure 2-2: Scheme the diagram of a typical salt dome and reservoirs forming near that (Levin, 2006).

Significance of the Vinton dome and availability of model of the Vinton dome area

An advantage of the Vinton dome area is that the geological model of the area and the cap rock have already been made, and the synthetic gravity signal of the cap rock of Vinton dome has been calculated (Murphy, 2004; Ennen, 2012). The full tensor gradiometery survey done by Bell Geospace over the Vinton salt dome is important because it was a FTG data set collected with the purpose of measuring gravity for reservoir levels.

CHAPTER 3. FULL TENSOR GRADIOMETERY DATA

A brief history

When at the beginning of the 20th century, von Eotvos made the first instrument for measuring gravity gradiometry (Domenico, 1994), the innovation was not considered practical, although “billions of barrels of oil” discoveries were attributed to the instrument. The slow speed of operation was the main reason that caused the rejection of the method even though it was extremely sensitive (Lumley et al., 2010). In a very short time since its inception, the airborne FTG method has gained prominence (DiFrancesco et al., 2009). This prominence can be easily understood from the number of workshops focused on the method, increase in the demand, and use and the number of surveys done and instruments sold.

In the 1970’s and 1980’s, Bell Aerospace used the gradiometer instrument as the main part of the FTG system in marine applications (Murphy, 2004). Until 2003, Bell Geospsace had flown 1202 km for Air-FTG surveys over North America and had collected data over 12000 km for commercial purposes in Africa (Hammond and Murphy, 2003). By 2004, Murphy claimed more than 60,000 line km of data were acquired using both marine and airborne platforms (Murphy, 2004). All of these parameters prove a growing trend in using gravity gradiometry and full tensor gravity (FTG) data. Figure 3-1 illustrates the cumulative line-kilometers of surveys done based on gravity gradiometery for a ten year period from 1999 to 2008 for all gravity gradiometry surveys.

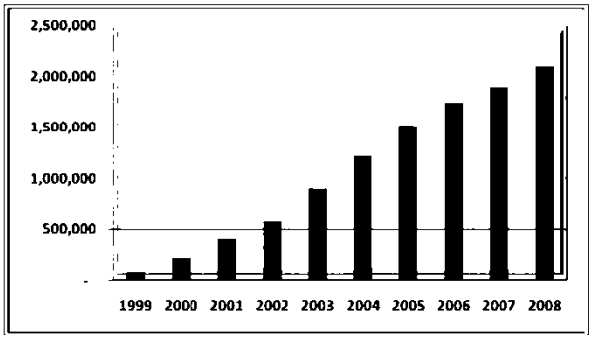

Figure 3-1: An upward trend emphasizing the market acceptance of gravity gradiometer as an exploration tool. Cumulative line-kilometers of the method in industry airborne and marine from 1999 till 2008 (DiFrancesco et al., 2009).

The first airborne gravity gradiometry survey started in October 1999 (Van Leeuwen, 2000). In 2001, Bell Geospace successfully started using an FTG platform on a single engine aircraft (Zuidweg and Mumaw, n.d.). Since then the company has flown airborne surveys over Africa, New Zealand, Australia, North America, South America and Europe (Bell Geospace, Inc., 2008). The Gulf of Mexico, the North Sea, and East Asia are some places that are investigated by the marine FTG by Bell Geospace. Companies, like ARKeX and Fugro are the other major companies that deal with airborne gravity gradiometry data and surveys (DiFrancesco et al., 2009). In 2008, BGI collected FTG data over the Vinton dome (Bell Geospace, Inc., 2008) and this is the data set that I worked with in my research.

Today, airborne Full Tensor Gravity (FTG) has been proven to be the "preferred technology" in both mineral and petroleum exploration projects (Dransfield et al., 2010). It is used in hydrocarbon exploration by detecting salt domes, fault blocks or structural closures (Murphy and Dickson, 2009). Other targets investigated with this method are base metals, precious metals, kimberlites, and even groundwater exploration (Hammond and Murphy, 2003) body (Zuidweg and Mumaw, n.d.).

There are a few examples of successful application of FTG data in oil and gas exploration including detection of salt domes, carbonate platforms and basement mapping. Other projects that used FTG methods include surveys in the Faroe-Shetland Basin area, Gulf of Mexico, the North Sea, East Asia (Bell Geospace, 2008), Northern Perth Basin (Norwest Energy NL), Chirete, Argentina (Dransfield et al., 2010), Ghana (Dransfield et al., 2010) and Vinton dome, Louisiana (Dickinson et al., 2009).

What is measured in gravity gradiometry?

Gravity potential is a scalar field, and thus it can be described as a vector. In the Cartesian coordinate system, it can be represented in terms of its components G_x, G_y and G_z (Stasinowsky, 2010). Gradiometers measure the spatial rate of change in these components in all three directions and, the term "tensor" refers to the elements of the rate of change of the gravity field or gradients of the components (Figure 3-2).

Only five components of the gradient tensor are independent. Due to the conservative characteristic of the gravity field, it can be shown that gravity gradient tensor is symmetric such that $T_{ij}=T_{ji}$ (Murphy, 2004). Considering symmetry in the FTG tensor, one expects 6 independent elements in the tensor. Gravitational potential obeys Laplace's equation; therefore each of the diagonal elements of the tensor is the negative of the sum of the two other components (Blakely, 1995). For example, T_{zz} equals the negative sum of T_{xx} and T_{yy}. Thus, it can be easily concluded that the FTG tensor has five independent elements (Murphy, 2004). The unit of gravity gradient is the Eotvos, with 1 Eo equals to 0.1 mGal/Km, which is equivalent to 10^{-9} s^{-2} (Murphy, 2004).

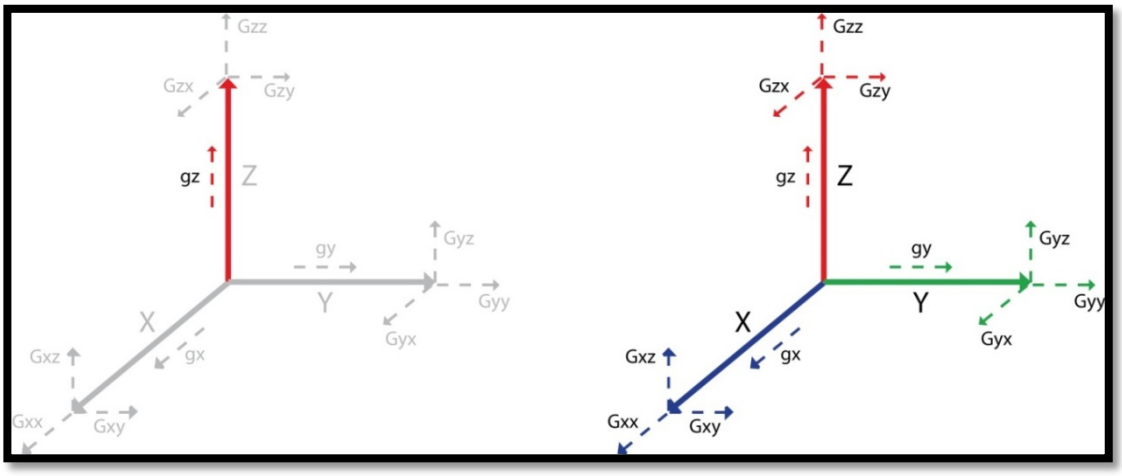

$$T_{ij} = \begin{bmatrix} T_{xx} & T_{xy} & T_{xz} \\ T_{yx} & T_{yy} & T_{yz} \\ T_{zx} & T_{zy} & T_{zz} \end{bmatrix}$$

Figure 3-2: Schematic diagram showing the conventional gravity measuring one component of the gravity field in the vertical direction Gz and the full tensor gravity gradiometry components Tij having 9 elements (from http://en.wikipedia.org/wiki/Gravity _gradiometry.)

Each of the five tensor components gives us unique information about the attributes of the target. While the horizontal tensor components T_{xx}, T_{yy}, T_{xy}, T_{xz} *and* T_{yz} are used to identify edges of the target and lineaments relevant to the structural and/or stratigraphic changes as well as the body thickness, T_{zz} is used for estimating the depth of the target (Murphy, 2004; Murphy and Brewster, 2007). They can be interpreted individually or combined in certain methods to best extract the pattern of interest (Murphy and Brewster,

2007). Table 3-1 shows what each element emphasizes assuming x axis is east-west, y axis is north-south, and z axis is vertical (Ennen, 2012).

Table 3-1: Six elements of the gradient tensor and what each element highlights (Ennen, 2012).

Element	Best to emphasize
T_{xx}	North-South trending features
T_{xy}	Northeast-Southwest trending features
T_{xz}	Central axis of a mass
T_{yy}	East-West trending features
T_{yz}	Central axis of a mass
T_{zz}	Edges

How the FTG data are measured

The Bell Geospace Full Tensor Gravity (FTG) system contains three Gravity Gradient Instruments (GGI). Each GGI has a rotating disk with 2 matched pairs of accelerometers (Figure 8.3). The gradient tensor can be obtained by observations of the two opposing accelerometers and taking into account the distance between them. Therefore the output of each GGI is two opposing gradients. The FTG tensor components are obtained by an appropriate linear combination of all six GGI outputs (Murphy, 2004)

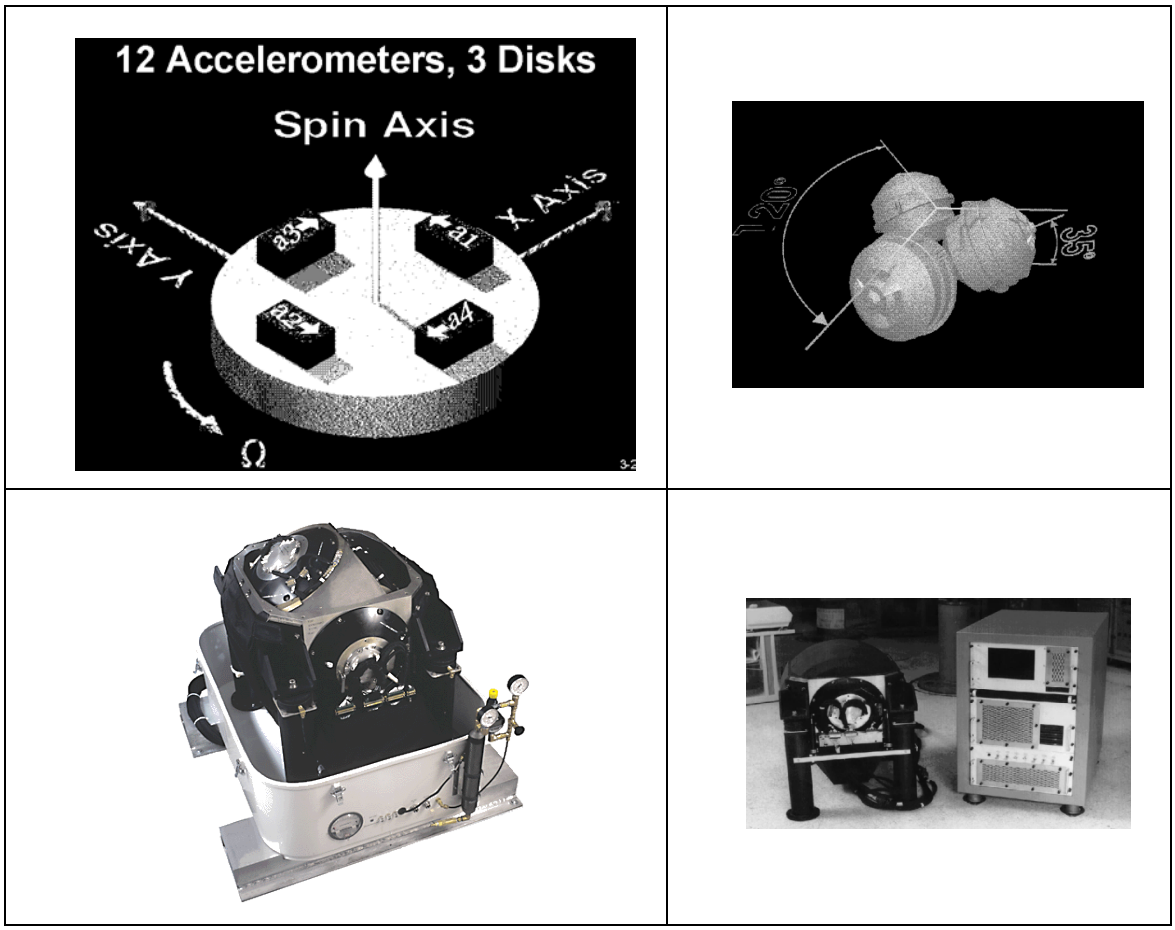

Figure 3-3: Air-FTG instrument: Inside a GGI (top left), three GGIs oriented at 120 degrees from each other (top right), Bell Geospace FTG system (bottom left) and FTG cabinet containing the GGI's and the controlling electronics cabinet (bottom right).

Full tensor gradiometry data versus conventional gravity data

Due to sampling difficulties of ground surveys and the inherent higher accuracy of the full tensor measurement, Full Tensor Gradient (FTG) measurements give us more information about the gravity field rather than partial tensor gradient (g_z) or a single vector field measurement. This means that, in case of a lateral density contrast, interpretation of FTG data of sub surface features would be more reliable compared with conventional gravity surveys (Murphy, 2004). The conventional gravity measures the component of the gravity field (most of the time g_z component) whereas gravity gradiometer measures the rate of the change in the gravity field in 3 perpendicular directions. So the FTG method is able to investigate the high frequency signals that are associated with near-surface lateral density variations while conventional vertical gravity

instruments cannot detect the lateral variations due to inadequate sampling (Figure 3-4) (Murphy, 2004). Higher spatial resolution of FTG method is due to the fact that gradiometer signal strength is proportional to $1/r^3$ where r is distance from the source while vertical gravity signal is proportional to $1/r^2$ (Figure 3-4) (Hammond and Murphy, 2003).

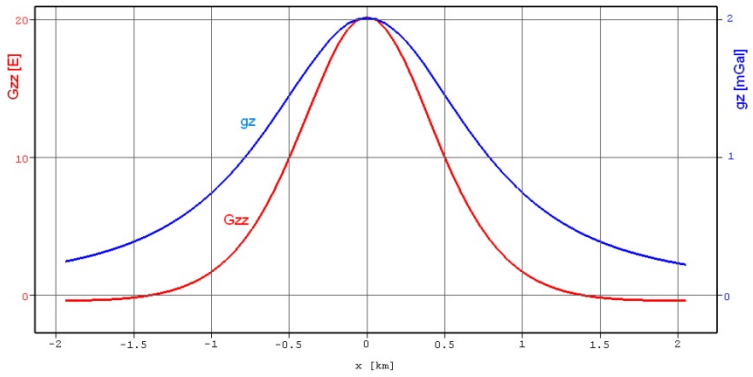

Figure 3-4: Comparing the Vertical gravity g_z and gravity gradient G_{zz} responses from a point source buried at 1 km depth (http://en.wikipedia.org/wiki/Gravity_gradiometry).

The characteristic that makes gradiometers the preferred technology for mineral exploration and high resolution oil and gas exploration is its sensitivity at short wavelengths. Because of station spacing, the conventional gravity information is limited to wavelengths above about 5 km in many places in the world, making them more useful in regional studies at basin scale whereas FTG provides dramatically better sensitivity at short wavelengths (Figure 3-4) (Dransfield et al., 2010).

In addition to greater information content and higher resolution, other advantages of FTG data over conventional gravity measurements include: improved constraints that enable expertise to clear signal from the measured data better (Murphy, 2010), speed of data acquisition and ease of covering the area of interest (Fullagar and Pears, 2010). One more point worth mentioning here is the high degree of confidence in FTG results: as geological signals in this method are extracted from 5 measured independent components, the signal is more reliable (Murphy, 2010).

The most important advantage of the method over the conventional gravimetry method is its better sensitivity at short wavelength (Dransfield et al., 2010), which allows it to provide higher resolution data. FTG surveys are sometimes preferred to seismic surveys

where the seismic method is considered too expensive or technically inadequate, like in the sub-salt, sub-basalt or sub-carbonate cases (Zuidweg and Mumaw, n.d).

CHAPTER 4. AN INTRODUCTION TO THE KALMAN FILTER

The Kalman filter is an optimal recursive data processing algorithm whose purpose is to produce values that tend to be closer to the true values of the measured parameters. Determining the "real" state of a physical system or deciding the true value of one of the dynamic attributes of a given system from a set of measurements is one of the objectives of the filtering process (Moriya, 2010). Suppose that we want to make the best possible estimate of a set of parameters that describes the state of a system, but all we have is a set of measurements affected by the presence of noise and the state of the system that is also perturbed by noise. The only way to get some information from this data set is using a filter.

When working with systems and also in system analysis, one should consider three basic sources of uncertainty in determining the actual system behavior. First, the mathematical system model is never perfect. For instance, the laws of Newtonian physics are accepted approximations to what is actually observed; their accuracy is adequate in most instances since we are unaccustomed to physical systems speeds near the speed of light. However, for processes closer to the speed of light, this approximation is not valid. We should therefore know that our approximated mathematical model can be a source of uncertainty especially when dealing with situations closer to the speed of light. Second, our own control input is not the only thing that drives the dynamic systems; there are also disturbances that we can neither control nor model effectively. Finally, we assume that sensors exactly measure our variable of interest, but in fact sensors are imperfect and cannot provide complete or accurate data about a system (Maybeck, 1979). A Kalman filter is able to tackle uncertainties of these assumptions. Figure 4-1 shows a typical Kalman filter application based on different sources of uncertainty involved in a measurement.

In general, we cannot imagine filtering our measurements without any information about our system or sensors. However, if we can answer the following three questions; (1) What is the system and measurement device dynamics? (2) What is the system noise and measurement error? (3) What is the initial condition of the desired variable?, then it has been suggested by researchers that the best possible way to determine the true state of

a system is by using the Kalman filter (Maybeck, 1979). We also can use the Kalman filter and be assured that this filter gives the best results compared to other filters if the following three basic assumptions are satisfied: (1) the system is linear; (2) the contaminated noise (both system and measurement noise) is white; and (3) the noise has a Gaussian distribution (Maybeck, 1979).

The filter, introduced by R.E. Kalman, in a paper called "A new approach to linear filtering and prediction problem" in 1960 in Journal of Basic Engineering, has been used for five decades. The Kalman filter is one of those rare topics that has maintained continued interest and has also a rich history in practical applications. What made the Kalman filter popular in the world of applications was its performance and ease of implementation rather than its analytical elegance (Zarchan and Musoff, 2000). Navigating the Apollo spacecraft, predicting short-term stock market fluctuations, and estimating location with relatively inexpensive hand-held receivers (global positioning systems) are some of the broad applications of the filter. It is recognized as the best performing filter in many disciplines. The Kalman filter is believed by some to be the second most important algorithm technique ever conceived after the Fast Fourier Transform (Zarchan and Musoff, 2000); some even consider it as the greatest discovery of the twentieth century (Haykin, 2001).

The Kalman filter attempts to minimize the mean of the squared error (Maybeck, 1979). This successful filter, which enjoys the benefits of using both least squares and probability theory, has been shown to be the optimal solution of a linear problem in the sense that no nonlinear filter designed so far can perform better than it, and even when the noise components are not Gaussian, it is the optimal filter among the entire family of linear filters (Moriya, 2010). One aspect of its optimality is that the filter incorporates all the information given to it. Regardless of measurement precision, the Kalman filter processes all available measurements to estimate the current value of the variables of interest.

Theoretically, the Kalman filter is an estimator that determines the state of a linear dynamic system which is perturbed by Gaussian white noise by using measurements that are linearly related to the state but corrupted by additive Gaussian white noise (Figure 4-1) (Maybeck, 1979; Grewal and Andrews, 2008). As mentioned earlier, the

filter is also a mathematical approach that estimates the state of a general system such that it minimizes the mean of the squared error (Welch and Bishop, 2006). The states of a system are those parameters that illustrate the internal condition or status of the system at a given instant of time (Simon, 2012). For example, the states of a moving object might include its velocity, position, and acceleration whereas for a chemical plant they could be pressure, temperature, flow rate, and gas analysis. Another example would be flood prediction: the dynamic system under investigation here being the river system and the states involved could be water level and rain gauges (Grewal and Andrews, 2008).

In applying the Kalman filter, it is not always possible or even required to measure every variable in a system — the filter is able to estimate the missing information from indirect and noisy measurements (estimating the state of a dynamic system). It is also used to predict the likely future courses of a dynamic system that cannot be controlled by people, for example the amount of flow of rivers during floods (performance analysis of estimation systems) (Grewal and Andrews, 2008).

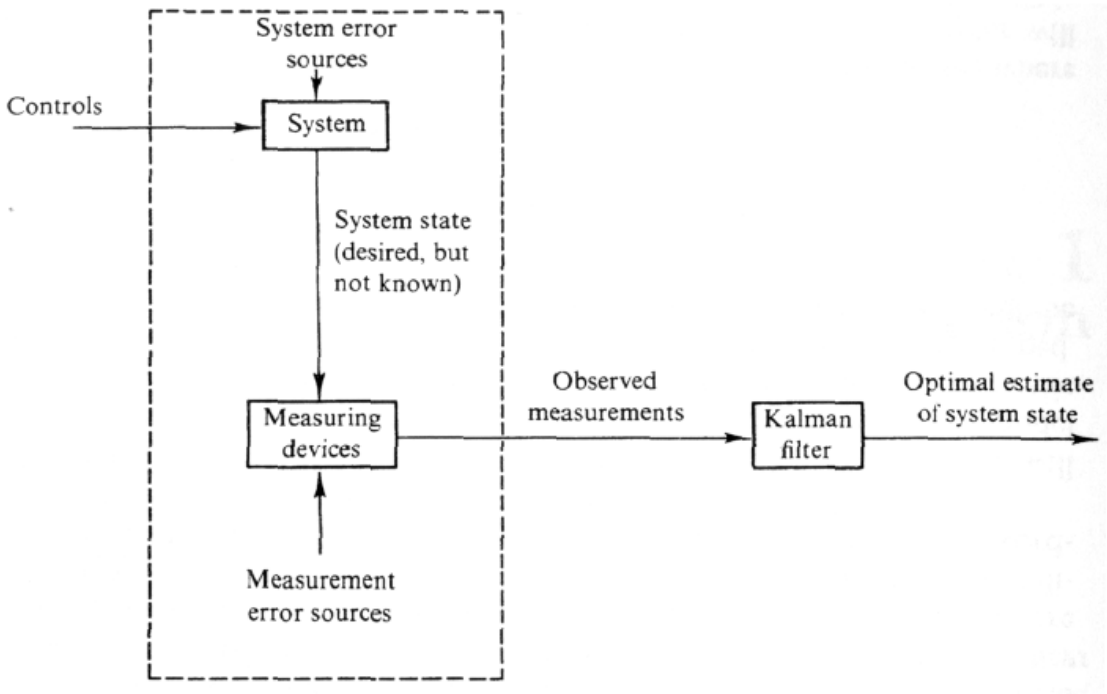

Figure 4-1: Different sources of uncertainty involved in a system and typical Kalman filter application (from Maybeck, 1979).

Historical Perspectives of the Kalman Filter

What is known today as stochastic filtering and estimation theory, leading to different versions of the Kalman filter in use today, is the result of the evolutionary development of ideas from many researchers. Galileo, Pascal, Huygens, Newton, Bernoulli, Riccati, Piazzi, Laplace, and Maxwell are some of the well-known scientists who contributed to the estimation theory. Although the fact that measurement errors are inevitable was known from the time of Galileo (1564-1642), the first method for calculating an optimal estimate from the noisy measurements, the method of least mean squares, was first discovered by Carl Friedrich Gauss in 1795 (Sorenson, 1970). Before Gauss had published his great achievement in 1805 in *Disquisitiones Arithmeticae*, there were other scientists who were challenged by the question of " how to estimate measured values a priori so that the estimate in combination with the measurement could be used to estimate better the measured parameter" (Moriya, 2010). The challenge for Pierre-Simon Laplace was the estimation of the motions of Jupiter and Saturn. The concept of parametric estimation was used also in addressing questions like estimating the motion of the moon and the dimensions of the Earth (Simon, 2006). By 1801, it had been nearly 30 years that an association of European astronomers had been searching for a "missing" planet based on Bode's law without any success. On the first day of the nineteenth century, Piazzi discovered a new celestial object and tracked it for 41 nights but after that it moved very close to the sun and disappeared. At that time, it was believed that there were only seven planets – proclaimed by the well-known philosopher George Hegel– and it would have been a waste of time to search for the eighth one. Despite this belief, the orbit of this new planet, Ceres, could be estimated by Gauss by the least mean square method and the planet was found again by its discoverer, Piazzi, on the last day of the year. The publication of this method placed him, along with Laplace, as one of the founders of the theory of probability (Moriya, 2010). Since its introduction, it has been an interesting subject for generations of scientists and technologists. This first optimal estimation method that was based on least squares and probability theory provided a connection between experimental and theoretical sciences and gave experimentalists a practical method for estimating the unknown parameters of theoretical methods.

The method of least squares is one fundamental part of the Kalman filtering; the other mathematical foundation is the probability theory or stochastic systems (Figure 4-2)It makes the estimation of the parameters of a dynamic system possible. Probability itself was developed by scientists like Pascal, Fermat, Huygens, Bernoulli, Laplace, and Legendre and, as described before, Gauss combined it with least square theory in the 19th century (Grewal and Andrews, 2008). Another concept needed in the dynamic estimation is that of the Markov chain. It was Andre Andreyevich Markov who first developed the theory of Markov process. In this process or "chain", the system undergoes transitions from one state to another, between a finite or countable number of possible states, and it is considered to be memoryless. This means that the next state depends only on the current state and not on the sequence of events that preceded it. Later on, Norbert Wiener (1984-1964), one of the geniuses of the 20th century, combined the probability theory with the knowledge of dynamic systems and developed a filter known as the Wiener filter. In the early years of World War II, Wiener was involved in a military project attempting to find an answer to the problem of "firing on moving targets" for the United States. He tried to figure out how to predict the future course of a target using noisy radar tracking data. The solution was derived from the least mean square prediction error in terms of the autocorrelation functions of the signal and the noise (Moriya, 2010). Wiener approached the problem from the frequency domain perspective. His filter was known to be very successful; therefore it was classified as "Top Secret" and was not published for years (Wiener reported his solution in the classified report in 1942, but it was not available to public until 1949) (Wiener, 1964). Almost at the same time that Wiener was developing his filter, but independently of him, a Soviet scientist Kolmogorov, published a method pertaining to least squares estimation on measurement theory. Kolmogorov's work, practically identical to Wiener's method, did not become well-known in the Western world until later since it was published in Russian (Kolmogorov, 1992). As Wiener and Kolmogorov's filters are identical, the filter is known today as the Wiener-Kolmogorov filter.

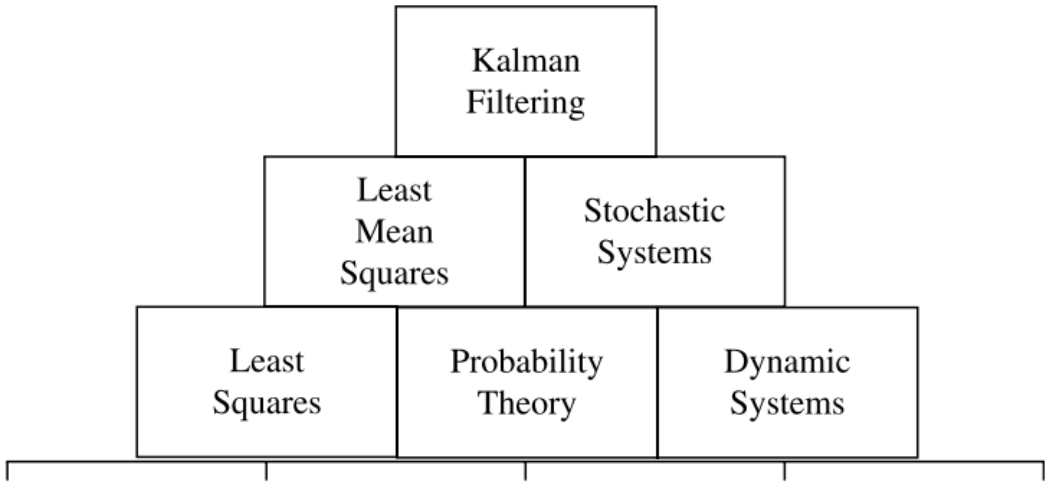

Figure 4-2: Foundational concepts leading to the Kalman filter (from Grewal and Andrews, 2008).

The Wiener-Kolmogorov filter became the basis of dynamic systems research in the 1950s. The Wiener-Kolmogorov filter is based heavily in statistics and requires information about covariances. For several years in the 1950s, NASA investigated a way to implement the Wiener-Kolmogorov filter and use it in space navigation problems, but without success (Schmidt, 1981), until they began to replace the covariance knowledge by state-space descriptions and the results were algorithms that are very close to the Kalman filter (Moriya, 2010). It was one of the first models connecting position and velocity (state) to measurements (space).

In 1958, Rudolph E. Kalman and Richard S. Bucy were given a fund to do advanced research in estimation and control at the Research Institute for Advanced Studies in Baltimore. Kalman followed the idea of applying the notion of state variables to the Wiener-Kolmogorov filter; he developed the equivalent estimation method from a time-varying state-space model and established what is now called the Kalman filter (Grewal and Andrews, 2008). Although the replacement of state-space form instead of the frequency domain formulation made the mathematical background needed for the derivation much simpler, Kalman's idea was not accepted among his peers in electrical engineering and so he chose a mechanical engineering journal to publish his new filter. Even later, when he wrote his second paper on the continuous-time case, it was rejected

because one of the referees stated that one step in the proof was not correct (but it was indeed correct). Kalman insisted on presenting his filter and finally the paper was accepted. Soon, it became one of the most interesting topics of study in many universities and in a single decade after its introduction, it was the subject of hundreds of doctoral theses in the electrical engineering field, a field where it originally met with severe skepticism (Grewal and Andrews, 2008).

Although prior to 1960, and before Kalman developed his filter, similar filters were introduced in fields other than engineering, such as statistics and economics. However, the filter was named after Kalman for several reasons. First, Kalman introduced his filter in a relatively straightforward way and even though he did not focus on any specific application, he laid out a strong theoretical foundation, and thus it was considered more general and useful. Second, at the time of the publication of his paper, digital computers were available and that made the use of the filter practical. Finally, Kalman introduced his work to NASA and they used the filter as an estimator for the Apollo space program successfully (Schmidt, 1981; McGee and Schmidt, 1985).

Later in 1962, the Kalman filter played an important role in the development of realization theory, a theory that deals with the problem of finding a model to explain the behavior of a system based on observed input/output data. In 1985, Kalman received the Kyoto Prize, the Japanese equivalent of the Nobel Prize (Grewal and Andrews, 2008).

The Kalman filter was one of the enabling technologies of the Space Age. Without it, the precise navigation of spacecrafts through solar system was completely impossible. It was also recognized as the best performing filter in many other disciplines. In general, the principal uses of the Kalman filter can be grouped into two categories: (1) estimating the state of dynamic systems and (2) performance analysis of estimation systems (Grewal and Andrews, 2008). Some of the applications of the Kalman filter are: tracking a user's position and orientation in virtual environments (Welch and Bishop, 1997), data fusion in navigation (Joost and and Krekel, 1993), data processing (Zhang, 1997), describing the water movement in river basins, coastal areas, and oceans (Madsen and Cañizares , 1999; and Drécourt and Madsen, 2001), maximizing equity market sector predictability (Johnson and Sakoulis, 2003), assimilation of observations in atmospheric models (Houtekamer et al., 2005), suppression of noise in a running car environment for hands-

free mobile telephony (Kybic, 1998), aerospace applications (Schmidt, 1981), and sales rate and cumulative sales forecasting (Munroe et al., 2009).

In recent years, more research topics are focusing on applications of the Kalman filter for non-linear systems, the systems whose noise has non-Gaussian characteristics, the systems that involve uncertainty in their contrasts, etc. These subjects have resulted in more than 100,000 publications by 2010, including a variety of academic publications, textbooks, and numerous patents (Moriya, 2010).

In the following chapters, I develop the Kalman filter for reducing noise in full tensor gravity gradiometry (FTG) data that were initially collected for testing the capabilities of airborne gradiometry in locating a known salt dome in Louisiana for oil and gas exploration. The data were provided by Bell Geospace Company. In this research, I have introduced new methodology in the application of the filter for reducing noise and I have also incorporated the constraint of Laplace's equation, for the first time, in the formulation of the filter. In order to illustrate basic concepts of the filter, I also use examples from a few books on the topic.

Inside the Black Box of the Kalman Filter

Starting With an Example

A simple example from Maybeck's (1979) book on the Kalman filter is widely used by other authors as it is helpful in understanding in simple steps how the Kalman filter works. In this single variable example, any kind of data would suffice but the determination of a position is chosen here since it is a familiar concept for dynamic systems.

Suppose we want to establish our position based on a set of measurements where the true location is not known. Our measurement of position for time t_1 is considered to be z_1. We know that there are some sources of uncertainty in our measurements like human error and measuring device inaccuracies, etc. Because of all different inaccuracies that are involved in measurements, we have the standard deviation σ_{z_1} to define the precision. With such a measurement (z_1) and corresponding standard deviation, we would be able to establish the conditional probability of x (x_1), i.e., the position at time t_1 (Figure 4-3).

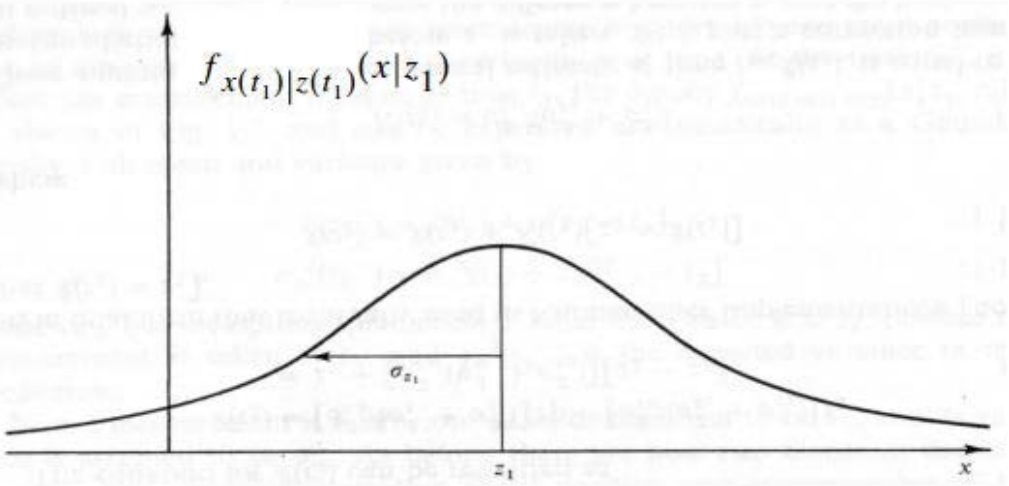

Figure 4-3: Conditional probability density of position based on first measured value z_1 (from Maybeck, 1979)

Figure 4-3 shows $f_{x(t_1)|z(t_1)}(x|z_1)$ as a function of location (x) and illustrates the probability of being at a location based only on the measurement z_1. It is also

understandable that the larger the σ_{z_1}, the broader the probability peak. Broader probability peak spreads the probability "weight" over a larger range of x values. From basic statistics, we know that for a Gaussian probability density, 68.3 % of the probability "weight" lies within ±1σ distance of the mean on both sides. With this explanation, the best estimate of the position ($\hat{x}(t_1)$) based on the conditional probability density is

$$\hat{x}(t_1) = z_1 \qquad 4\text{-}1$$

And the variance of the error in the estimate is:

$$\sigma_x{}^2(t_1) = \sigma_{z_1}{}^2 \qquad 4\text{-}2$$

In this perfect Gaussian case, the best estimate ($\hat{x}$) is equal to the mode, the median and also the mean of the measurements. If another measurement is taken at the same time so that t2 ≅ t1, we can say the position has not changed from measurement 1 to 2 while the second measurement (z_2) has the variance σ_{z_2}. Let's suppose that for any reason (for example the second observer is better trained or more skilled), and hence σ_{z_2} is smaller than σ_{z_1}. Figure 4-4 illustrates how the conditional density of the position would be at time t2 based on only the second measurement z_2. As we expect, due to smaller variance, the peak is narrower and one's ability to locate the position in the case of the second observation is greater (Figure 4-4).

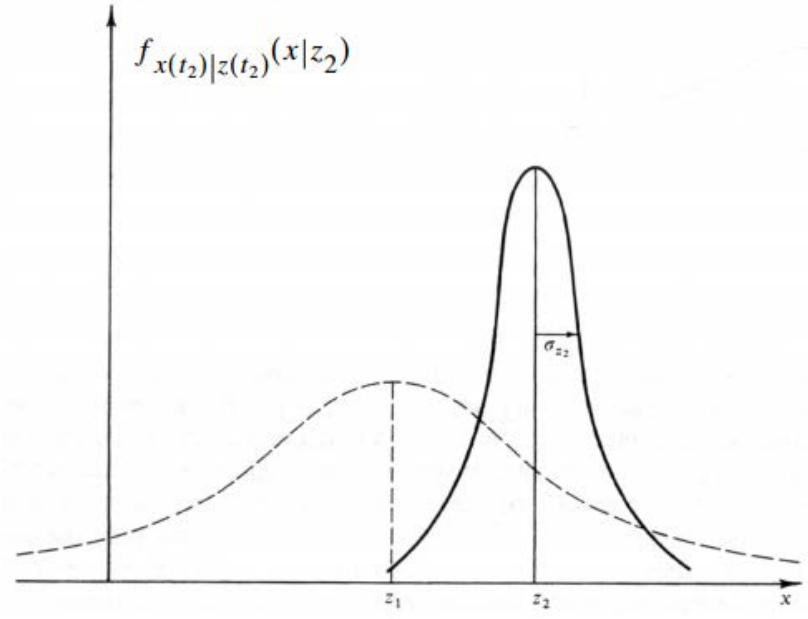

Figure 4-4: Conditional probability density of position based on the second measured value z2 (from Maybeck, 1979).

The next question is whether we can have a better estimate based on both the measurements and whether we can combine the results to obtain a better estimate (Figure 4-4). The best estimate of the position, at time $t_2 \cong t_1$ based on both available measurements z_1 and z_2 has a Gaussian probability density with mean μ and variance σ^2 (Figure 4-5) such that

$$\mu = \left[\frac{{\sigma_{z_2}}^2}{({\sigma_{z_1}}^2+{\sigma_{z_2}}^2)}\right] z_1 + \left[\frac{{\sigma_{z_1}}^2}{({\sigma_{z_1}}^2+{\sigma_{z_2}}^2)}\right] z_2 \qquad 4\text{-}3$$

and

$$\frac{1}{\sigma^2} = \left(\frac{1}{{\sigma_{z_1}}^2}\right) + \left(\frac{1}{{\sigma_{z_1}}^2}\right) \qquad 4\text{-}4$$

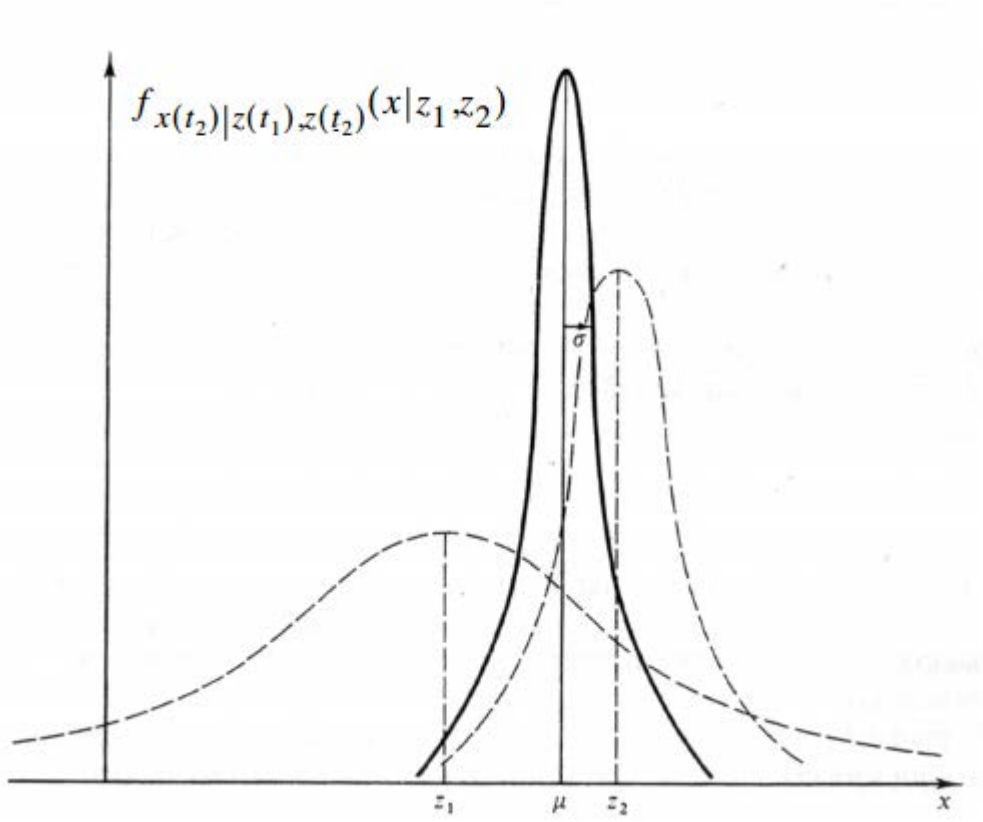

Figure 4-5: Conditional probability density of position based on both measured values z1 and z2 (from Maybeck, 1979).

If the uncertainty is equal for both $Z_1$and Z_2in equation 4-3, then the weights in the equation will be 0.5 for each measurement

$$\mu = \left[\frac{1}{2}\right] z_1 + \left[\frac{1}{2}\right] z_2 \qquad 4\text{-}5$$

And if $\sigma_{z_1}$is larger than σ_{z_2}, then the measurement z_2 will appropriately have more weight, and vice versa. Similarly, one can observe from Equation 4-4 that the variance of the best estimate is smaller than either of the two measurements. It means that even if one of the measurements is of poor quality and consequently has large uncertainty, then the variance of the estimate is again less than that of each measurement; it is reasonable because even a poor quality data can provide some information and should thus increase the precision of the prediction.

In order to put the above concepts in the iterative form needed for the Kalman filter, the best or maximum likelihood estimate of position involving the two measurements can be written as:

$$\hat{x}(t_2) = \mu \qquad 4\text{-}6$$

and whose error variance is σ^2 .

While the associated error variance is σ^2, we refer to $\hat{x}(t_2)$ as the best estimate since it is the maximum likelihood estimate. It is also a linear estimate whose variance is less than any other linear estimate (Maybeck, 1979).

If the first and second measurements have the same precision, then Equation 4-3 will be

$$\mu = \left[\frac{1}{2}\right] z_1 + \left[\frac{1}{2}\right] z_2 \qquad 4\text{-}7$$

That is simply, as would be expected, the average of the two measurements. When uncertainty involved in measuring z_1 is more than that of z_2, $\sigma_{z_1}$is larger than σ_{z_2}, then the equation will dictate more weight to z_2 (Equation 4-3).

Considering Equations 4-3 and 4-6 simultaneously, and because the weights on z_1 and z_2 in Equation 4-3 add up to 1, we arrive at

$$\hat{x}(t_2) = \left[\frac{{\sigma_{z_2}}^2}{\left({\sigma_{z_1}}^2 + {\sigma_{z_2}}^2\right)}\right] z_1 + \left[\frac{{\sigma_{z_1}}^2}{\left({\sigma_{z_1}}^2 + {\sigma_{z_2}}^2\right)}\right] z_2$$

$$= \frac{{\sigma_{z_2}}^2 z_1 + {\sigma_{z_1}}^2 z_2 + {\sigma_{z_1}}^2 z_1 - {\sigma_{z_1}}^2 z_1}{\left({\sigma_{z_1}}^2 + {\sigma_{z_2}}^2\right)}$$

$$= z_1 + \left[\frac{{\sigma_{z_1}}^2}{({\sigma_{z_1}}^2 + {\sigma_{z_2}}^2)}\right][z_2 - z_1] \qquad 4\text{-}8$$

Finally, using Equation 4-1, Equation 4-6 can be rewritten in a form known in the Kalman filter literature:

$$\hat{x}(t_2) = \hat{x}(t_1) + K(t_2)[z_2 - \hat{x}(t_1)] \qquad 4\text{-}9$$

where

$$K(t_2) = \left[\frac{{\sigma_{z_1}}^2}{\left({\sigma_{z_1}}^2 + {\sigma_{z_2}}^2\right)}\right]$$

Equation 4-9 illustrates that the optimal estimate at time t_2, $\hat{x}(t_2)$, is equal to the best prediction of its value *before* the second measurement, z_2, is taken plus an iterative correction term, *K*, composed of the gain value times the difference between z_2 and the best prediction of its value before the last measurement, $\hat{x}(t_1)$ (Maybeck, 1979). Equation 4-9 and the associated discussion explain the "predictor-corrector" structure of the filter. First, based on all previous information, a "prediction" of the desired variables at the next measurement time is made. Then, when the next measurement is taken, the difference between it and the predicted value is used for "correction".

Substituting *K* in Equation 4-4, the variance of the position can be rewritten as

$${\sigma_x}^2(t_2) = {\sigma_x}^2(t_1) - K(t_2){\sigma_x}^2(t_1) \qquad 4\text{-}10$$

In this form, the terms $\hat{x}(t_2)$ and ${\sigma_x}^2(t_2)$ include all of the information in the function $f_{x(t_2)\,|z(t_1),z(t_2)}(x\,|z_1, z_2)$ and propagate conditional probability density of the position at time t_2 considering measurements $z_1$and z_2.

The above framework can be used to estimate static problems, but how will the equations change in a dynamic problem? What will happen if the object of interest travels for some time before another measurement is taken? If we suppose that the best model has the following form:

$$\frac{dx}{dt} = u + w \qquad 4\text{-}11$$

where *u* is the nominal velocity and *w* is a noise term representing uncertainty in our knowledge of the actual velocity. It might be due to disturbances or the effects that have been neglected, so that we can consider the model as a first order equation which may have non-optimum conditions. The noise is considered to be a white Gaussian noise with a mean of zero and variance $\sigma_w{}^2$(Maybeck, 1979).

Figure 4-6 shows how the conditional probability density propagates. The probability density shifts along the x-axis with the nominal speed of *u* and spreads out in time about its mean. Addition of uncertainty over time, reduces confidence in the knowledge of the exact position, and hence the increased spread of the probability density at position z_3 (Figure 4-6).

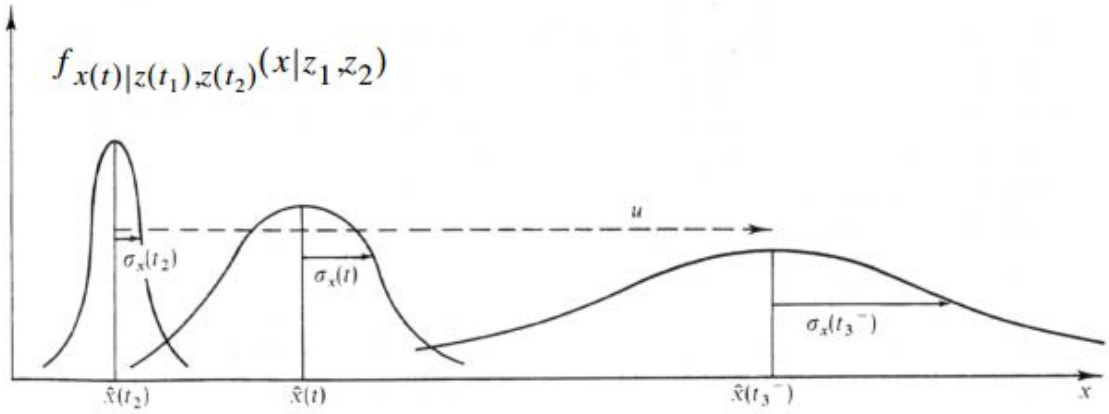

Figure 4-6: Propagation of conditional probability density of position based on all three measured values z1, z2 and z3, (from Maybeck, 1979).

At the time $t_3{}^-$, right before the third measurement is taken at time t_3 (superscripts minus indicate pre-measurement values), the desired probability density has a Gaussian distribution and it is expressed mathematically as a function having a conditional probability of $f_{x(t_3)\ |z(t_1),z(t_2)}(x\ |z_1,z_2)$ and that probability can be represented by its mean and variance using the following equations (Maybeck,1979):

$\hat{x}(t_3{}^-) = \hat{x}(t_2) + u[t_3 - t_2]$, and

$\sigma_x{}^2(t_3{}^-) = \sigma_x{}^2(t_2) + \sigma_w{}^2[t_3 - t_2]$ 4-12

At time t_3, the measurement z_3, with the variance of $\sigma_x{}^2(t_3{}^-)$, is taken. At this point, as before, there are two available Gaussian probability densities: one is the density that encompasses all the information before the measurement and the other is the information that comes from the measurement itself. Like in the static case, the predicted probability density of $\hat{x}(t_3{}^-)$ and $\sigma_x{}^2(t_3{}^-)$ is combined with the density of z_3 and $\sigma_{z_3}{}^2$ to yield a Gaussian density having the best estimate at time t_3 as given below by the values of $\hat{x}(t_3)$ and $\sigma_x{}^2(t_3)$

$\hat{x}(t_3) = \hat{x}(t_3{}^-) + K(t_3)[z_3 - \hat{x}(t_3{}^-)]$,

and

$$\sigma_x{}^2(t_3) = \sigma_x{}^2(t_3{}^-) - K(t_3)\sigma_x{}^2(t_3{}^-) \qquad 4\text{-}13$$

where the gain value of $K(t_3)$ is calculated as

$$K(t_3) = \frac{\sigma_x{}^2(t_3{}^-)}{[\sigma_x{}^2(t_3{}^-)+\sigma_{z_3}{}^2]} \qquad 4\text{-}14$$

The optimal estimate at time t_3 is $\hat{x}(t_3)$; it is formed by the prediction of its value before the measurement z_3 is taken and is corrected by the gain value times the difference between z_3 and the prediction of its value.

Equation 4-14 suggests that if the variance of the measurement noise, σ_{z_3}, is large, then the corresponding gain value $K(t_3)$ will be small. Equation 4-13 shows that the smaller gain value implies that we should give less weight to a noisy measurement and more weight should be given to the optimal estimate made before the measurement is taken, $\hat{x}(t_3{}^-)$. Mathematically, if at the extreme $\sigma_{z_3} \to \infty$, $K(t_3)$ approaches zero, and as we would expect the best estimate at this point, $\hat{x}(t_3)$, is $\hat{x}(t_3{}^-)$.

On the other hand, if the dynamic system noise, σ_w (later which will also be called the process noise covariance), is large, then $\sigma_x{}^2(t_3{}^-)$ will be large (Equation 4-12), and consequently $K(t_3)$ will be large. Literally, it means that when we are not sure about our system model and its output, we should give more weight to the measurement. In the limit, when $\sigma_w \to \infty$, $\sigma_x{}^2(t_3{}^-) \to \infty$, and $K(t_3) \to 1$, thus the best estimate from the filter, $\hat{x}(t_3)$, calculated from Equation 4-13, will be

$\hat{x}(t_3) = \hat{x}(t_3{}^-) + 1.[z_3 - \hat{x}(t_3{}^-)] = z_3$.

So in the limit of complete lack of confidence in the system model, the best choice would be ignoring the model completely and relying on only the new measurement as the optimal estimate.

In understanding the Kalman filtering process, there is one other limiting case to consider: i.e. when ${\sigma_x}^2(t_3^-)$ becomes zero. When this occurs, $K(t_3)$ will be zero. It means that if we have absolute confidence in our estimate before the measurement, z_3, is taken, then we do not need to include the measurement itself in adjusting our estimate. In this case, we can accept the estimate before the measurement is taken, i.e., $\hat{x}(t_3^-)$, as the best estimate, $\hat{x}(t_3)$, in Equation 4-13 as

$$\hat{x}(t_3) = \hat{x}(t_3^-) + 0.[z_3 - \hat{x}(t_3^-)] = \hat{x}(t_3^-)$$

$$Thus, \qquad \sigma_x(t_3^-) \to 0 \quad then \quad \hat{x}(t_3) = \hat{x}(t_3^-) \qquad 4\text{-}15$$

How the Kalman Filter Works

As mentioned before, the Kalman filter, i.e., an optimal state estimator, is made of two different steps and equations: ***Time Update*** or the prediction step as well as ***Measurement update*** which is known as the correction step. The filter uses a form of feedback control to make the estimate. It means that, first, the filter estimates the process state and then obtaining the feedback from the noisy measurement, it corrects its estimate (Figure 4-7). In other words, the time update equations are designed to project current state and error covariance estimates forward, and obtain the *a priori* estimates for the next time step. Whereas the measurement update equations try to incorporate a new measurement into the *a priori* estimate and calculate *a posteriori estimate* (Moriya, 2010).

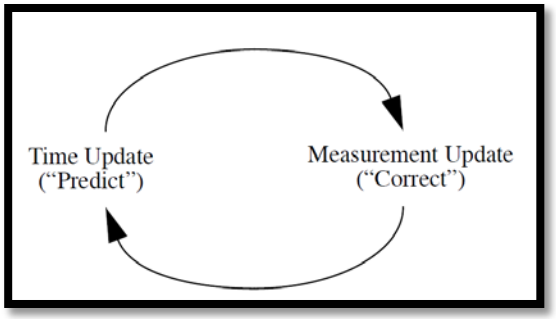

Figure 4-7: The Kalman filter recursive feedback loop (from Welch and Bishop, 2006).

In chapter 5, to understand the workings of the Kalman filter, I explain the measurement and time update procedures as well as the corresponding equations. The measurement update is obtained with iterative least-squares estimation. I found the book, "Optimal State Estimation: Kalman, H∞, and Nonlinear Approaches", by D. Simon very helpful in understanding the filter, and so I use the examples from that book in addition to my own examples.

CHAPTER 5. THE MEASUREMENT UPDATE AND TIME UPDATE STEPS

From Least-Squares Estimation to Iterative Least-Squares

Carl Friedrich Gauss discovered in 1795 and published later in 1809 (Simon, 2006) that “the most probable value of the unknown quantities will be that in which the sum of the squares of differences between the actually observed and computed values multiplied by numbers that measure the degree of precision is a minimum” (2004). This is the basis of the measurement update step of the Kalman filter (Simon, 2006).

In this step of the Kalman filter, the best value of a state is determined given our noisy measurements. This is done using an iterative least-squares approach and it is the starting point of all Kalman filters. As it mentioned before, the states of a system are those parameters that illustrate the internal condition or status of the system at a given instant of time (Simon, 2012). In the following, I introduce two linear least-squares examples, which are first converted to the iterative least-squares method, and then in the form of equations for the measurement update (Simon, 2006). I took the next 2 examples from Simon (2006).

Example 1: Estimation of a constant by the least-squares with measurements having the same degree of accuracy

In the simplest case, the desired state is a constant vector, where all available measurements have the same accuracy and therefore the same level of confidence. It is an example for determining the resistance of a resistor. We do not know the resistance and we have taken several measurements (with noise) with a cheap multimeter to estimate its resistance. In this example, the desired state (resistance) is a constant scalar but, in general the state can involve more than one element and have the form of a constant vector (Simon, 2006). Stating these explanations in mathematical language, we have state vector "x" that contains “n” unknown elements, and vector "y" that involves “k” noisy measurements. The question is how we can determine the “best” estimate of "x" which is called "$\hat{x}$". With the assumptions of the Kalman filter, consider that there is a linear

relation between the elements of the measurement vector, *y,* and the state vector, x, and there exists some measurement noise (v), so

$$y_1 = H_{11}x_1 + \cdots H_{1n}x_n + v_1$$

.

.

.

$$y_k = H_{k1}x_1 + \cdots + H_{kn}x_n + v_k \quad \text{5-1}$$

where H is the measurement matrix.

Writing in the matrix form, we have

$$y = Hx + v \quad \text{5-2}$$

The difference between noisy measurements and vector $H\hat{x}$ which is known as measurement residual is given as

$$\epsilon_y = y - H\hat{x} \quad \text{5-3}$$

From the least-squares method (Gauss, 2004), to find the most probable value of the vector, $\hat{x}$, we need to minimize the sum of the squares between the measured values, y, and the vector $H\hat{x}$. To accomplish this, we minimize the cost function J, where J is defined as

$$J = {\epsilon_{y1}}^2 + \cdots + {\epsilon_{yk}}^2$$

$$= {\epsilon_y}^T \quad \text{5-4}$$

Substituting 6-3 in 6-4, we have,

$$J = (y - H\hat{x})^T(y - H\hat{x})$$

$$= y^Ty - \hat{x}^TH^Ty - y^TH\hat{x} + \hat{x}^TH^TH\hat{x} \quad \text{5-5}$$

Since we are looking for the unknown $\hat{x}$ that minimizes the cost function J, we need to compute the partial derivative of J with respect to $\hat{x}$ and set it equal to zero. Thus,

$$\frac{\partial J}{\partial \hat{x}} = -y^TH - y^TH + 2\hat{x}^TH^TH$$

$$= 0 \quad \text{5-6}$$

The $\hat{x}$ that can satisfy the above equation can be calculated as

$$H^T y = H^T H\hat{x}$$

$$\hat{x} = (H^T H)^{-1} H^T y$$

$$= H^L y \qquad 5\text{-}7$$

In the above equation H^L exists if $k \geq n$ and H is a full rank matrix, then H^L is the left pseudo inverse of H. One of the two criteria for the existence of H is that the number of measurements, k, must be greater than the number of variables, n, that we want to estimate ($k \geq n$). The second criterion is that the measurements need to be linearly independent.

In the above equations, we used the following mathematical properties of matrix algebra and matrix calculus.

$$(AB)^T = B^T A^T$$

$$\frac{\partial (x^T y)}{\partial x} = y^T$$

$$\frac{\partial (x^T y)}{\partial y} = x^T$$

$$\frac{\partial (x^T Ax)}{\partial x} = x^T A + A^T \mathrm{x}^{\mathrm{T}} \qquad 5\text{-}8$$

For estimating the unknown resistance, x, of the resistor, based on k available noisy measurements from a multimeter, we can write

$$y_1 = x + v_1$$

.

.

.

$$y_k = x + v_k \qquad 5\text{-}9$$

Since there is only one resistor, x is a scalar. Equation ◦-9 can be written in the form of a single matrix as,

$$\begin{bmatrix} y_1 \\ \cdot \\ \cdot \\ \cdot \\ y_k \end{bmatrix} = \begin{bmatrix} 1 \\ \cdot \\ \cdot \\ \cdot \\ 1 \end{bmatrix} x + \begin{bmatrix} v_1 \\ \cdot \\ \cdot \\ \cdot \\ v_k \end{bmatrix} \qquad 5\text{-}10$$

Equation 5-7 illustrates that the optimal estimate, $\hat{x}$, of the unknown resistance, x, can be calculated as

$$\hat{x} = (H^T H)^{-1} H^T y$$

$$= \left([1 \dots 1] \begin{bmatrix} 1 \\ \cdot \\ \cdot \\ 1 \end{bmatrix} \right)^{-1} [1 \dots 1] \begin{bmatrix} y_1 \\ \cdot \\ \cdot \\ y_k \end{bmatrix}$$

$$= \frac{1}{k}(y_1 + \cdots y_k) \qquad \text{5-11}$$

where H is as defined previously in Equations 5-10. The result gives the average of the measurements as the best estimate of the unknown resistance and thus agrees with one's intuition.

Example 2: Estimation of a constant when measurements have different degree of accuracy

In the above example, we studied the case that we had equal amount of confidence in all our measurements. But that is not a general case. In practice, we have more confidence in some measurements than the others. So we need to give more weight to the measurements having greater confidence. Nevertheless, we would like to use measurements with greater uncertainty in our estimation, because they still have *some* information.

Mathematically stated, like before, we have an unknown constant, which is represented by an n-element vector, x, and a k-element vector of measurements, y. We also assume that there is a linear relationship between each element of y with the elements of x, and we have some measurement noise (v) whose variance might be different for each element of y. Thus,

$$\begin{bmatrix} y_1 \\ \cdot \\ \cdot \\ y_k \end{bmatrix} = \begin{bmatrix} H_{11} & \cdot & \cdot & \cdot & H_{1n} \\ \cdot & & & & \cdot \\ \cdot & & \ddots & & \cdot \\ H_{k1} & \cdot & \cdot & \cdot & H_{kn} \end{bmatrix} \begin{bmatrix} x_1 \\ \cdot \\ \cdot \\ x_k \end{bmatrix} + \begin{bmatrix} v_1 \\ \cdot \\ \cdot \\ v_k \end{bmatrix}$$

$$E({v_i}^2) = {\sigma_i}^2 \qquad (i = 1, \dots, k) \qquad \text{5-12}$$

If the measurement noise has zero-mean and is independent, the measurement covariance matrix has the form

$$R = E(vv^T)$$

$$= \begin{bmatrix} {\sigma_1}^2 & \cdots & 0 \\ \vdots & & \cdots \\ 0 & \cdots & {\sigma_k}^2 \end{bmatrix} \quad \text{5-13}$$

To find the optimum value of x, we need to minimize the cost function, J, with respect to $\hat{x}$. So

$$J = \frac{{\epsilon_{y1}}^2}{{\sigma_1}^2} + \cdots + \frac{{\epsilon_{yk}}^2}{{\sigma_k}^2} \quad \text{5-14}$$

If we compare Equation 5-14 with 5-4, we see that in 5-4 we tried to minimize the sum of the squares of the elements of ϵ_y, while in 5-14 we minimize the *weighted* sum of the squares. The weighted minimization makes it possible to consider relative variances of the errors in observations. It means that, if one of our measurements, let's say y_1, is a relatively noisy measurement, then as we do not have that much confidence in it, we place less emphasis on minimizing the difference between it and the first element of $H\hat{x}$, and we put more effort in minimizing this difference for those measurements that are less noisy. In this case, the cost function can be written as

$$\begin{aligned} J &= {\epsilon_y}^T R^{-1} \epsilon_y \\ &= (y - H\hat{x})^T R^{-1} (y - H\hat{x}) \\ &= y^T R^{-1} y - \hat{x}^T H^T R^{-1} y - y^T R^{-1} H\hat{x} + \hat{x}^T H^T R^{-1} H\hat{x} \end{aligned} \quad \text{5-15}$$

To compute the best estimate of x, which is $\hat{x}$, like before, we need to take the partial derivative of the cost function, J, with respect to $\hat{x}$ and set it equal to zero:

$$\begin{aligned} \frac{\partial \mathrm{J}}{\partial \hat{x}} &= -2y^T R^{-1} H + 2\hat{x}^T H^T R^{-1} H \\ &= 0 \end{aligned}$$

Therefore,

$$H^T R^{-1} y = H^T R^{-1} H\hat{x}$$

and

$$\hat{x} = (H^T R^{-1} H)^{-1} H^T R^{-1} y \quad \text{5-16}$$

For the example of estimating the resistance based on k available measurements with different levels of uncertainty, our system of equations becomes:

$$y_i = x + v_i$$

$$E({v_i}^2) = {\sigma_i}^2 \qquad (i = 1, \dots, k) \tag{5-17}$$

Like Equation 5-10, the relation between the unknown values and measurement can be written as

$$\begin{bmatrix} y_1 \\ \cdot \\ \cdot \\ \cdot \\ y_k \end{bmatrix} = \begin{bmatrix} 1 \\ \cdot \\ \cdot \\ \cdot \\ 1 \end{bmatrix} x + \begin{bmatrix} v_1 \\ \cdot \\ \cdot \\ \cdot \\ v_k \end{bmatrix} \tag{5-18}$$

The measurement noise covariance has the following form

$$R = diag({\sigma_1}^2 \dots {\sigma_k}^2) \tag{5-19}$$

and substitution of the above vectors in Equation 5-16 results in

$$\hat{x} = (H^T R^{-1} H)^{-1} H^T R^{-1} y$$

$$\hat{x} = \left(\begin{bmatrix} 1 & \cdots & 1 \end{bmatrix} \begin{bmatrix} {\sigma_1}^2 & \cdots & 0 \\ \vdots & \ddots & \vdots \\ 0 & \dots & {\sigma_k}^2 \end{bmatrix}^{-1} \begin{bmatrix} 1 \\ \vdots \\ 1 \end{bmatrix} \right)^{-1} \times \begin{bmatrix} 1 & \cdots & 1 \end{bmatrix} \begin{bmatrix} {\sigma_1}^2 & \cdots & 0 \\ \vdots & \ddots & \vdots \\ 0 & \dots & {\sigma_k}^2 \end{bmatrix}^{-1} \begin{bmatrix} y_1 \\ \cdot \\ \cdot \\ \cdot \\ y_k \end{bmatrix}$$

$$= \left(\sum {1}/{{\sigma_i}^2} \right)^{-1} \left({y_1}/{{\sigma_1}^2} + \cdots + {y_k}/{{\sigma_k}^2} \right) \tag{5-20}$$

Thus, when the measurements are weighted by the inverse of their uncertainty, less emphasis is placed on measurements having greater uncertainty. When all of the data have the same accuracy, ($i.e., when\ \partial_i$ is constant), Equation 5-20 reduces to Equation 5-11.

Converting the Linear Estimator to the Linear Recursive Estimator

Equations 5-7 and 5-16 calculate the optimum estimate of a constant vector; If we update our estimate of x each time for all measurements sequentially, it means that we obtain measurements gradually and include them into the estimation procedure subsequently, we will need to augment the H matrix and recompute our best estimate, $\hat{x}$, each time. If the number of measurements gets large, then the computation could become very time consuming and will need large memory and storage space. So rewriting the estimator equation recursively is an important step in making it an effective estimator. In this form of equation, after $(k-1)$ measurements, we obtain a new measurement, y_k, the iterative least-squares equations can be written as

$$y_k = H_k x + v_k$$

$$\hat{x}_k = \hat{x}_{k-1} + K_k(y_k - H_k\hat{x}_{k-1}) \quad 5\text{-}21$$

In the above equation, all matrices are known except K_k, which is called the estimator gain matrix.

The $(y_k - H_k\hat{x}_{k-1})$ term is known as the correction term. If either the correction term or the gain matrix becomes zero, then the estimate does not change from time step $(k-1)$ to k.

We need a criterion to determine the gain matrix. Here the criterion is to minimize the sum of the variances of the estimation errors for each time step,

$$\begin{aligned} J_k &= E[(x_{1k} - \hat{x}_2)^2] + \cdots + E[(x_{nk} - \hat{x}_n)^2] \\ &= E\left(\epsilon^2{}_{x1,k} + \cdots + \epsilon^2{}_{xn,k}\right) \\ &= E\left(\epsilon^T{}_{x,k}\epsilon_{x,k}\right) \\ &= E\left[Tr\left(\epsilon^T{}_{x,k}\epsilon_{x,k}\right)\right] \\ &= TrP_k \end{aligned} \quad 5\text{-}22$$

In the above equation, P_k is the estimation error covariance and can be written in a recursive form as

$$\begin{aligned} P_k &= E\left(\epsilon_{x,k}\epsilon^T{}_{x,k}\right) \\ &= E\left\{\left[(I - K_kH_k)\epsilon_{x,k-1} - K_kv_k\right][\ldots]^T\right\} \\ &= (I - K_kH_k)E\left(\epsilon_{x,k-1}\epsilon^T{}_{x,k-1}\right)(I - K_kH_k)^T - K_kE(v_k\epsilon^T{}_{x,k-1})(I - K_kH_k)^T \\ &\quad -(I - K_kH_k)\,E\left(\epsilon_{x,k-1}v^T{}_k\right)K^T{}_k + K_kE(v_kv^T{}_k)K_k{}^T \end{aligned} \quad 5\text{-}23$$

The estimation error at time $(k-1)$ is independent of the measurement noise at time k (i.e., $\epsilon_{x,k-1}$ is independent of v_k) and the probability theory tells us that

$$E(AB) = E(A)E(B) \quad 5\text{-}24$$

If we further suppose that both the measurement noise and estimation error have zero mean, then,

$$E\left(v_k\epsilon^T{}_{x,k-1}\right) = E(v_k)E^T\left(\epsilon_{x,k-1}\right) = 0 \quad 5\text{-}25$$

With the same logic,

$$E\left(\epsilon_{x,k-1}v^T{}_k\right) = E\left(\epsilon_{x,k-1}\right)E^T(v_k) = 0 \quad 5\text{-}26$$

Using Equation 5-13, Equation 5-23 can be written as

$$P_k = (I - K_k H_k) P_{k-1} (I - K_k H_k)^T + K_k R_k K_k{}^T \quad 5\text{-}27$$

where R_k is the covariance of v_k. Equation 5-27 is the recursive formula that gives us the covariance of the least-squares estimation error. It tells us that as the measurement noise covariance (R_k) increases, the uncertainty in the estimate (P_k) also increases. That is exactly what one expects.

The issue of the value of K_k that will make the cost function (J) in Equation 5-22 the minimum is still unaddressed. For this, we need to calculate $\frac{\partial J_k}{\partial K_k}$ and set it equal to zero. Taking into account Equations 5-22 and 5-27 and considering

$$\frac{\partial Tr(ABA^T)}{\partial A} = 2AB$$

From matrix calculus, we have

$$\frac{\partial J_k}{\partial K_k} = \frac{\partial (Tr P_k)}{\partial K_k} = \frac{\partial [Tr\left((I - K_k H_k) P_{k-1} (I - K_k H_k)^T + K_k R_k K_k{}^T\right)]}{\partial K_k}$$

$$= 2(I - K_k H_k) P_{k-1} \left(-H_k{}^T\right) + 2 K_k R_k = 0 \quad 5\text{-}28$$

If we solve the above equation for K_k:

$$K_k R_k = (I - K_k H_k) P_{k-1} H_k{}^T,$$

and therefore

$$K_k \left(R_k + H_k P_{k-1} H_k{}^T\right) = P_{k-1} H_k{}^T$$

and

$$K_k = P_{k-1} H_k{}^T (H_k P_{k-1} H_k{}^T + R_k)^{-1} \quad 5\text{-}29$$

Table 5-1: Measurement update equations. shows the basic recursive least squares estimation equations, which form the measurement update equations of the Kalman filter.

Table 5-1: Measurement update equations.

$\hat{x}_k = \hat{x}_{k-1} + K_k \left(y_k - H_k \hat{x}_{k-1}\right)$	5-21
$P_k = \left(I - K_k H_k\right) P_{k-1} \left(I - K_k H_k\right)^T + K_k R_k K_k{}^T$	5-27
$K_k = P_{k-1} H_k{}^T (H_k P_{k-1} H_k{}^T + R_k)^{-1}$	5-29

Table 5-2: Components of the full tensor gradiometry matrix and their mathematical meaning.

$\hat{x}_k$	State estimate	Output
K_k	Gain matrix (in some sources it is called blending factor)	Intermediary variables
y_k	Actual measurement	Input
H_k	Measurement matrix (relates the state to the measurement)	Constant
P_k	Estimation error covariance	Output
R_k	Measurement error covariance	Input

The steps for the recursive least-squares estimator are summarized in Simon's book (2006) as:

1. Initializing the estimator, the best values for the estimation, and its corresponding covariance,

   $\hat{x}_0 = E(x)$

   $P_0 = E[(x - \hat{x}_0)(x - \hat{x}_0)^T]$ 5-30

   If the values of x are not known before measurements are taken, then we set $P_0 = \infty$, and if x is perfectly known, then $P_0 = 0$;
2. For $k = 1, 2, ...,$ repeat the following in a loop
   (a) Obtain the measurement y_k, and
   (b) Update the estimate of x and estimate the error covariance P (using equations in Table 5-1).

Alternative forms of the estimator

In scientific literature, the equations of the Kalman filter are given in different forms. These alternative forms are mathematically identical, but some of them are more practical from a computational point of view. If we start with Equation 5-27 and substitute K_k from Equation 5-29 we obtain

$$P_k = (I - K_k H_k) P_{k-1} (I - K_k H_k)^T + K_k R_k {K_k}^T$$
$$= \left[I - P_{k-1} {H_k}^T {S_k}^{-1} H_k\right] P_{k-1} [...]^T + K_k R_k {K_k}^T \quad 5\text{-}31$$

In the above equation a new variable S_k is introduced which is defined as

$$S_k = \left(H_k P_{k-1} {H_k}^T + R_k\right) \quad 5\text{-}32$$

If we again substitute K_k from 5-29 in 5-31, using the following rule of matrix computations

$(ABC \dots MN)^T = N^T M^T \dots C^T B^T A^T$,

then,

$$P_k = P_{k-1} - P_{k-1}{H_k}^T {S_k}^{-1} H_k P_{k-1} - P_{k-1}{H_k}^T {S_k}^{-1} H_k P_{k-1} +$$
$$P_{k-1}{H_k}^T {S_k}^{-1} H_k P_{k-1}{H_k}^T {S_k}^{-1} H_k P_{k-1} + P_{k-1}{H_k}^T {S_k}^{-1} R_k {S_k}^{-1} H_k P_{k-1}$$
$$= P_{k-1} - 2 P_{k-1}{H_k}^T {S_k}^{-1} H_k P_{k-1} + P_{k-1}{H_k}^T {S_k}^{-1} (H_k P_{k-1}{H_k}^T + R_k) {S_k}^{-1} H_k{}^T P_{k-1}$$
$$= P_{k-1} - 2 P_{k-1}{H_k}^T {S_k}^{-1} H_k P_{k-1} + P_{k-1}{H_k}^T {S_k}^{-1} S_k {S_k}^{-1} H_k{}^T P_{k-1}$$
$$= P_{k-1} - 2 P_{k-1}{H_k}^T {S_k}^{-1} H_k P_{k-1} + P_{k-1}{H_k}^T {S_k}^{-1} H_k{}^T P_{k-1}$$
$$= P_{k-1} - P_{k-1}{H_k}^T {S_k}^{-1} H_k P_{k-1} \qquad 5\text{-}33$$

If we review equations 5-29 and 5-32 that calculate K_k and S_k, respectively, P_k can be rewritten as

$$P_k = P_{k-1} - P_{k-1}{H_k}^T \left(H_k P_{k-1}{H_k}^T + R_k\right)^{-1} H_k P_{k-1}$$
$$= P_{k-1} - K_k H_k P_{k-1}$$
$$= (I - K_k H_k) P_{k-1} \qquad 5\text{-}34$$

Equation 5-34 has a simpler form compared with Equation 5-27 but on the other hand it has a numerical problem. Sometimes, it gives a negative value for P_k which is not realistic.

If we start with Equation 5-34 again and take the inverse of the both sides of the equation, we can write

$$P_k = P_{k-1} - P_{k-1}{H_k}^T \left(H_k P_{k-1}{H_k}^T + R_k\right)^{-1} H_k P_{k-1}$$
$${P_k}^{-1} = [P_{k-1} - P_{k-1}{H_k}^T \left(H_k P_{k-1}{H_k}^T + R_k\right)^{-1} H_k P_{k-1}]^{-1} \qquad 5\text{-}35$$

Considering the following matrix inversion lemma

$$(A - BD^{-1}C)^{-1} = A^{-1} + A^{-1}B\,(D - CA^{-1}B)^{-1}CA^{-1} \ , \qquad 5\text{-}36$$

Equation 5-35 can be written as

$${P_k}^{-1} = {P_{k-1}}^{-1}$$
$$+{P_{k-1}}^{-1} P_{k-1}{H_k}^T (H_k P_{k-1}{H_k}^T + R_k - H_k P_{k-1}{P_{k-1}}^{-1} P_{k-1}{H_k}^T)^{-1} H_k P_{k-1}{P_{k-1}}^{-1}$$

$$P_k^{-1} = P_{k-1}^{-1} + H_k^T R_k^{-1} H_k \quad 5\text{-}37$$

So P_k can be calculated as

$$P_k = (P_{k-1}^{-1} + H_k^T R_k^{-1} H_k)^{-1} \quad 5\text{-}38$$

This form seems more complicated since three matrix inversions are needed to calculate it but has a computational advantage. It is never negative.

To get an alternative form of the gain matrix we start from Equation 5-29

$$K_k = P_{k-1} H_k^T (H_k P_{k-1} H_k^T + R_k)^{-1}$$

Multiplying both sides of the equation by $P_k P_k^{-1}$ which is equal to identity matrix gives us

$$P_k P_k^{-1} K_k = P_k P_k^{-1} P_{k-1} H_k^T (H_k P_{k-1} H_k^T + R_k)^{-1} \quad 5\text{-}39$$

Substituting P_k^{-1} from Equation 5-37 leads to

$$\begin{aligned} K_k &= P_k (P_{k-1}^{-1} + H_k^T R_k^{-1} H_k) P_{k-1} H_k^T (H_k P_{k-1} H_k^T + R_k)^{-1} \\ &= P_k (H_k^T + H_k^T R_k^{-1} H_k P_{k-1} H_k^T)(H_k P_{k-1} H_k^T + R_k)^{-1} \\ &= P_k H_k^T (I + R_k^{-1} H_k P_{k-1} H_k^T)(H_k P_{k-1} H_k^T + R_k)^{-1} \end{aligned} \quad 5\text{-}40$$

Multiplying the right hand side of the equation by another identity matrix ($R_k R_k^{-1}$)

$$\begin{aligned} K_k &= P_k H_k^T R_k^{-1} (R_k + H_k P_{k-1} H_k^T)(H_k P_{k-1} H_k^T + R_k)^{-1} \\ &= P_k H_k^T R_k^{-1} \end{aligned} \quad 5\text{-}41$$

In Table 5-3 the above recursive form of the least-squares equations are summarized.

Table 5-3: Different forms of measurement update equations.

$K_k = P_{k-1} H_k^T (H_k P_{k-1} H_k^T + R_k)^{-1}$	5-29
$= P_k H_k^T R_k^{-1}$	5-41
$\hat{x}_k = \hat{x}_{k-1} + K_k \left(y_k - H_k \hat{x}_{k-1}\right)$	5-21
$P_k = \left(I - K_k H_k\right) P_{k-1} \left(I - K_k H_k\right)^T + K_k R_k K_k^T$	5-27
$= (P_{k-1}^{-1} + H_k^T R_k^{-1} H_k)^{-1}$	5-38
$= (I - K_k H_k) P_{k-1}$	5-34

Now, going back to the simple example of estimating a constant value from a set of measurements, and using the equations in Table 5-3, one can write

$$K_k = P_{k-1}{H_k}^T(H_k P_{k-1}{H_k}^T + R_k)^{-1}$$

In this case, $H_k = 1$ and we suppose that R is a constant, i.e., all measurements have the same covariance. So

$$K_1 = P_0(P_0 + R)^{-1}$$

$$\hat{x}_k = \hat{x}_{k-1} + K_k(y_k - H_k\hat{x}_{k-1})$$

$$\hat{x}_1 = \hat{x}_0 + \frac{P_0}{P_0 + R}(y_1 - \hat{x}_0)$$

$$P_k = (I - K_k H_k)P_{k-1}(I - K_k H_k)^T + K_k R_k {K_k}^T$$

$$P_1 = \frac{P_0 R}{P_0 + R} \qquad \text{5-42}$$

Then for the best estimate of x and the related covariance, one can write the equation for $k = 2$ and obtain

$$K_2 = \frac{P_1}{P_1 + R} = \frac{P_0}{2P_0 + R}$$

$$P_2 = \frac{P_1 R}{P_1 + R} = \frac{P_0 R}{2P_0 + R}$$

$$\hat{x}_2 = \hat{x}_1 + \frac{P_1}{P_1 + R}(y_2 - \hat{x}_1)$$

$$= \frac{P_0 + R}{2P_0 + R}\hat{x}_1 + \frac{P_0}{2P_0 + R} \qquad \text{5-43}$$

Considering equations 5-42 and 5-43, we can write a general expression for calculating the estimate ($\hat{x}$), the estimation error covariance (P_k), and the gain matrix (K_k) as

$$P_{k-1} = \frac{P_0 R}{(k-1)P_0 + R}$$

$$K_k = \frac{P_0}{kP_0 + R}$$

$$\hat{x}_k = \hat{x}_{k-1} + K_k(y_k - \hat{x}_{k-1})$$

$$= (1 - K_k)\hat{x}_{k-1} + K_k y_k$$

$$= \frac{(k-1)P_0 + R}{kP_0 + R}\hat{x}_{k-1} + \frac{P_0}{kP_0 + R}y_k \qquad \text{5-44}$$

The above equations show that when x is perfectly known before any measurements are obtained, i.e. when $P_0 = 0$, then $K_k = 0$ and $\hat{x}_k = \hat{x}_0$. It means that the optimal estimate of x is known, constant, and completely independent of the measurements. It is the case when we are completely sure about our first estimation and clearly we do not need the measurements to calculate the best estimation of the variable. On the other hand, in the case when x is completely unknown before the measurements, $P_0 \to \infty$, and the best estimate of the variable would be:

$$\begin{aligned}\hat{x}_k &= \frac{(k-1)P_0}{kP_0}\,\hat{x}_{k-1} + \frac{P_0}{kP_0}y_k \\ &= \frac{(k-1)}{k}\,\hat{x}_{k-1} + \frac{1}{k}y_k \\ &= \tfrac{1}{k}\,[(k-1)\,\hat{x}_{k-1} + y_k]\end{aligned} \qquad 5\text{-}45$$

But what will be the best estimate of a state when the state is completely unknown? Intuitively, we know that it should be the average of the measurements. If we rewrite the average of the measurements in an iterative form as

$$\begin{aligned}\bar{y}_k &= \frac{1}{k}\sum_{j=1}^{k} y_j \\ &= \frac{1}{k}\left(\sum_{j=1}^{k-1} y_j + y_k\right) \\ &= \frac{1}{k}\left[(k-1)\left(\frac{1}{k-1}\sum_{j=1}^{k-1} y_j\right) + y_k\right] \\ &= \tfrac{1}{\mathrm{k}}[(\mathrm{k}-1)\bar{\mathrm{y}}_{\mathrm{k}-1} + \mathrm{y}_{\mathrm{k}}]\end{aligned} \qquad 5\text{-}46$$

Comparing equations 5-45 and 5-46 one can see that the optimal estimate of a state, when the estimate is completely unknown, is the average of the measurements.

Examples illustrating how the measurement update equations make an estimation

Below are two examples that show how the linear recursive estimator works. The first example is about a system that has one measurement set (y) and one variable to be

estimated (x) (the same as Example 1 at the beginning of the chapter). The second example considers a system that has again one measurement set but the state consists of two variables$(x_1 \; and \; x_2)$.

Suppose we have a data set collected with a voltmeter having the accuracy R and the true voltage of the system is known accurately. The example illustrates how a linear recursive estimator can yield the desirable result. The matrices needed for this example are

$$H = 1$$
$$P_0 = 1$$
$$x_0 = 15 \qquad \text{5-47}$$

$P_0 = 1$ implies that we are not sure about the initial estimate $x_0 = 15$. Figure 5-1 illustrates that the estimates will converge to the true value of 12 (in this case, within 10 iterations), and the estimation error variance (P_k) approaches zero whose low value assures us that the estimates are trustable.

On the other hand, if we trust the initial estimate of 15 more than before by supplying a smaller estimation variance of $P_0 = 0.2$, then the linear recursive estimator cannot reach the true voltage in ten time steps. Figure 5-2 shows that 80 iterations are needed to approach the true value in this case.

In the case of more precise measurements, *R*, the measurement error, is smaller and clearly it means that we believe we should trust our measurements more and our estimates need to be closer to our measurements. As Figure 5-3 shows, even though our first estimate ($x_0 = 15$) is not close to the true value (12), since the measurement error is smaller than the previous examples (R= 0.1 instead of 1), the second estimation can get very close to the true value of 12. Both the estimation and the corresponding variance illustrate this point (i.e., variance of the estimation gets close to 0.1 as soon as the second estimation was made).

If we incorrectly specify that our measurements are 100% correct and no noise is present (i.e. R=0), it is expected that the later estimations will be the same as the first measurement (z_1), regardless of the number of iterations. This occurs even if future

measurements may be more precise, and the equations from Table 5-3 rewritten for this case show why:

$$\text{If } R = 0, \begin{cases} K_1 = P_0 {H_1}^T \left(H_1 P_0 {H_1}^T + R_1\right)^{-1} = P_0^2 = 1 \\ P_1 = (1 - K_1 H_1) P_0 (1 - K_1 H_1)^T + K_1 R_1 {K_1}^T = 0 \\ \hat{x}_1 = \hat{x}_0 + K_1 (y_1 - H_1 \hat{x}_0) = y_1 \end{cases}$$

$$\begin{cases} K_2 = P_1 {H_2}^T \left(H_2 P_1 {H_2}^T + R_2\right)^{-1} = NAN \\ P_2 = (1 - K_2 H_2) P_1 (1 - K_2 H_2)^T + K_2 R_2 {K_2}^T = NAN \\ \hat{x}_2 = \hat{x}_1 + K_2 (y_2 - H_2 \hat{x}_1) = NAN \end{cases} \quad \text{5-48}$$

a

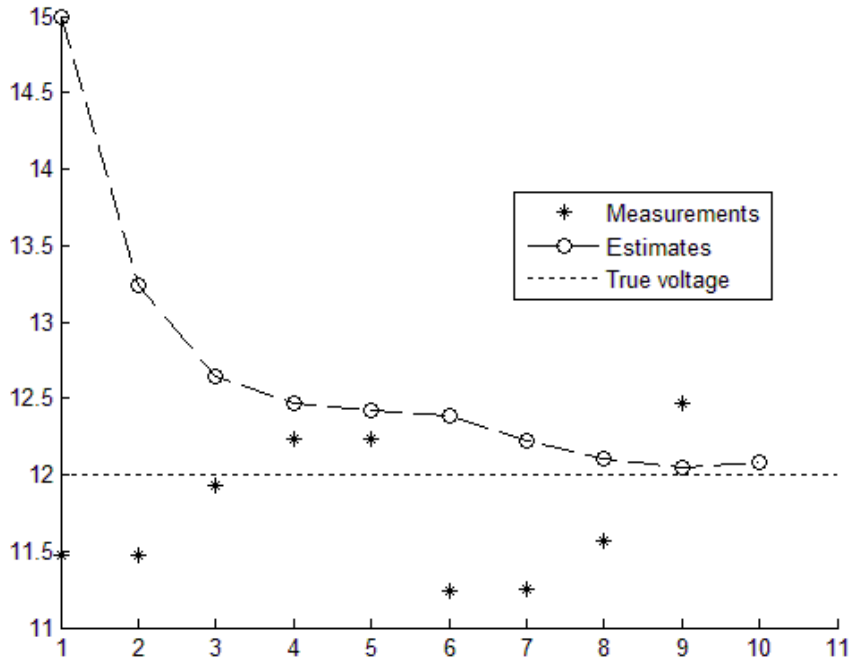

b

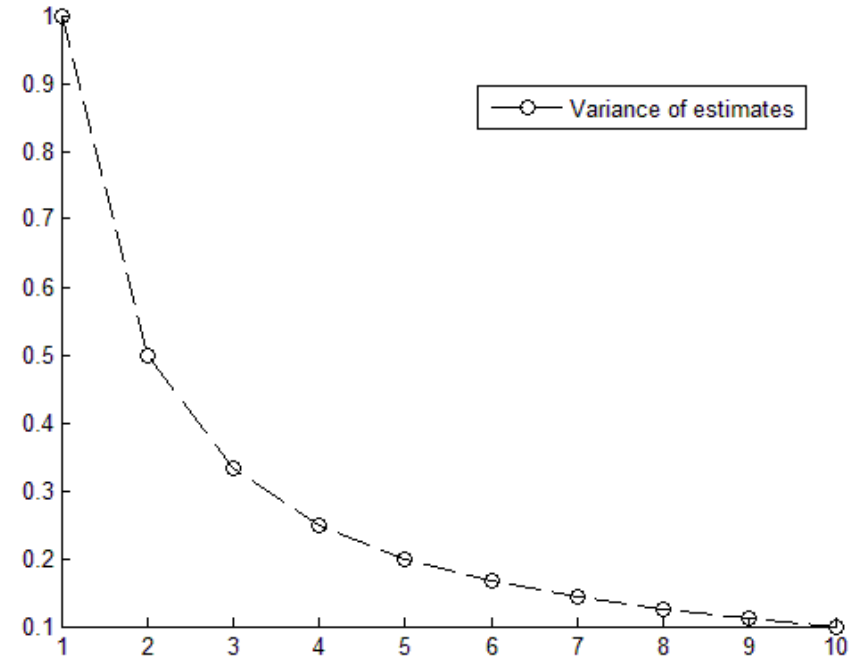

Figure 5-1: Importance of measurement error and initial estimate covariance; the first simulation: Measurement error R = 1 and the uncertainty in the initial estimate covariance P_0 =1. (a) State estimates and (b) the corresponding estimation variance.

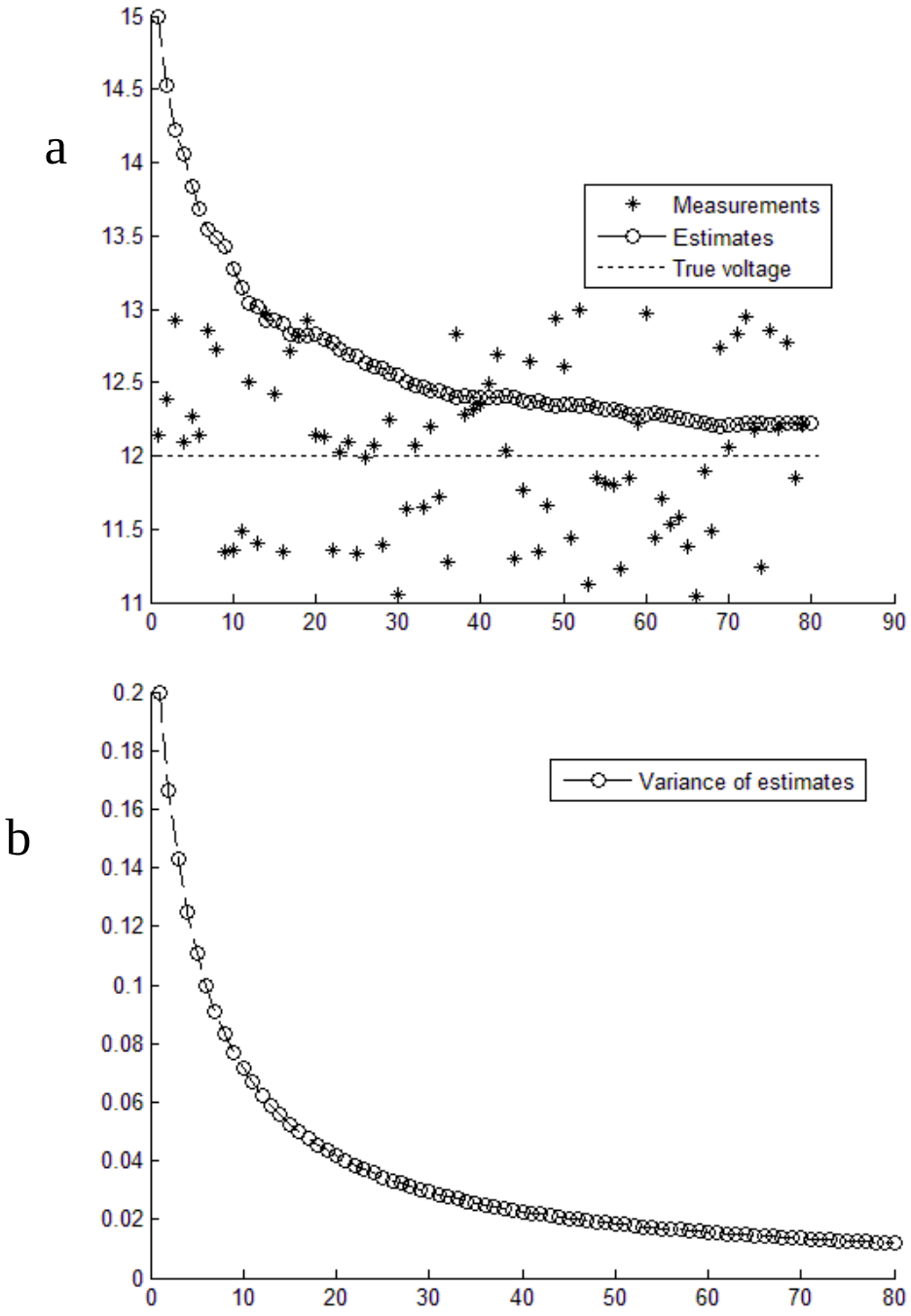

Figure 5-2: Importance of measurement error and initial estimate covariance; The second simulation: Measurement error R = 1 and the uncertainty in the initial estimate covariance P_0 =2. (a) State estimates and (b) the corresponding estimation variance for the second simulation. 80 estimations were made to reach the target.

a

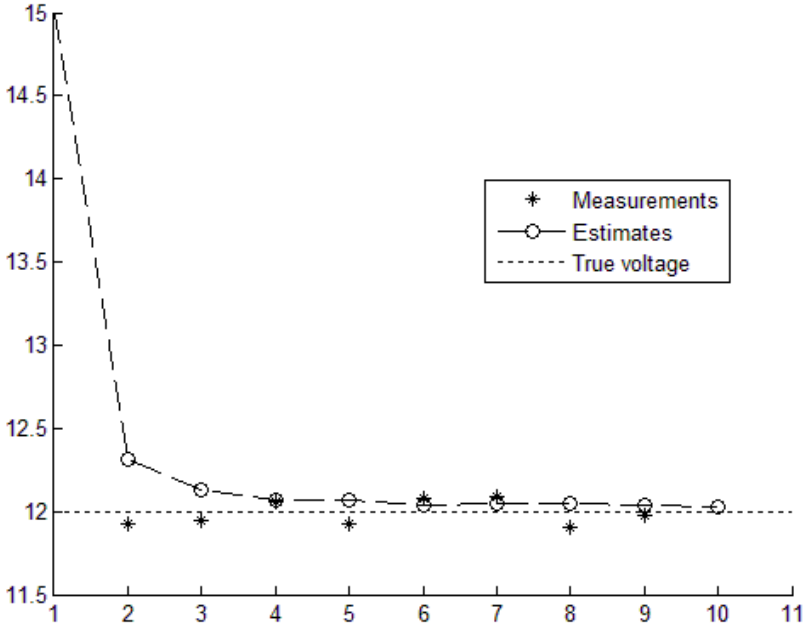

b

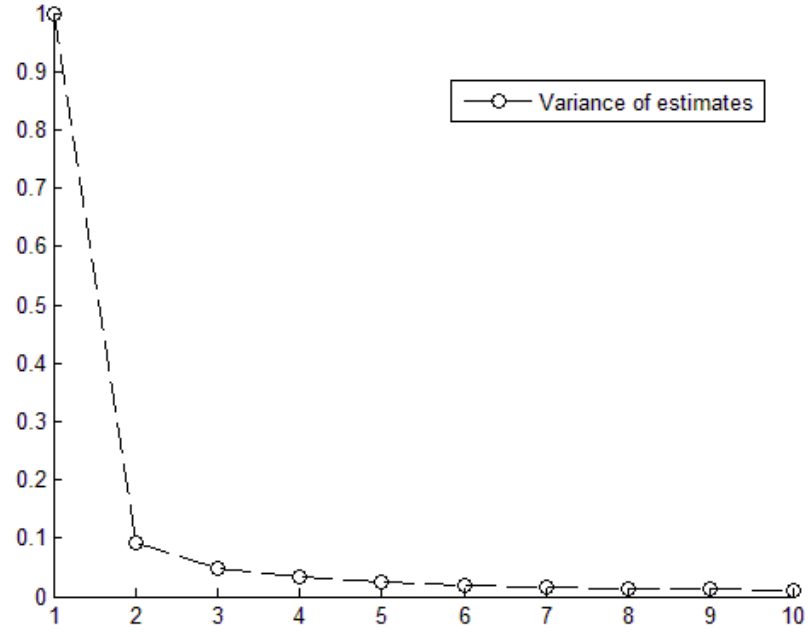

Figure 5-3: Importance of measurement error and initial estimate covariance; the Third simulation: measurement error R is considered 0.1 (see the reduced spread of measurements around the true value of 12) and the initial estimation error variance P_0 =1. In this case, the filter responds to measurements quickly, increasing the estimate variance so it was very "quick" to believe the noisy measurements. (a) State estimates and (b) the corresponding estimation variance.

As for this case, $P_1 = 0$ and $K_1 = 1$, both K_2 and P_2 are undefined and the second iteration breaks down.

On the other hand, if one assumes that x is perfectly known before measurements, then $P_0 = 0$, which upon substitutions into equations in Table 5-3 yields,

$$\begin{cases} K_1 = P_0 {H_1}^T \left(H_1 P_0 {H_1}^T + R_1\right)^{-1} = 0 \\ P_1 = (1 - K_1 H_1) P_0 (1 - K_1 H_1)^T + K_1 R_1 {K_1}^T = 0 \\ \hat{x}_1 = \hat{x}_0 + K_1 (y_1 - H_1 \hat{x}_0) = \hat{x}_0 = x_0 \end{cases}$$

$$K_1 = K_2 = \ldots = K_n = 0$$

$$P_1 = P_2 = \ldots = P_n = 0$$

$$\hat{x}_1 = \hat{x}_2 = \ldots = \hat{x}_n = x_0$$

Below I give an example taken from Simon's book, "Optimal State Estimation", that is very useful for illustrating how the linear recursive estimator works. I, however, used different models to illustrate how parameters (initial estimation error and measurement error) can affect the behavior of the system.

In this example the instrument can detect the concentration of two mixed chemicals but it cannot distinguish between two or measure them separately. However, we are interested in the concentration of each chemical individually. Suppose in our system chemical 1 is constant but the system has a leakage so that chemical 2 is decreased by 1% from one measurement time to the next time step. So the measurement equation can be written as

$$y_k = x_1 + 0.99^{k-1} x_2 + v_k \qquad 5\text{-}49$$

In this equation v_k is the measurement noise, which is a random variable with zero-mean and variance *R*.

And *H*, is a (1×2) measurement matrix:

$$[1 \qquad 0.99^k] \qquad 5\text{-}50$$

From Table 5-3, the states of the system are x_1 and x_2 in this example and the corresponding covariances are P_1 and P_2. Supposing that the initial estimates of the states are 8 and 6, respectively, the initial state matrix can be written as

$$x_0 = \begin{bmatrix} 8 \\ 6 \end{bmatrix} \quad \text{5-51}$$

P, which is the estimation covariance matrix, is a (2×2) matrix and the elements on its diagonal are the ones that are used in determining the state variances. As we do not have confidence in our initial estimate, the initial estimation error variance matrix has the form

$$P_0 = \begin{bmatrix} 1 & 0 \\ 0 & 1 \end{bmatrix} \quad \text{5-52}$$

In this example, we will use a random function to create measurements, so for each separate run, we will have different measurements but what matters is that we expect the linear recursive estimator to show a certain behavior. We expect the variances of the estimations to approach zero after a couple dozen time steps, and estimations approaching their true values. The following figures illustrate the parameter estimates and the corresponding variances for different simulations.

In all examples, the estimates approach their true values after several iterations and the corresponding variances decrease to zero rapidly, assuring us that the estimates must be reaching their true values.

If we have more confidence in our initial estimate, we can start with a smaller value of P.

$$P_0 = \begin{bmatrix} 0.1 & 0 \\ 0 & 0.1 \end{bmatrix} \quad \text{5-53}$$

Figure 5-5 illustrates that when we have more confidence in our initial estimate, the results will be smoother. Eventually, we will come to the same result but the number of time steps that we need to estimate to get the same result becomes larger. In the case where we use the smaller initial estimation covariance, at time step 2, we would reach 0.1 for the estimation error (Figure 5-5) whereas for the case of lesser confidence in our initial estimate, this value cannot be reached in first 40 time steps (Figure 5-4).

We should notice here the role of the measurement error (R) and how it can affect the result. Large R means that we cannot trust measurements very much and we should rely on the previous estimation more (Table 5-3). Mathematically, high value of R results in a smaller gain value (K_k)

$$\mathrm{K_k = P_{k\text{-}1} H_k^{\,T} (H_k P_{k\text{-}1} H_k^{\,T} + R_k)^{\text{-}1}} \quad \text{5-29}$$

So the next estimate is calculated as

$$\hat{x}_k = \hat{x}_{k-1} + K_k\left(y_k - H_k\hat{x}_{k-1}\right) \quad 5\text{-}21$$

$$\hat{x}_k = \hat{x}_{k-1}(1 - KH_k) + K_k\, y_k \quad 5\text{-}54$$

Thus, the smaller gain value results in lesser weight to the measurement and, consequently, relatively more weight will be placed in the prior estimates.

If the initial estimation error covariance (P_0) is defined as the identity matrix, and supposing a larger measurement error, ($R = 10$), the resultant estimation and the related covariance results in Figure 5-6. The figure shows that, noisy data set results in estimations that have small degree of confidence. Even after 50 time steps, *P* (estimation error covariance) of 0.2 cannot be reached. As one may instinctively conclude, for noisy data set, more measurements are needed to obtain a considerable level of confidence.

a)

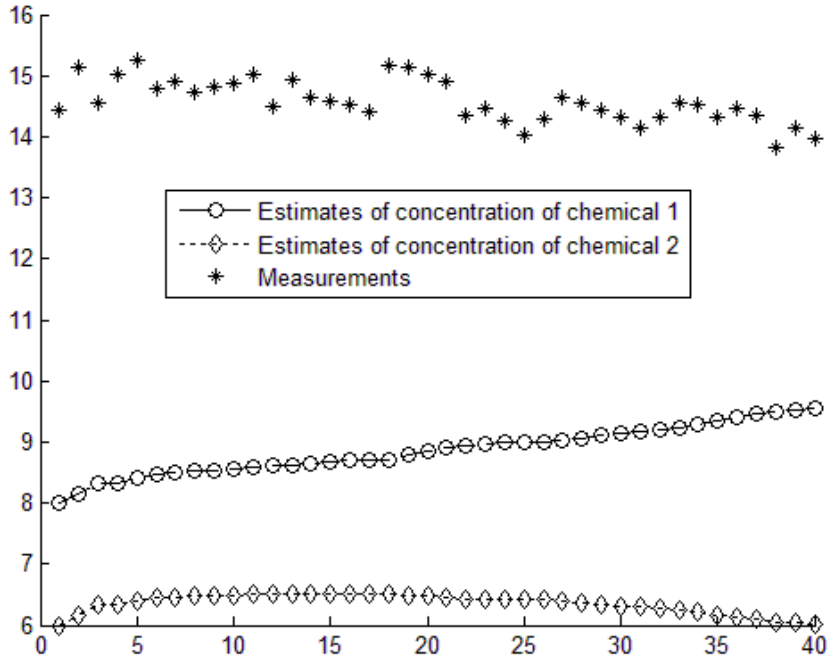

b)

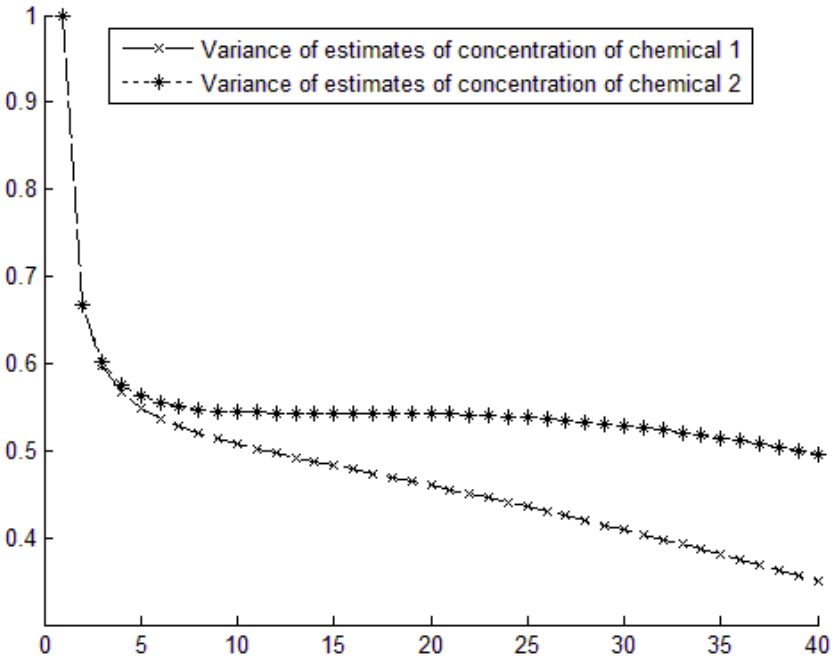

Figure 5-4: Simon's (2006) example 3.5: First simulation; modified for $R = 1$ *and* $p = \begin{bmatrix} 1 & 0 \\ 0 & 1 \end{bmatrix}$ *(a) State estimates and (b) the corresponding variances.*

a)

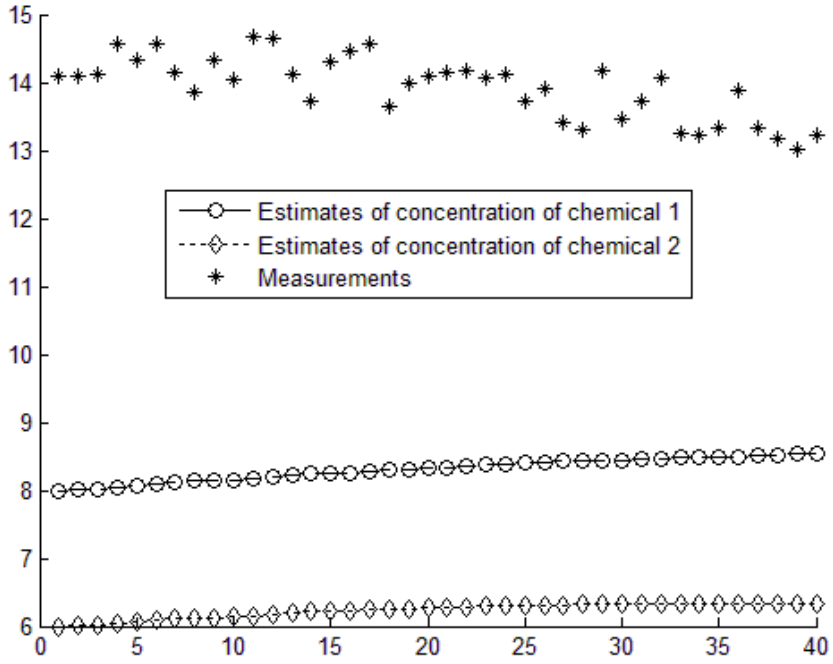

b)

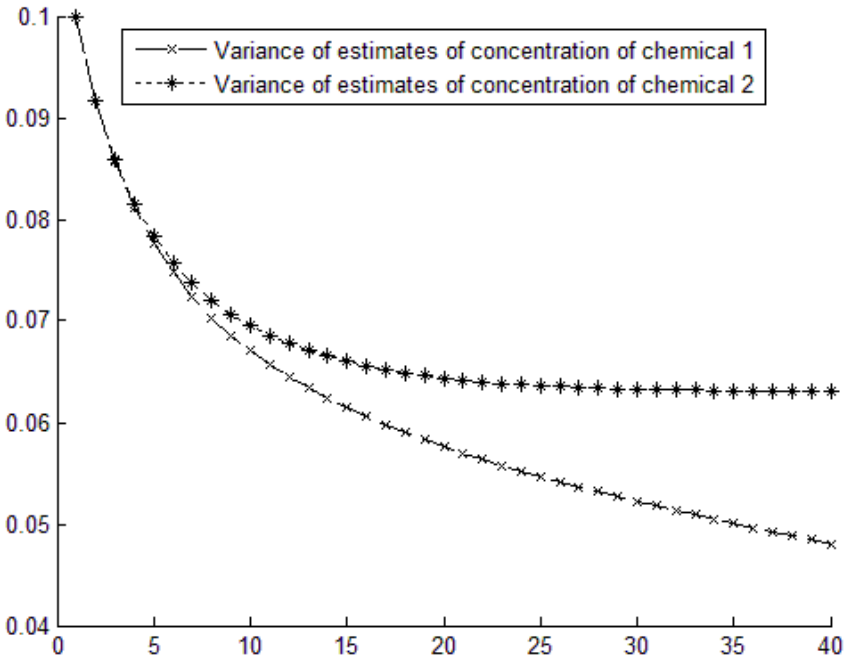

Figure 5-5: Simon's (2006) example 3.5: Second simulation; the same example when $R = 1$ *and* $p = \begin{bmatrix} 0.1 & 0 \\ 0 & 0.1 \end{bmatrix}$. *(a) State estimates and (b) the corresponding variances.*

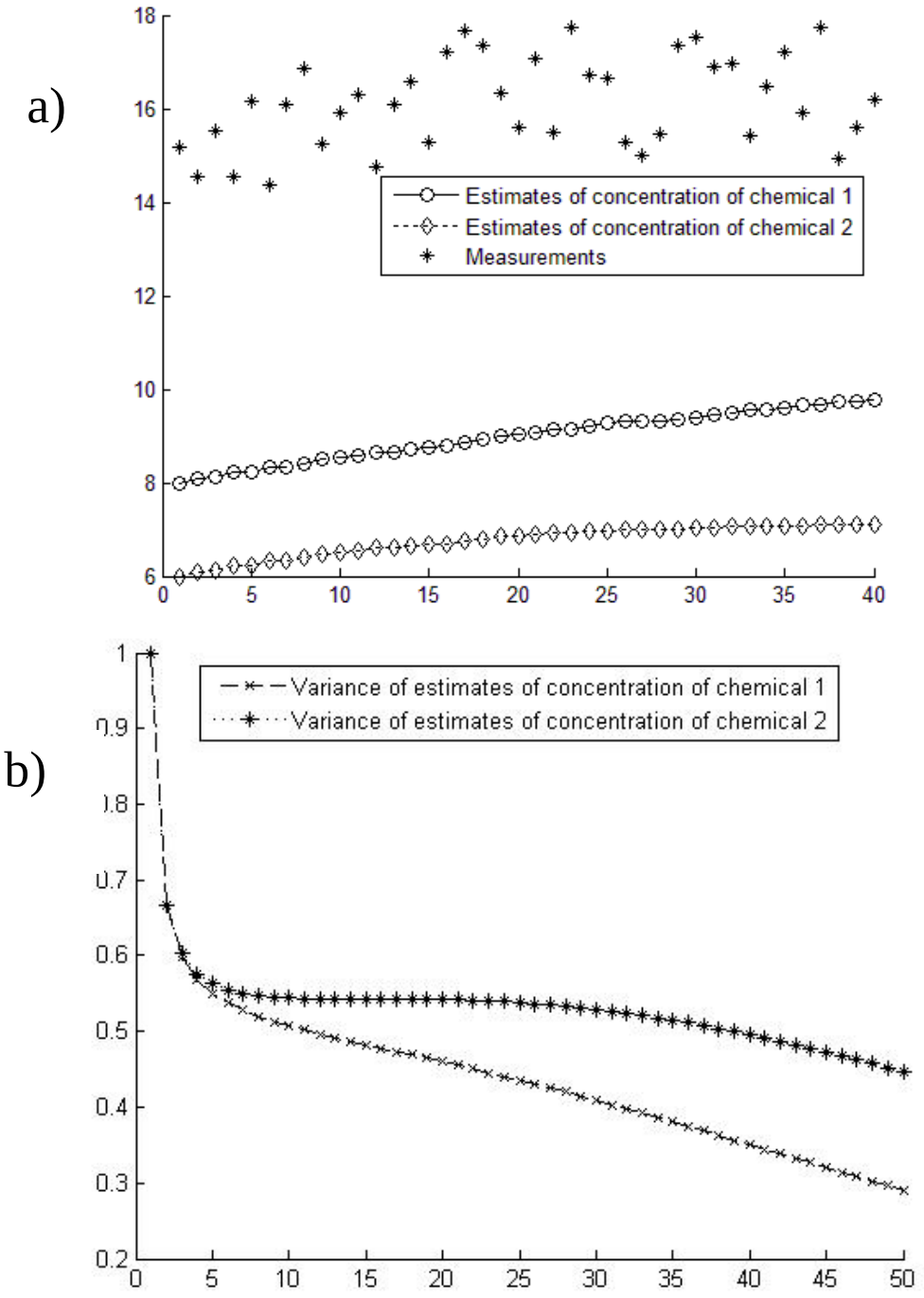

Figure 5-6: Simon's (2006) example 3.5: Third simulation; R =10 and $p = \begin{bmatrix} 1 & 0 \\ 0 & 1 \end{bmatrix}$. *The filter responds to measurements quickly, increasing the estimate variance so it was very "quick" to believe the noisy measurements. (a) State estimates and (b) the corresponding variances.*

The time update

Chapter 4 discussed how the Kalman filter equations can be categorized in two groups as measurement update equations and time update equations. The measurement update equations are responsible for feedback in such a way that they incorporate a new measurement into the *a priori* estimate and the result is the *a posteriori* estimate. They act as the corrector equations while time update equations function as the predictor equations. Time update equations project the current state and error covariance forward in time to calculate the *a priori* estimate that will be the input to the measurement update subsequently (Welch and Bishop, 2006).

In this section, I illustrate the examples of the time update equations used in the Kalman filter and the criteria that control their stability.

Supposing we can define our discrete-time system by a linear equation as

$$x_k = F_{k-1}x_{k-1} + G_{k-1}u_{k-1} + \omega_{k-1} \qquad 5\text{-}55$$

where F is a matrix that relates the current estimation to the previous one (called the state transition matrix), u_k is a known control vector, G is a control matrix defining linear equations for any control factors, and w_k is Gaussian zero-mean white noise with covariance Q_k. The expected value of both sides of the equation is written as

$$\bar{x}_k = F_{k-1}\bar{x}_{k-1} + G_{k-1}u_{k-1} \qquad 5\text{-}56$$

To calculate the change in the covariance of the state (x_k) with time, using Equations 5-55 and 5.56, we can write

$$\begin{aligned}(x-\bar{x}_k)(x-\bar{x}_k)^T &= (F_{k-1}x_{k-1} + G_{k-1}u_{k-1} + \omega_{k-1} - \bar{x}_k)(\dots)^T \\ &= [F_{k-1}(x_{k-1}-\bar{x}_{k-1}) + \omega_{k-1}][F_{k-1}(x_{k-1}-\bar{x}_{k-1}) + \omega_{k-1}]^T \\ &= F_{k-1}(x_{k-1}-\bar{x}_{k-1})(x_{k-1}-\bar{x}_{k-1})^T {F^T}_{k-1} + \omega_{k-1}{\omega^T}_{k-1} + \\ &\quad F_{k-1}(x_{k-1}-\bar{x}_{k-1})\,{\omega^T}_{k-1} + \omega_{k-1}(x_{k-1}-\bar{x}_{k-1})^T {F^T}_{k-1}\end{aligned} \qquad 5\text{-}57$$

Therefore, the covariance of x_k is calculated as

$$\begin{aligned}P_k &= E[(x-\bar{x}_k)(x-\bar{x}_k)^T] \\ &= E[F_{k-1}(x_{k-1}-\bar{x}_{k-1})(x_{k-1}-\bar{x}_{k-1})^T {F^T}_{k-1} + \omega_{k-1}{\omega^T}_{k-1} +\end{aligned}$$

$$F_{k-1}(x_{k-1} - \bar{x}_{k-1})\omega^T{}_{k-1} + \omega_{k-1}(x_{k-1} - \bar{x}_{k-1})^T F^T{}_{k-1}] \quad 5\text{-}58$$

Considering that $(x_{k-1} - \bar{x}_{k-1})$ and ω_{k-1} are uncorrelated, the last two terms in the above equations are zero. So P_k is written as

$$P_k = F_{k-1}\, P_{k-1} F^T{}_{k-1} + Q_{k-1} \quad 5\text{-}59$$

Table 5-4: Time update measurements.

$\bar{x}_k = F_{k-1}\bar{x}_{k-1} + G_{k-1}u_{k-1}$ 5-56
$P_k = F_{k-1}\, P_{k-1} F^T{}_{k-1} + Q_{k-1}$ 5-59

The following worked example from Simon (2006) is useful in illustrating and understanding the process of time update.

Examples illustrating how the time update equations predict an estimation

Suppose we have a system consisting of predator $x(1)$ and its prey $x(2)$, and we want to predict their population as a function of time. We would also like to know the accuracy of our estimation. Further suppose that the system of predator and prey can be described as

$$x_{k+1}(1) = x_k(1) - 0.8\, x_k(1) + 0.4\, x_1(2) + \omega_k(1)$$
$$x_{k+1}(2) = x_k(2) - 0.4\, x_k(1) + u_k + \omega_k(2) \quad 5\text{-}60$$

The first equation relates to the change in the population of predator from one time step to the next one; it shows that the predator population decreases when overcrowding occurs, but the prey population causes the predator population to increase. The second equation explains how the population of prey decreases through time due to predator population and increases due to a controlling parameter (u_k), which in this case can be the external food supply. Both the populations are subjected to environmental factors which disturb them randomly ($\omega_k(1)\ and\ \omega_k(2)$). The above equations can be written in the form of the state-space vectors and matrices as

$$x_{k+1} = \begin{bmatrix} 0.2 & 0.4 \\ -0.4 & 1 \end{bmatrix} x_k + \begin{bmatrix} 0 \\ 1 \end{bmatrix} u_k + \omega_k \qquad 5\text{-}61$$

In this example $F = \begin{bmatrix} 0.2 & 0.4 \\ -0.4 & 1 \end{bmatrix}$ and $G = \begin{bmatrix} 0 \\ 1 \end{bmatrix}$.

We can predict how the mean and covariance of the population (predator and prey) change with time using Equations 5-56 and 5-59. Suppose $u_k = 1$, the initial state is $\bar{x}_0 = \begin{bmatrix} 10 \\ 20 \end{bmatrix}$, $P_0 = \text{diag}\ (40,40)$, and $Q = \begin{bmatrix} 1 & 0 \\ 0 & 2 \end{bmatrix}$. Then the first five time steps can be calculated as follows:

Initiate the filtering process by setting the values of the initial state vector and its covariance

$$x_0 = \begin{bmatrix} 10 \\ 20 \end{bmatrix} \qquad \text{and} \qquad P_0 = \begin{bmatrix} 40 & 0 \\ 0 & 40 \end{bmatrix}.$$

First iteration:

$$x_1 = \begin{bmatrix} 0.2 & 0.4 \\ -0.4 & 1 \end{bmatrix} \begin{bmatrix} 10 \\ 20 \end{bmatrix} + \begin{bmatrix} 0 \\ 1 \end{bmatrix} 1 = \begin{bmatrix} 10 \\ 17 \end{bmatrix}$$

$$P_1 = \begin{bmatrix} 0.2 & 0.4 \\ -0.4 & 1 \end{bmatrix} \begin{bmatrix} 40 & 0 \\ 0 & 40 \end{bmatrix} \begin{bmatrix} 0.2 & 0.4 \\ -0.4 & 1 \end{bmatrix}^T + \begin{bmatrix} 1 & 0 \\ 0 & 2 \end{bmatrix} = \begin{bmatrix} 9 & 12.8 \\ 12.8 & 48.4 \end{bmatrix}$$

Second iteration:

$$x_2 = \begin{bmatrix} 0.2 & 0.4 \\ -0.4 & 1 \end{bmatrix} \begin{bmatrix} 10 \\ 17 \end{bmatrix} + \begin{bmatrix} 0 \\ 1 \end{bmatrix} 1 = \begin{bmatrix} 8.8 \\ 14 \end{bmatrix}$$

$$P_2 = \begin{bmatrix} 0.2 & 0.4 \\ -0.4 & 1 \end{bmatrix} \begin{bmatrix} 9 & 12.8 \\ 12.8 & 48.4 \end{bmatrix} \begin{bmatrix} 0.2 & 0.4 \\ -0.4 & 1 \end{bmatrix}^T + \begin{bmatrix} 1 & 0 \\ 0 & 2 \end{bmatrix} = \begin{bmatrix} 11.15 & 19.15 \\ 19.15 & 41.6 \end{bmatrix}$$

Third iteration:

$$x_3 = \begin{bmatrix} 0.2 & 0.4 \\ -0.4 & 1 \end{bmatrix} \begin{bmatrix} 8.8 \\ 14 \end{bmatrix} + \begin{bmatrix} 0 \\ 1 \end{bmatrix} 1 = \begin{bmatrix} 7.36 \\ 11.48 \end{bmatrix}$$

$$P_3 = \begin{bmatrix} 0.2 & 0.4 \\ -0.4 & 1 \end{bmatrix} \begin{bmatrix} 11.15 & 19.15 \\ 19.15 & 41.6 \end{bmatrix} \begin{bmatrix} 0.2 & 0.4 \\ -0.4 & 1 \end{bmatrix}^T + \begin{bmatrix} 1 & 0 \\ 0 & 2 \end{bmatrix} = \begin{bmatrix} 11.17 & 16.51 \\ 16.51 & 30.06 \end{bmatrix}$$

Fourth iteration:

$$x_4 = \begin{bmatrix} 0.2 & 0.4 \\ -0.4 & 1 \end{bmatrix} \begin{bmatrix} 7.36 \\ 11.48 \end{bmatrix} + \begin{bmatrix} 0 \\ 1 \end{bmatrix} 1 = \begin{bmatrix} 6.04 \\ 9.54 \end{bmatrix}$$

$$P_4 = \begin{bmatrix} 0.2 & 0.4 \\ -0.4 & 1 \end{bmatrix} \begin{bmatrix} 11.17 & 16.51 \\ 16.51 & 30.06 \end{bmatrix} \begin{bmatrix} 0.2 & 0.4 \\ -0.4 & 1 \end{bmatrix}^T + \begin{bmatrix} 1 & 0 \\ 0 & 2 \end{bmatrix} = \begin{bmatrix} 8.9 & 11.79 \\ 11.79 & 20.64 \end{bmatrix}$$

Fifth iteration:

$$x_5 = \begin{bmatrix} 0.2 & 0.4 \\ -0.4 & 1 \end{bmatrix} \begin{bmatrix} 6.04 \\ 9.54 \end{bmatrix} + \begin{bmatrix} 0 \\ 1 \end{bmatrix} 1 = \begin{bmatrix} 5.03 \\ 8.11 \end{bmatrix}$$

$$P_5 = \begin{bmatrix} 0.2 & 0.4 \\ -0.4 & 1 \end{bmatrix} \begin{bmatrix} 8.9 & 11.79 \\ 11.79 & 20.64 \end{bmatrix} \begin{bmatrix} 0.2 & 0.4 \\ -0.4 & 1 \end{bmatrix}^T + \begin{bmatrix} 1 & 0 \\ 0 & 2 \end{bmatrix} = \begin{bmatrix} 6.54 & 8.01 \\ 8.01 & 14.63 \end{bmatrix}$$

Figure 5-7 shows the first 15 time steps and illustrates the propagation of the mean and the covariance of predator and prey populations with time. After a few iterations, *P* reaches a steady-state value indicating convergence.

However, if we suppose that overcrowding does not affect the predator population then the Equations 5-60 can be rewritten as

$$x_{k+1}(1) = x_k(1) + 0.4\, x_1(2) + \omega_k(1)$$
$$x_{k+1}(2) = x_k(2) - 0.4\, x_k(1) + u_k + \omega_k(2) \qquad \text{5-62}$$

Hence, $= \begin{bmatrix} 1 & 0.4 \\ -0.4 & 1 \end{bmatrix}$.

All other parameters are unchanged with respect to the first example.

Unlike the previous case, the mean and the covariance of the estimation are not convergent here.

Whether convergence will occur or not in a particular case can be deduced from the following conditions on the existence of the solution. The theorem states that when the state transition matrix (F) is *stable* and the process error covariance (Q) is positive definite, the estimation error covariance (P) has a "unique positive definite steady-state solution" (Simon, 2006). One of the conditions of this stability is that each of the eigenvalues of matrix *F* be < 1 and their product be $\neq 1$ (Simon, 2006). For the second case discussed above, *F* is not stable and therefore the variances diverge from one step to the next.

A comparison of the transition matrixes and their eigenvalues from the two examples are given below. They show the cause of the difference in the propagation of means and covariances is in the stability criteria given above.

$$F = \begin{bmatrix} 0.2 & 0.4 \\ -0.4 & 1 \end{bmatrix} \longrightarrow \lambda_1(F) = 0.6 \quad \& \quad \lambda_2(F) = 0.6 \qquad \text{5-63}$$

$$F = \begin{bmatrix} 1 & 0.4 \\ -0.4 & 1 \end{bmatrix} \longrightarrow \lambda_1(F) = 1 + 0.4\,i \quad \& \quad \lambda_2(F) = 1 - 0.4\,i$$

Now going back to the voltmeter example discussed in the measurement update part (Chapter 6), a system can be written as

$$\bar{x}_k = \bar{x}_{k-1} \qquad 5\text{-}64$$

Further supposing that our initial estimates are the same as the first assumption

$$P_0 = 1$$

$$x_0 = 15 \qquad 5\text{-}65$$

A slight modification in the magnitude of the one by one F matrix, from 1.25 to even 0.75 can make a divergent problem convergent (Figure 5-9 and 5-10).

Thus, even before computing the covariance, just by calculating the eigenvalues, we can say if there is a unique positive definite steady-state solution for P or not. When $F = 1.25$, its eigenvalue is 1.25 and the system is unstable and the estimation and the corresponding estimation error covariance are not convergent. Whereas when $F = 0.75$, $\lambda(F)=0.75$ and the system is stable. So the mean and covariance tend to a certain value after adequate number of iterations. One of the reasons that makes the Kalman filter practical is that it can solve this problem by its time and measurement update loop.

a)

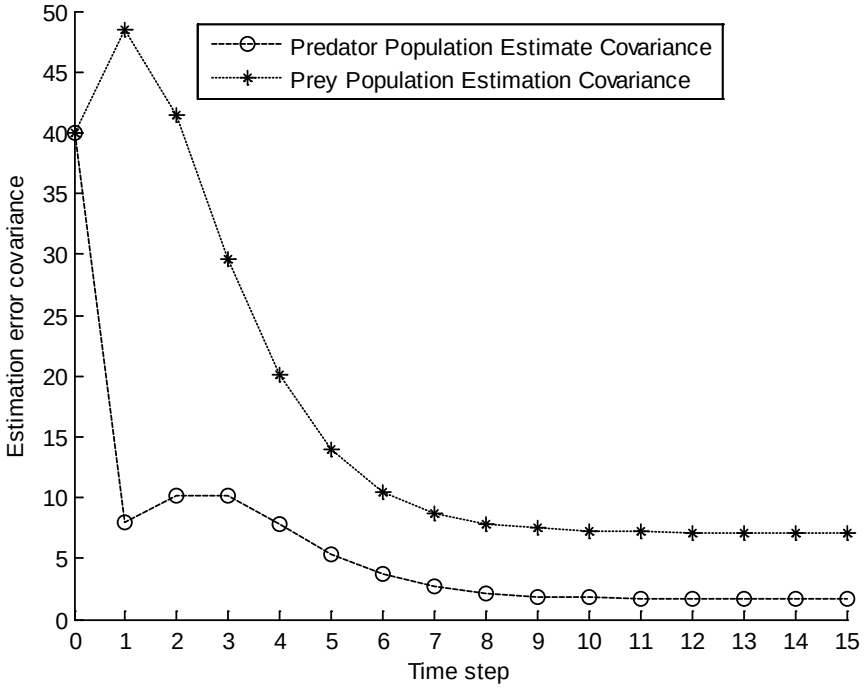

b)

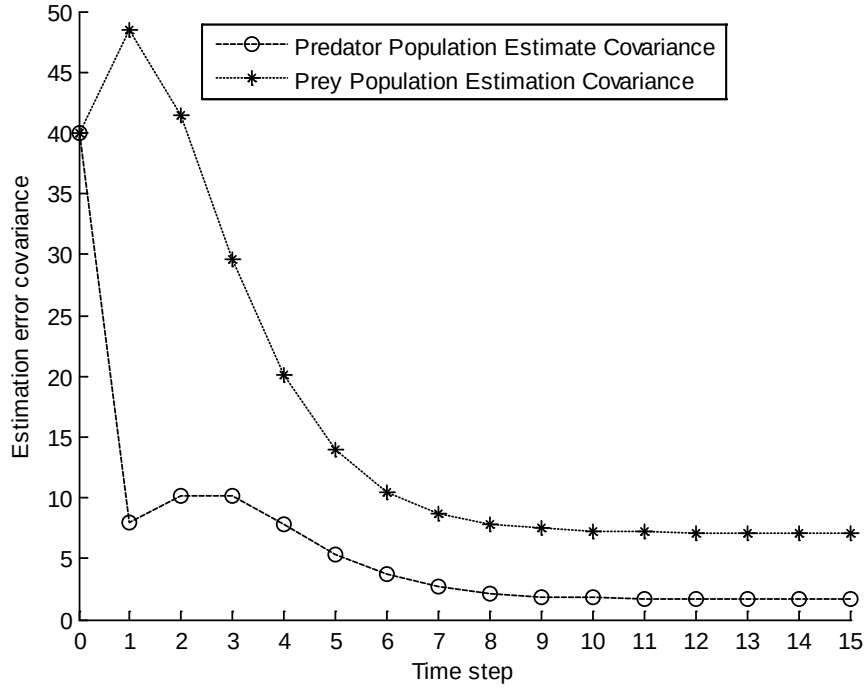

Figure 5-7: (a) The state mean and (b) covariance of the predator and prey population. First simulation of the Simon's (2006) Example 4.1 with the assumption that overcrowding affects the predator population.

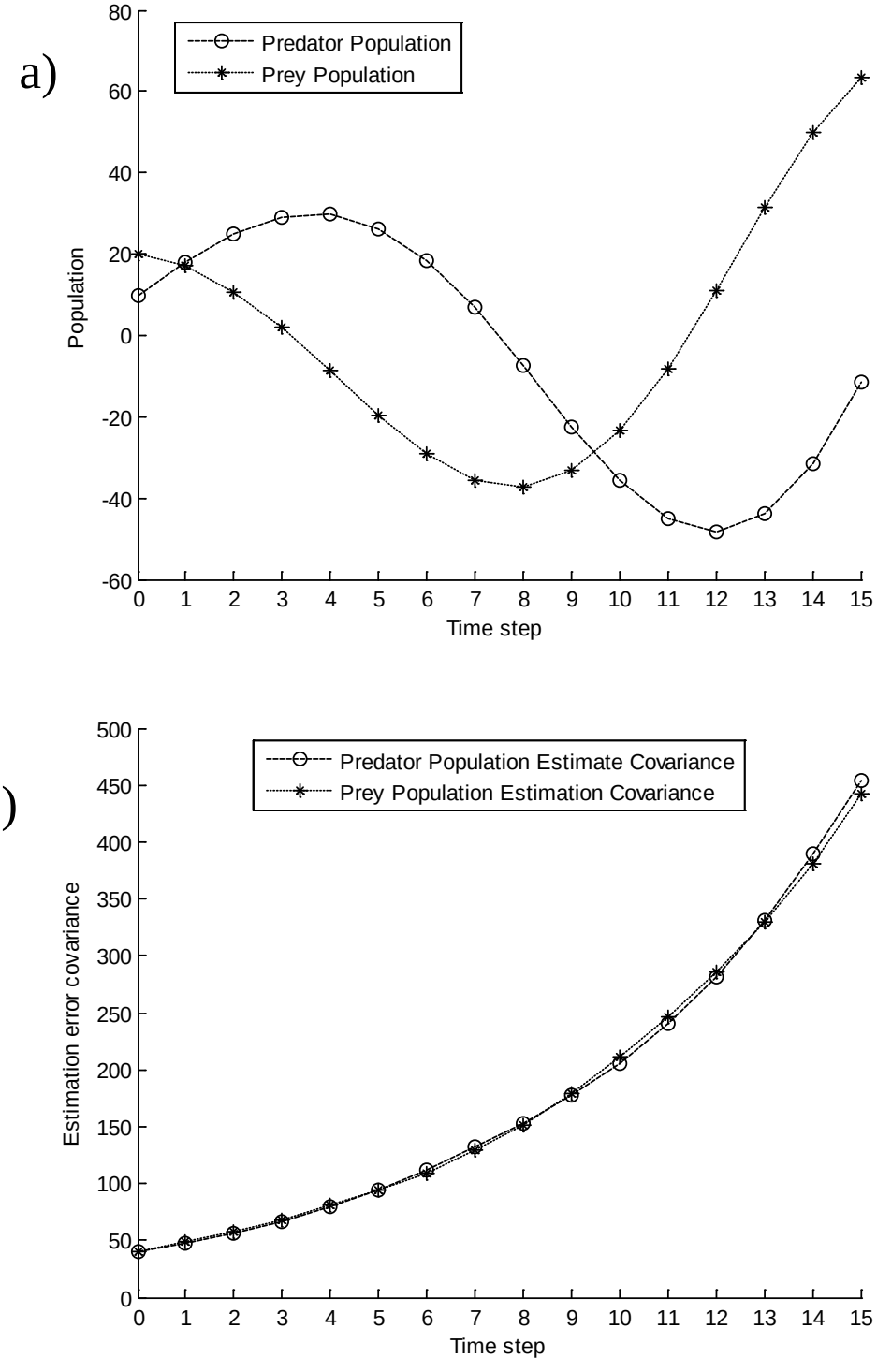

Figure 5-8: (a) State mean and (b) Covariance of the predator and prey population. Second simulation supposing that overcrowding does not affect the predator population.

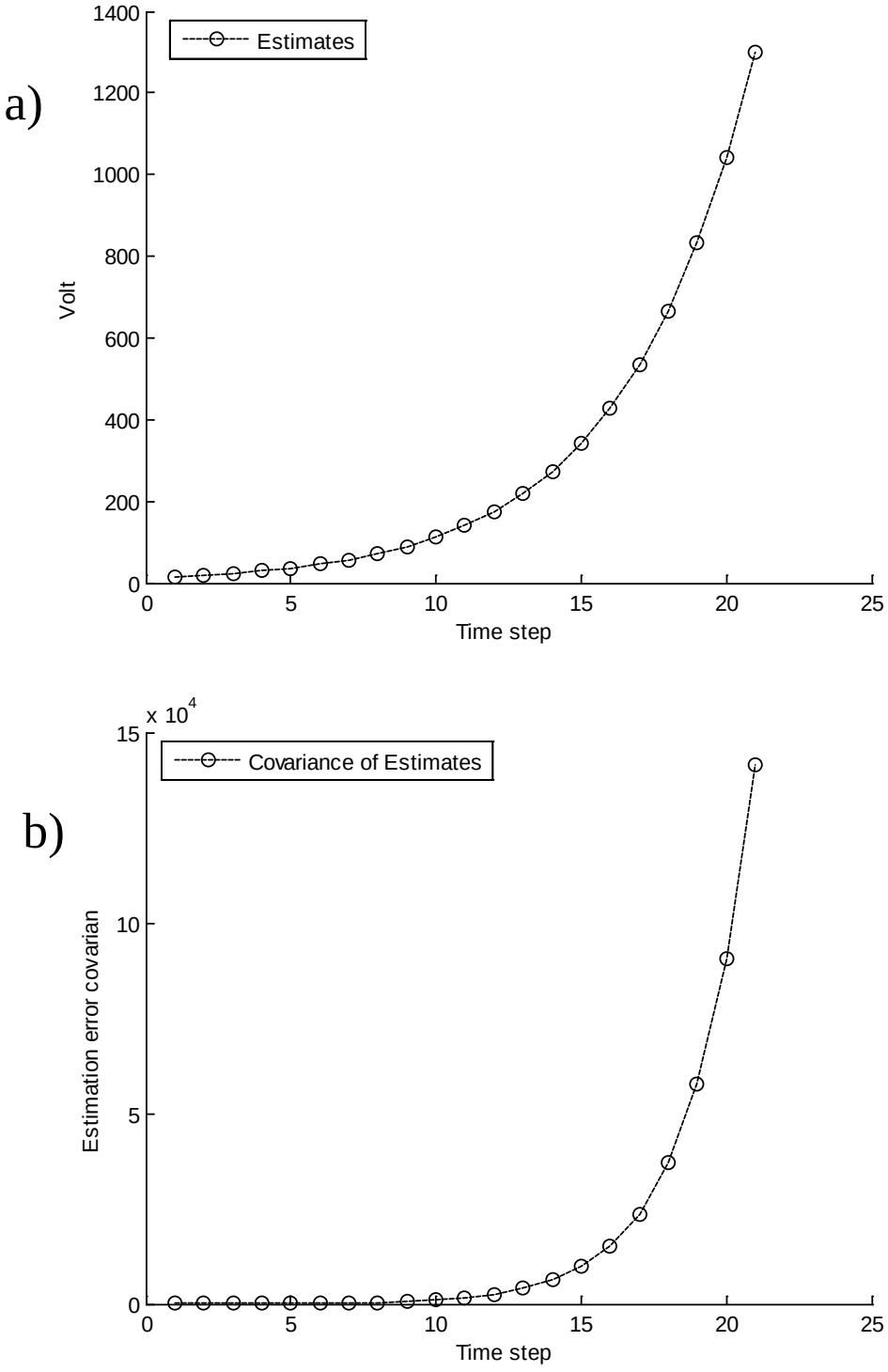

Figure 5-9: (a) State mean and (b) covariance of the voltmeter example studied in measurement update section. First simulation: F=1.25, R=1, and P_0 =1.

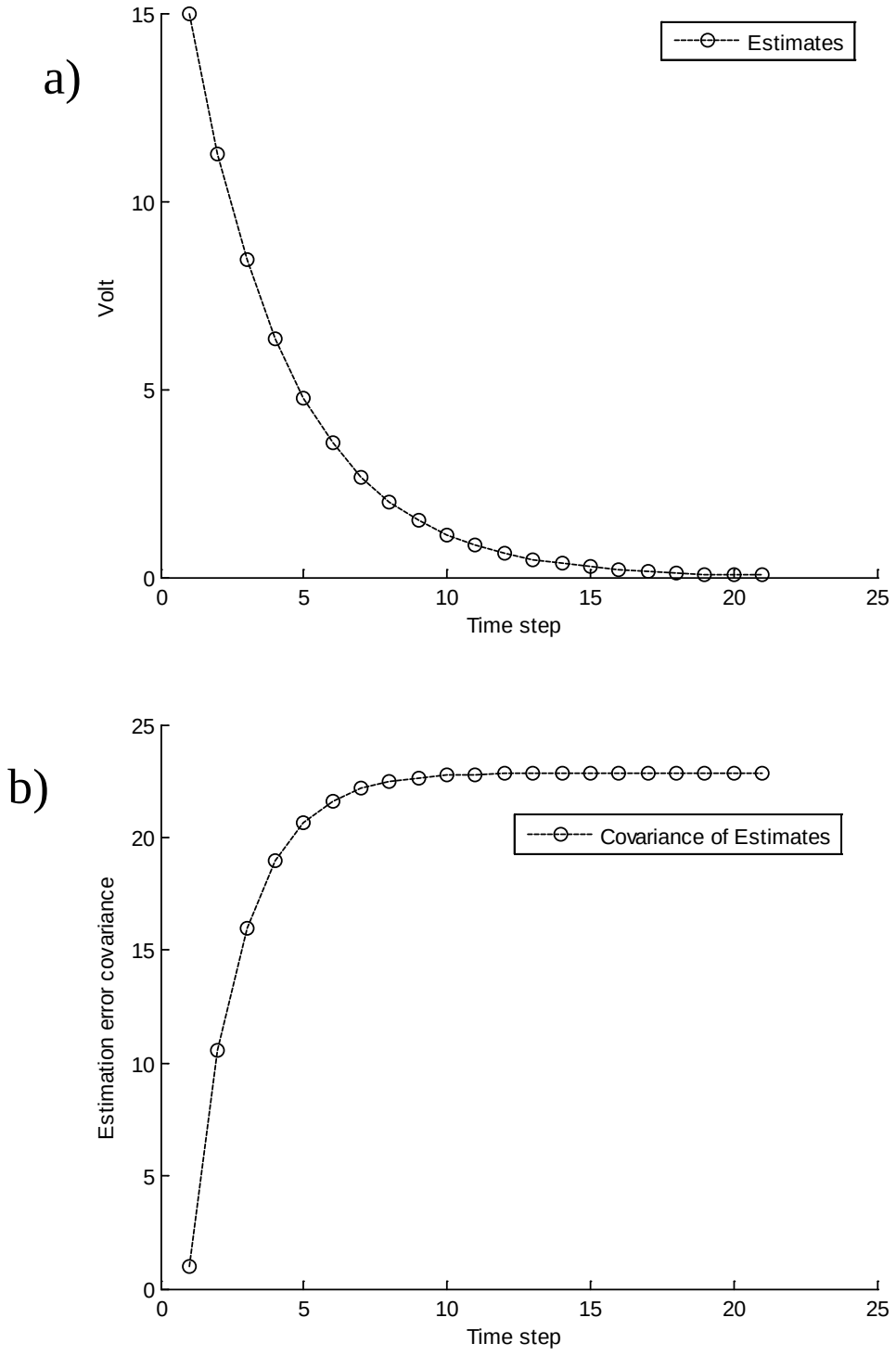

Figure 5-10: (a) State mean and (b) covariance of the voltmeter example studied in measurement update section. Second simulation: F=0.75, R=1, and P_0 =1.

CHAPTER 6. THE DISCRETE- TIME KALMAN FILTER EQUATIONS

The understanding developed in the chapters on the measurement and time update will be used here to derive the discrete-time Kalman filter equations. For understanding the equations that follow, the notation used is very important and therefore it is given when appropriate.

If we suppose that a linear discrete-time system can be defined as

$$x_k = F_{k-1}x_{k-1} + G_{k-1}u_{k-1} + \omega_{k-1}$$
$$y_k = H_k x_k + v_k \qquad 6\text{-}1$$

where F is a matrix that relates the current estimation (x_k) to the previous one (x_{k-1}), known as the state transition matrix, G_k is Control matrix , and u_k is a known optional control vector, and w_k is the process noise. Moreover, H is a matrix that relates the state vector matrix (x_k) to the measurement vector (y_k), whereas v_k is the measurement noise. Both ω_k and v_k are assumed to be white, with normal probability distribution (Gaussian) and uncorrelated which means that they are independent of each other; the corresponding covariance matrices are Q_k and R_k, respectively (Welch and Bishop, 2006). Mathematically, these previous statements related to the characteristics of noise denoted as

$$\omega_k \sim (0, Q_k)$$
$$v_k \sim (0, R_k)$$
$$E\left[v_k \omega_j^T\right] = 0 \qquad 6\text{-}2$$

The role of the filter is to estimate the state vector (x_k) based on the dynamics of the system which is known to us to a certain degree and the noisy measurement (y_k) that are available to us. How accurate our filter is able to estimate the state of the system depends on the amount of information we have about our system. For example, to estimate x_k, it is important whether the measurement at time step k (z_k) is available to use or not. If the measurements cover all the measurements up to and including time k, then it is possible to have *a posteriori* estimate $(\hat{x}_k^+)$, where if the measurement z_k is not available, and only the measurements prior to time k are available, it is possible to estimate only *a priori* estimate $(\hat{x}_k^-)$ (Grewal and Andrews, 2011). Mathematically, this is denoted as

$$\hat{x}_k^+ = E[\, x_k \mid y_1, y_2, \ldots y_k] = a\ posteriori\ estimate$$
$$\hat{x}_k^- = E[\, x_k \mid y_1, y_2, \ldots y_{k-1}] = a\ priori\ estimate \qquad 6\text{-}3$$

Both $\hat{x}_k^+$ and $\hat{x}_k^-$ are the estimates of the same quantity (x_k) but $\hat{x}_k^+$ should be a better estimate. These two estimates are the ones that are used later in deriving the Kalman filter equations. However, following Simon's book (2006), I want to discuss other kinds of estimations since they are used in smoothing methods.

If, in estimating x_k, measurements after time k are available and are taken into account in our estimation, then we can form a smoothed estimate. If the value of x_k is estimated based on the measurements more than one step behind, then the estimation is known as the predicted estimate.

$$\hat{x}_{k \mid k+N} = E[\, x_k \mid y_1, y_2, \ldots y_k, \ldots y_{k+N}] = a\ smoothed\ estimate$$
$$\hat{x}_{k \mid k-M} = E[\, x_k \mid y_1, y_2, \ldots y_{K-M},] = a\ predicted\ estimate \qquad 6\text{-}4$$

where N is the number of estimates considered after the current estimate, k, being considered and M are the number of estimates considered prior to the current estimate.

Figure 6-1 illustrates different forms of estimations. Here it is assumed that we have measurements up to and including time step $k = 10$. Any estimation of the state at $k < 10$ is called the smoothed estimate ($\hat{x}_{5|10}$ is an example). An estimate of the state at time $k = 10$ is known as the *a posteriori* estimate ($\hat{x}_{10|10}$) and the estimate of the state at $k = 11$ is called *a priori* estimate ($\hat{x}_{11|10}$). Any estimation of the state at time steps $k > 11$, is a prediction estimate ($\hat{x}_{15|10}$ is shown as an example of this type).

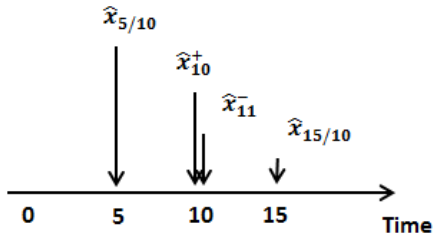

Figure 6-1: Illustration of the smoothed, a priori, a posteriori, and the predicted notation of estimates.

The two primary estimations that are used in the Kalman filter are the *a priori* estimate ($\hat{x}_k^-$) and *a posteriori* estimate ($\hat{x}_k^+$). As discussed in Chapter 5, each estimation has a corresponding covariance of the estimation error (P_K) and, consequently, the covariance of the estimation error of the *a priori* estimate is shown as P_k^- whereas for the *a posteriori* estimate is denoted as P_k^+ (Welch and Bishop, 2006). Mathematically, the *a priori* and *a posteriori* covariance are written as

$$P_k^- = E[(x - \hat{x}_k^-)(x - \hat{x}_k^-)^T]$$
$$P_k^+ = E[(x - \hat{x}_k^+)(x - \hat{x}_k^+)^T] \quad 6\text{-}5$$

Figure 6-2, taken from Simon (2006), can help further in understanding the concept of *a priori* and a *posteriori* estimation and the corresponding estimation error covariance. With the notation in Figures 6-1 and 6-2, it is possible to synthesize the understanding developed from chapter 5 about time and measurement update equations to derive the Kalman filter equations.

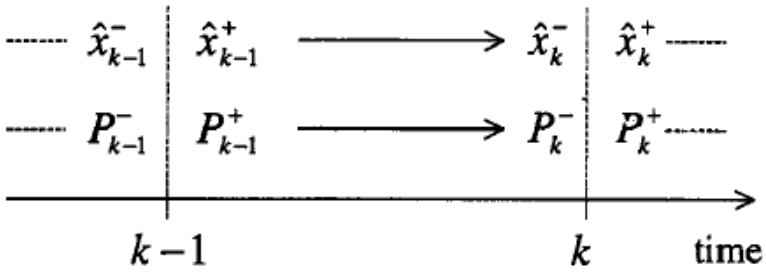

Figure 6-2: Timeline illustrating the concept of a priori and a posteriori estimation and their corresponding estimation error covariance. (from Simon, 2006).

Suppose that we have access to measurements up to and including time step k. To illustrate how the filter performs, assume that we have calculated the best estimate of the state at time step $k-1$, ($\hat{x}_{k-1}^+$), and therefore we know the comparable covariance of the estimation error, ($\hat{p}_{k-1}^+$). It means that we have considered and taken into account $k-1$ measurements for the state estimation at time step $k-1$. With Equation 5-56, we can predict the state of the system at time step k as

$$\bar{x}_k = F_{k-1}\bar{x}_{k-1} + G_{k-1}u_{k-1} \quad 5\text{-}56$$

As we have considered $k-1$ measurements to estimate the state at time step k, and since there is no other measurement between time $(k-1)^+$ and k^-, the calculation from Equation 5-56 which is based on our knowledge of the system dynamics (F_k and G_k), is actually the *a posteriori* estimate, $\hat{x}_k^+$. Thus, Equation 5-56 can be rewritten as

$$x_k^- = F_{k-1}\hat{x}_{k-1}^+ + G_{k-1}u_{k-1} \qquad 6\text{-}6$$

Also, as soon as the prediction of an estimation is made, the corresponding covariance estimation error needs to be calculated to tell us how accurate the estimation is. Equation 5-59 can help with that

$$\mathrm{P_k} = \mathrm{F_{k\text{-}1}}\,\mathrm{P_{k\text{-}1}}\mathrm{F^T_{k\text{-}1}} + \mathrm{Q_{k\text{-}1}} \qquad 5\text{-}59$$

And, in terms of the notation of the *a priori* and *a posteriori* estimates, it can be written as

$$P_k^- = F_{k-1}P_{k-1}^+F_{k-1}^T + Q_{k-1} \qquad 6\text{-}7$$

At this point, the last measurement, y_k, can be taken into account in the estimation of x_k. From the measurement update equations and Table 5-1 we have

$$\hat{\mathrm{x}}_\mathrm{k} = \hat{\mathrm{x}}_{\mathrm{k\text{-}1}} + \mathrm{K_k}\left(\mathrm{y_k}\text{-}\mathrm{H_k}\hat{\mathrm{x}}_{\mathrm{k\text{-}1}}\right) \qquad 5\text{-}21$$

$$\mathrm{P_k} = \left(\mathrm{I}\text{-}\mathrm{K_k}\mathrm{H_k}\right)\mathrm{P_{k\text{-}1}}\left(\mathrm{I}\text{-}\mathrm{K_k}\mathrm{H_k}\right)^{\mathrm{T}} + \mathrm{K_k}\mathrm{R_k}\mathrm{K_k}^{\mathrm{T}} \qquad 5\text{-}27$$

$$= (\mathrm{P_{k\text{-}1}}^{\text{-}1} + \mathrm{H_k}^{\mathrm{T}}\mathrm{R_k}^{\text{-}1}\mathrm{H_k})^{\text{-}1} \qquad \textit{5-38}$$

$$= (\mathrm{I}\text{-}\mathrm{K_k}\mathrm{H_k})\mathrm{P_{k\text{-}1}} \qquad 5\text{-}34$$

$$\mathrm{K_k} = \mathrm{P_{k\text{-}1}}\mathrm{H_k}^{\mathrm{T}}(\mathrm{H_k}\mathrm{P_{k\text{-}1}}\mathrm{H_k}^{\mathrm{T}} + \mathrm{R_k})^{\text{-}1} \qquad 5\text{-}29$$

$$= \mathrm{P_k}\mathrm{H_k}^{\mathrm{T}}\mathrm{R_k}^{\text{-}1} \qquad 5\text{-}41$$

In the above equations, $\hat{x}_{k-1}$ is the estimate we have before the last measurement (y_k) is processed; thus, in the Kalman filter notation given above, it is shown as $\hat{x}_k^-$ (*a priori* estimate). Similarly, $\hat{x}_k$ is the estimate which is calculated after y_k is taken into account in the estimation of the state at time step k, and so it can be denoted as the *a posteriori* estimate. P_{k-1} and P_k that are the covariances before and after y_k is considered, respectively, and can be designated as the *a priori* and *a posteriori* covariance matrices. Using these notation changes, the above previous equations can be restated as

$$\hat{x}_k^+ = \hat{x}_k^- + K_k(y_k - H_k\hat{x}_k^-) \quad 6\text{-}8$$

$$P_k^+ = (I - K_kH_k)P_k^-(I - K_kH_k)^T + K_kR_k{K_k}^T$$

$$= [(P_k^-)^{-1} + {H_k}^T{R_k}^{-1}H_k]^{-1} = (I - K_kH_k)P_k^- \quad 6\text{-}9$$

$$K_k = P_k^-{H_k}^T(H_kP_k^-{H_k}^T + R_k)^{-1} = P_k^+{H_k}^T{R_k}^{-1} \quad 6\text{-}10$$

The five equations from 6-6 to 6-10 are recognized as the basic equations of the Kalman filter. The filtering procedure starts with the prediction step with the time update equations and goes to the measurement update equations to correct its estimations. Then the correction output is fed back to predict the next point and this is process is repeated until the last measurement (Figure 6-3).

The filter procedure starts with our best estimate of the initial state at step 0 ($\hat{x}_0^+$) and the related covariance of the state estimation error (P_0^+) which are defined as

$$\hat{x}_0^+ = E(x_0) \quad 6\text{-}11$$

$$P_0^+ = E[(x_0 - \bar{x}_0)(x_0 - \bar{x}_0)^T]$$

$$= E[(x_0 - \hat{x}_0^+)(x_0 - \hat{x}_0^+)^T] \quad 6\text{-}12$$

Once again, it should be mentioned that P_0^+ tells us about the level of uncertainty in the initial estimation of x_0. Therefore, if the initial state is known perfectly, then $P_0^+ = 0$. On the other hand, if we have no idea of the value of the initial state estimate, then $P_0^+ = \infty I$, where *I* is the identity matrix.

Given $\hat{x}_0^+$ and P_0^+, the Kalman filter goes through the time update step and the output would be the predictions for x_1^- and P_1^- (the *a priori* estimate and the corresponding covariance), here the filter computes the measurement update steps and the output of the previous time update step would be the input of this step. At this stage, using the measurement taken at time $k = 1$, i.e., y_1, the correction is made. The outputs of this step are x_1^+ and P_k^+ (the *a posteriori* estimate and the corresponding covariance) which will be fed to the loop as the input of the next time update step, k = 2, and so on.

Time update (Prediction)		Measurement update (Correction)
1) *A priori* update: Project the state ahead $x_k^- = F_{k-1}\hat{x}_{k-1}^+ + G_{k-1}u_{k-1}$	⇒	3) Compute the Kalman gain $K_k = P_k^- H_k{}^T (H_k P_k^- H_k{}^T + R_k)^{-1}$ 4) *A posteriori* update: Update estimate with measurement y_k $\hat{x}_k^+ = \hat{x}_k^- + K_k(y_k - H_k\hat{x}_k^-)$
2) *A Priori* error covariance: Project the error covariance ahead $P_k^- = F_{k-1}P_{k-1}^+F_{k-1}^T + Q_{k-1}$	⇐	5) *A posteriori* error covariance: Update the error covariance $P_k^+ = (I - K_k H_k)P_k^-$

Figure 6-3: The Kalman filter operation loop: Five basic filter equations and their concise meaning stating the filtering operation.

Table 6-1: Parameters in the Kalman filter

x_k^-	State prediction	Intermediary variables
$\hat{x}_k^+$	State update	Output
P_k^-	Covariance prediction	Intermediary variable
P_k^+	Covariance update	Output
K_k	Gain matrix (in some sources it is called blending factor)	Intermediary variable
y_k	Actual measurement	Input
H_k	Measurement matrix (relates the state to the measurement)	Should be modified at each step
F_k	State transition matrix (relates the state at the previous time step to the state at the current step)	Should be modified at each step
G_k	Control matrix (relates the optional control input to the state)	Should be modified at each step
u	Control input (indicates the magnitude of any system's or user's control on the situation)	Input
R_k	Measurement error covariance	Input
Q_k	Process noise covariance	Should be modified at each step

The concept and equations of one-step Kalman filter

One-step Kalman filter simplifies the computer implementation of the equations (Simon, 2006). Equation 5-6 which is used to predict the *a priori* estimate can be rewritten with the time index increased by one as

$$\mathrm{x_k^-} = \mathrm{F_{k-1}\hat{x}_{k-1}^+} + \mathrm{G_{k-1}u_{k-1}} \quad 6\text{-}6$$

$$\hat{x}_{k+1}^- = F_k\hat{x}_k^+ + G_k u_k \quad 6\text{-}13$$

Substituting $\hat{x}_k^+$ from Equation 6-8 into 6-13 results in

$$\mathrm{\hat{x}_k^+} = \mathrm{\hat{x}_k^-} + \mathrm{K_k}\left(\mathrm{y_k}\text{-}\mathrm{H_k\hat{x}_k^-}\right) \quad 6\text{-}8$$

$$\begin{aligned}\hat{x}_{k+1}^- &= F_k[\hat{x}_k^- + K_k(y_k - H_k\hat{x}_k^-)] + G_k u_k \\ &= F_k(I - K_k H_k)\,\hat{x}_k^- + F_k K_k y_k + G_k u_k\end{aligned} \quad 6\text{-}14$$

Equation 6-14 shows that we can compute *a priori* state estimate directly from the previous *a priori* estimate without computing the *a posteriori* state estimate in between. A similar approach can be used to obtain the one-step expression for the *a priori* covariance of the estimation error. Starting from Equation 6-7and increasing the time step by one yields

$$\mathrm{P_k^-} = \mathrm{F_{k-1}P_{k-1}^+F_{k-1}^T} + \mathrm{Q_{k-1}} \quad 6\text{-}7$$

$$P_{k+1}^- = F_k P_k^+ F_k^T + Q_k \quad 6\text{-}15$$

Substituting Equation 6-9 into 6-15 results in

$$\mathrm{P_k^+} = \mathrm{(I\text{-}K_kH_k)P_k^-} \quad 6\text{-}9$$

$$\begin{aligned}P_{k+1}^- &= F_k(P_k^- - K_k H_k P_k^-){F_k}^T + Q_k \\ &= F_k P_k^- F_k^T - F_k K_k H_k P_k^-{F_k}^T + Q_k \\ &= F_k P_k^- F_k^T - F_k P_k^-{H_k}^T(H_k P_k^-{H_k}^T + R_k)^{-1} H_k P_k^-{F_k}^T + Q_k\end{aligned} \quad 6\text{-}16$$

In the above calculation, the Kalman gain is substituted from Equation 6-10

$$\mathrm{K_k} = \mathrm{P_k^-H_k^T(H_kP_k^-H_k^T + R_k)^{-1}} = \mathrm{P_k^+H_k^TR_k^{-1}} \quad 6\text{-}10$$

Equation 6-16 is called a discrete Riccati equation and along with Equation 6-14 it forms the equations of the one-step Kalman filter. They can be used to compute the *a priori* state and the corresponding covariance of the estimation on the basis of the

previous *a priori* state and covariance without intermediate calculations of the *a posteriori* state estimate and covariance.

The same logic can be applied to the *a posteriori* state and covariance. They can be calculated directly from the previous *a posteriori* quantities without going through the equations determining the *a priori* state and covariance. Table 6-2 illustrates the one-step Kalman filter.

Table 6-2: The one-step Kalman filter using only the a priori estimations (top) and the a posteriori estimations (bottom).

$K_k = P_k^- H_k^T (H_k P_k^- H_k^T + R_k)^{-1}$	6-10
$\hat{x}_{k+1}^- = F_k(I - K_k H_k)\hat{x}_k^- + F_k K_k y_k + G_k u_k$	6-14
$P_{k+1}^- = F_k P_k^- F_k^T - F_k P_k^- H_k^T (H_k P_k^- H_k^T + R_k)^{-1} H_k P_k^- F_k^T + Q_k$	6-16
$K_k = P_k^+ H_k^T R_k^{-1}$	6-10
$\hat{x}_k^+ = (I - K_k H_k)(F_{k-1}\hat{x}_{k-1}^+ + G_{k-1}u_{k-1}) + K_k y_k$	6-17
$P_k^+ = (I - K_k H_k)(F_{k-1}P_{k-1}^+ F_{k-1}^T + Q_{k-1})$	6-18

Running and tuning the Kalman filter

Like any other filter or estimator, the Kalman filter needs to be tuned and has certain steps. These steps can be described as:

I. ***<u>Building a model.</u>*** This is the most important step which determines the system's dynamic and illustrates how the current state is related to the previous step as well as how the measurement is linked to the state (the first two equations below). Also, in this step we need to estimate the measurement and process noise (the two middle equations below) and make sure they are uncorrelated (the last equation).

$x_k = F_{k-1}x_{k-1} + G_{k-1}u_{k-1} + \omega_k$

$y_k = H_k x_k + v_k$

$\omega_k \sim (0, Q_k)$

$v_k \sim (0, R_k)$

$$E\left[v_k \omega_j^T\right] = 0 \qquad 6\text{-}19$$

In the actual implementation of the filter, the measurement error covariance, R, is usually known prior to operating the filter; one way to achieve this is through sample measurements. On the other hand, the determination of the process noise covariance, Q, is generally more difficult. That is why we usually do not have the ability to observe how uncertain we are about the system that we have defined. Sometimes one needs to run the filter several times so that one would be able to tune it (i.e., to determine parameters such as Q).

It is very important to consider that determining the process noise appropriately is critical. When Q is set large, the estimation error covariance increases (Equation 6-7) and this eventually results in a higher gain value, making the filter give more weight to the measurements (Equation ٦-10), and thereby making the state estimation difficult. On the other hand, if Q is assigned a small value, the estimation covariance will decrease rapidly from one time step to the next and eventually might converge to zero (Equation 6-16). Consequently, a zero value for P_k^- will result which will in turn lead to $K_k = 0$ (Equation 6-10). This means that the measurement update equation (Equation 6-8) will not consider the measurement itself in calculating the *a posteriori* estimate; and from that step on all measurements, y_k, will be completely ignored and the filter will become inactive in the sense that it will not respond to the measurements from that time step onward. Thus, it is essential to remember the general principle that for the Kalman filter, an assumption of an imperfect model (or the presence of a certain amount model noise) is important (Simon, 2006), and it is essentially a part of the process of building the model.

II. ***Initializing the process: Estimating the initial model state and its covariance.*** To initiate the Kalman filter, we need to know $\hat{x}_0^+$ and P_0^+, our best estimates of the initial state and the covariance of our initial estimate. They have been defined previously as follows

$$\hat{x}_0^+ = E(x_0) \quad 6\text{-}11$$

$$P_0^+ = E\left[(x_0 - \hat{x}_0^+)(x_0 - \hat{x}_0^+)^T\right] \quad 6\text{-}12$$

III. ***<u>The iterations.</u>*** After all the above information is gathered, we can start the process by plugging these values in the three equations of the measurement update (Figure 6-3) and iterate till the required convergence is obtained.

Once again I illustrate the filter process with examples.

<u>Example 1</u>

Going back to the simple voltmeter example examined in chapter 5, the true value of the state is 12 volts. Following the steps explained above:

i. Building the model. As the signal is constant, *F = 1*, and the filter is run assuming different levels of process noise covariance (*Q=1, Q=5, and Q=0.1*). There is no control signal (*B=0*). Some know that our measurement is the state value which is contaminated with measurement noise that has a standard deviation of 1 (*R=1*).

$$x_k = F_{k-1}x_{k-1} + G_{k-1}u_{k-1} + \omega_k$$
$$= x_{k-1}$$
$$y_k = H_k x_k + v_k$$
$$y_k = x_k + v_k$$

ii. We need to start the procedure from the initial state estimation. Here we suppose that the system has the characteristics of Figure 5-1, i.e., x_0 *=15 and* P_0*=1.*

iii. Now we can iterate the Kalman filter cycle.

a)

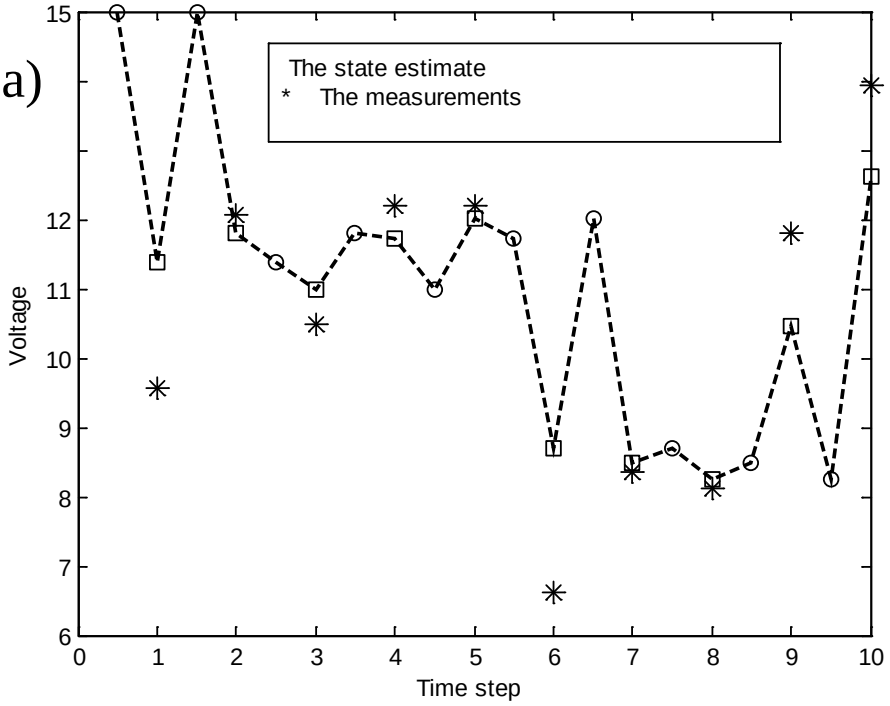
The state estimate
* The measurements
Voltage
Time step
15
12
11
10
9
8
7
6
0
1
2
3
4
5
6
7
8
9
10

b)

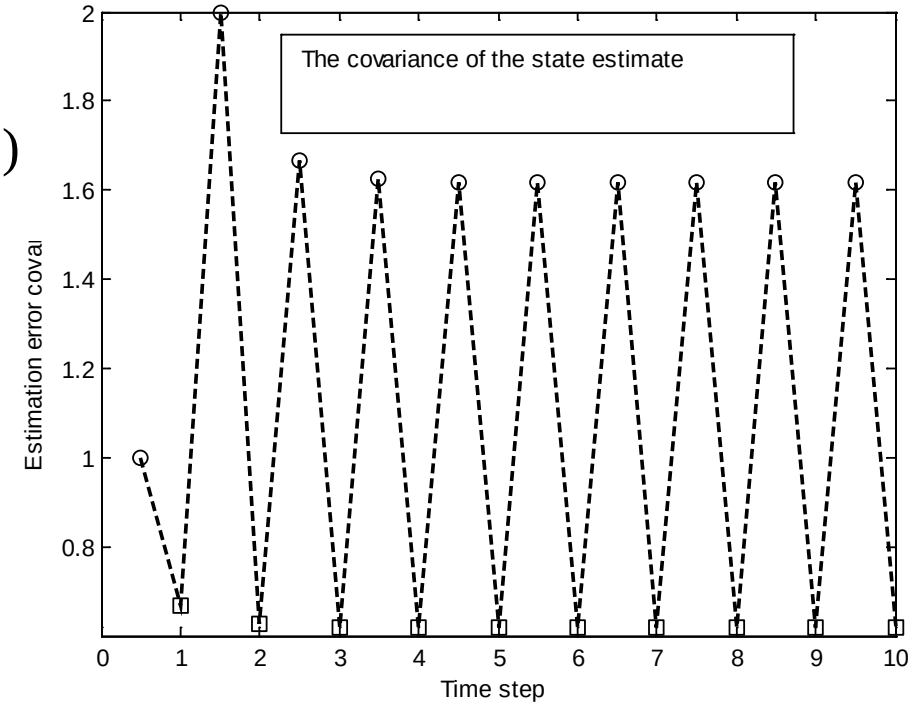
The covariance of the state estimate
Estimation error covai
Time step
2
1.8
1.6
1.4
1.2
1
0.8
0
1
2
3
4
5
6
7
8
9
10

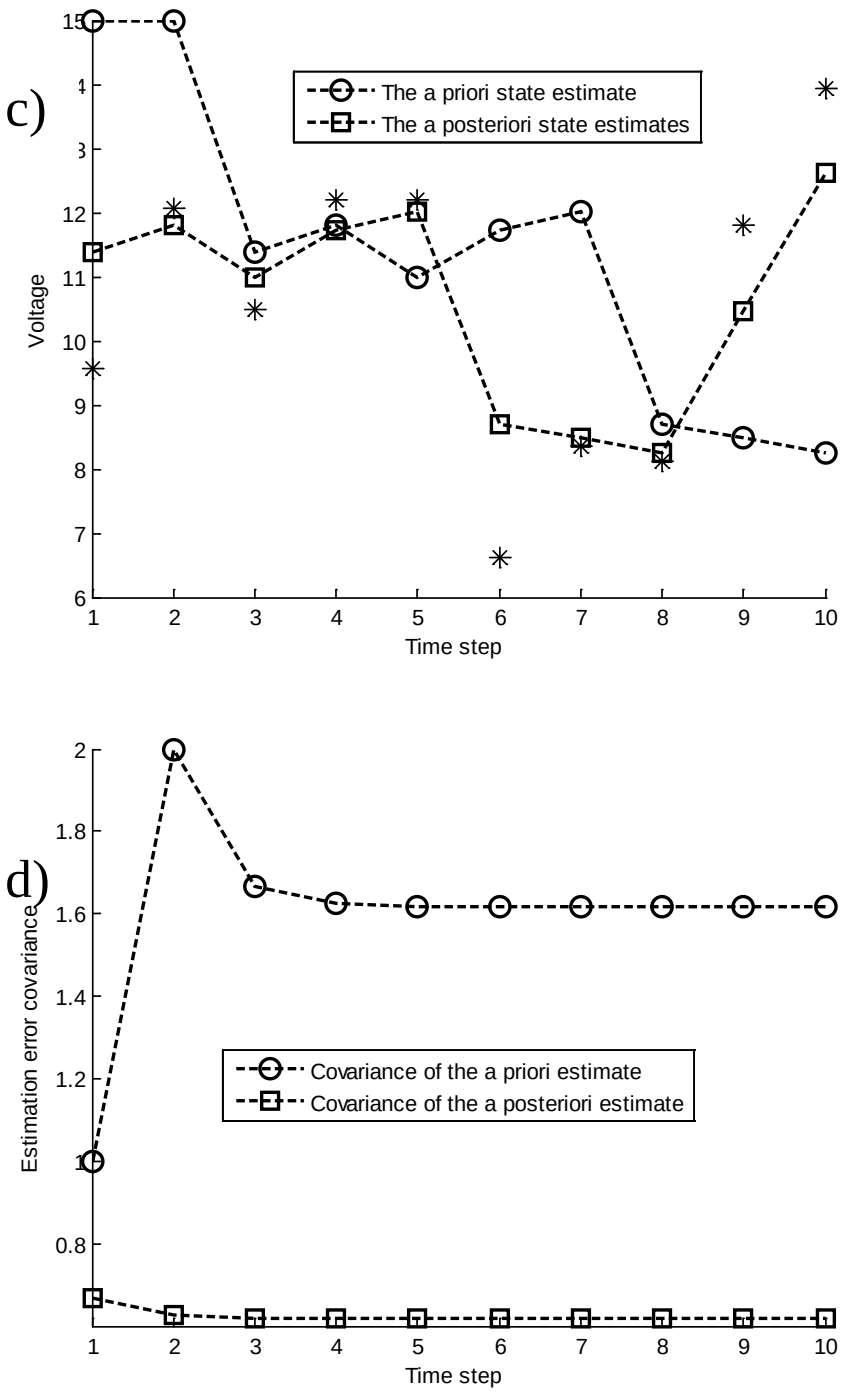

Figure 6-4: Illustrations of different estimations in the Kalman filter. Circles show the a priori estimations and squares illustrate the a posteriori estimations. (a) State estimations and the measurements, (b) covariance of the estimation, (c) propagation of estimations with time, and (d) changes in the covariance of the estimations. Parameters: R=1, Q=1 and P_0 =1.

a)

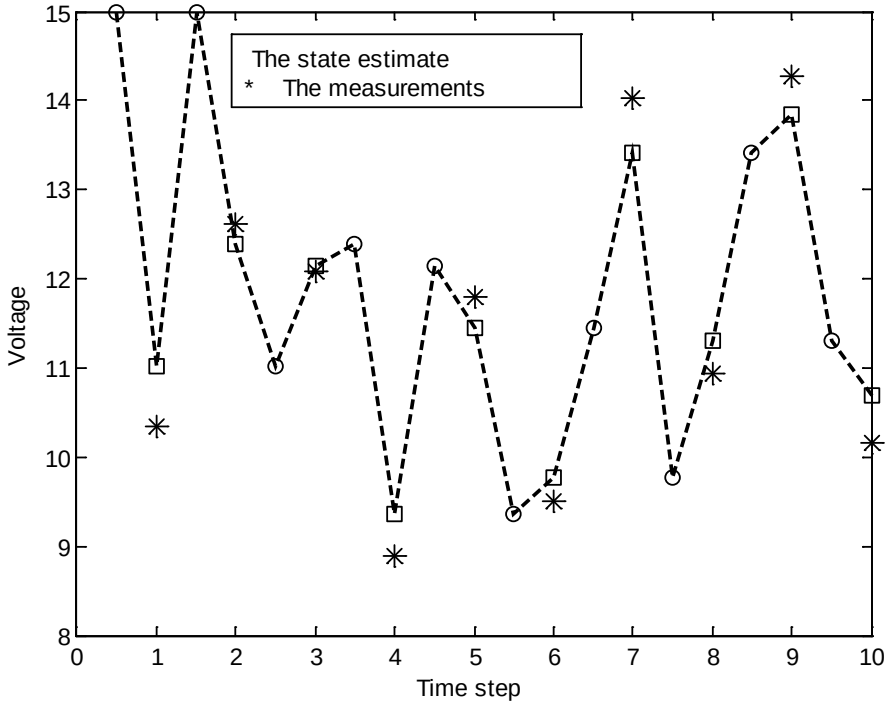
The state estimate
* The measurements
Voltage
Time step
15
14
13
12
11
10
9
8
0
1
2
3
4
5
6
7
8
9
10

b)

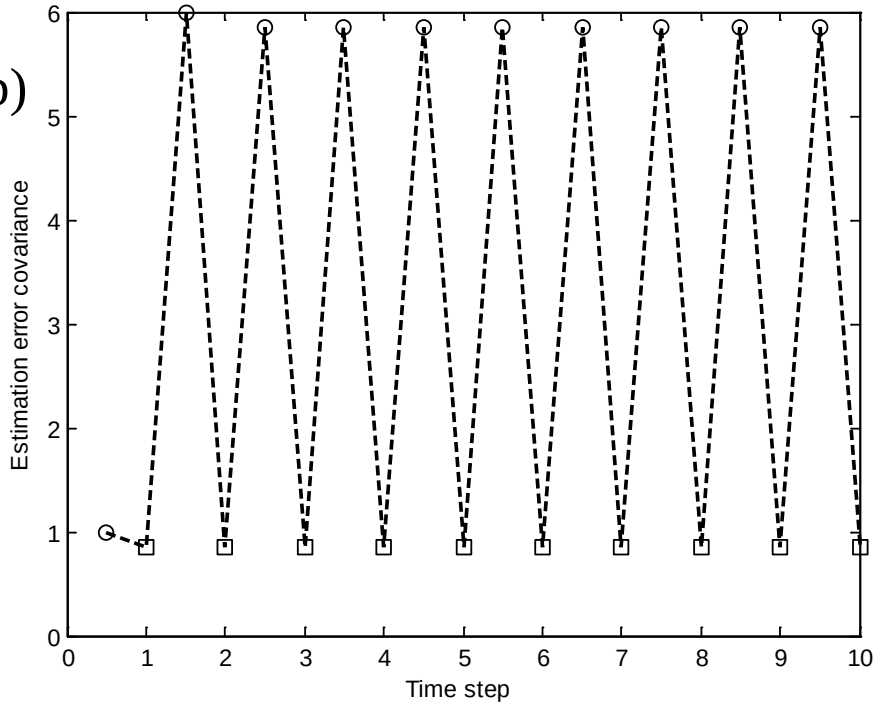
Estimation error covariance
Time step
6
5
4
3
2
1
0
0
1
2
3
4
5
6
7
8
9
10

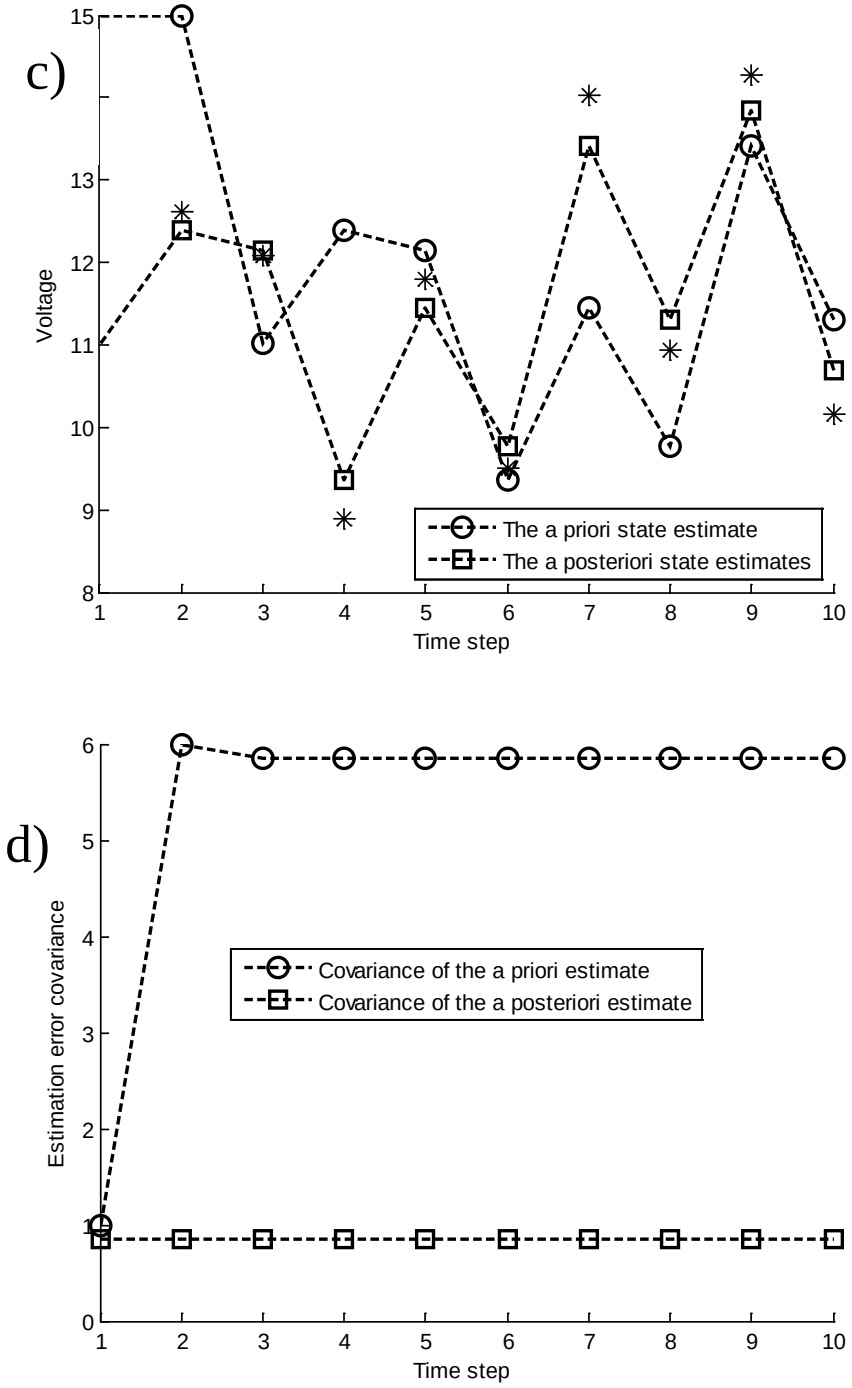

Figure 6-5: (a) State estimations (Circles show the priori estimations and squares illustrate the posteriori estimations) and the measurements, (b) covariance of the estimation, (c) how the estimations propagate with time, and (d) how the covariance of the estimations changes. Second simulation: R=1, Q=5 and P_0 =1.

a)

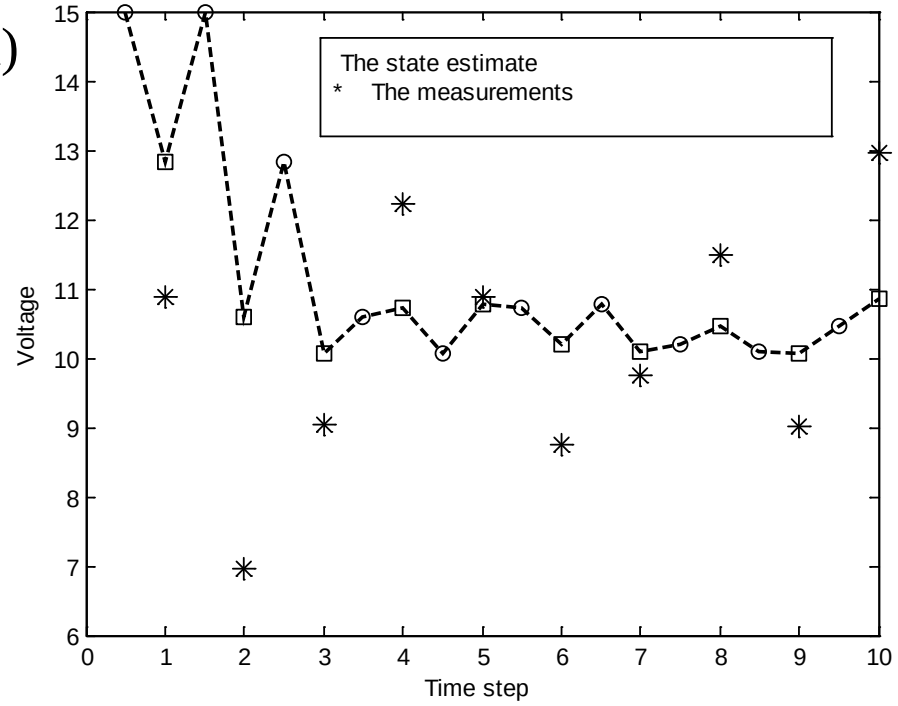
The state estimate
* The measurements
Voltage
Time step
15
14
13
12
11
10
9
8
7
6
0
1
2
3
4
5
6
7
8
9
10

b)

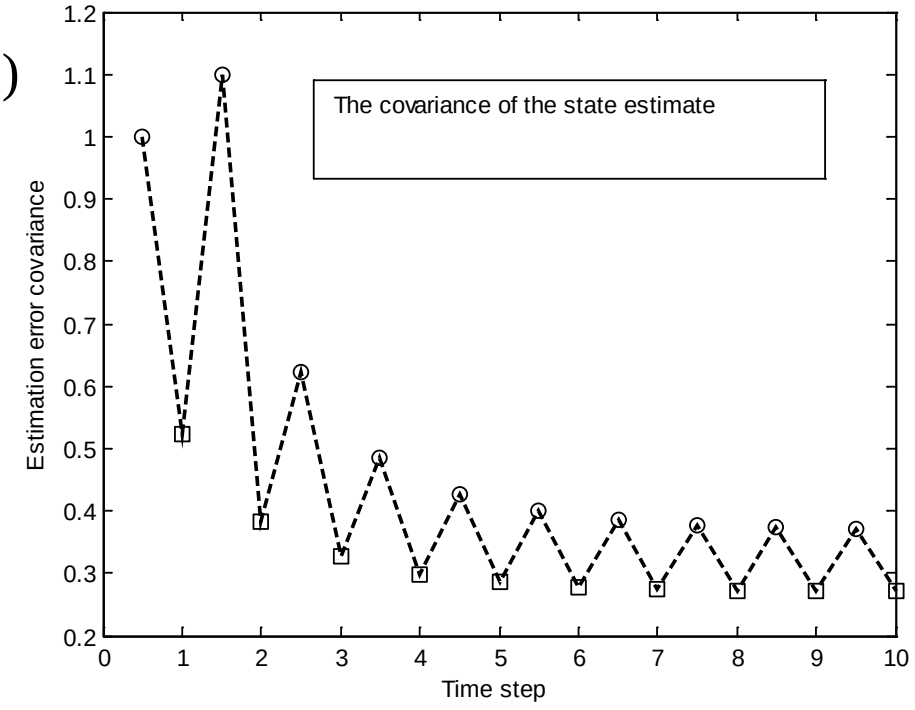
The covariance of the state estimate
Estimation error covariance
Time step
1.2
1.1
1
0.9
0.8
0.7
0.6
0.5
0.4
0.3
0.2
0
1
2
3
4
5
6
7
8
9
10

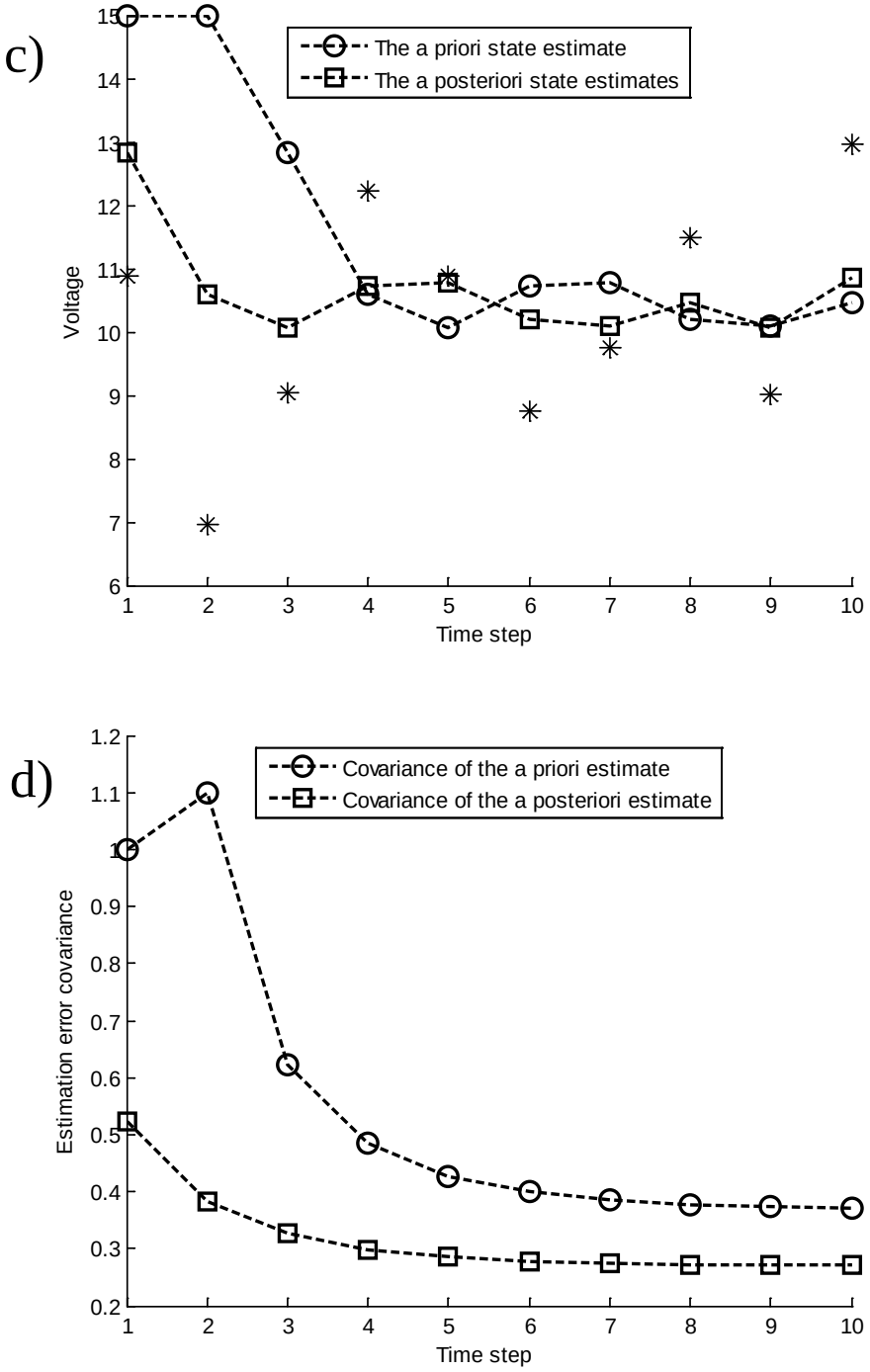

Figure 6-6: (a) State estimations (Circles show the priori estimations and squares illustrate the posteriori estimations) and the measurements, (b) covariance of the estimation, (c) how the estimations propagate with time, and (d) how the covariance of the estimations changes. Third simulation: R=1, Q=0.1 and P_0 =1.

The above examples and figures illustrate the importance of Q and the effect of its value relative to R. The first simulation shows the case where Q and R have equal values (Figure 6-4). In this case, the *a posteriori* estimation would be an estimation carried out between the measurement at a given time step and the *a priori* estimation at the same time step. After some iteration, our estimations approach the true value of the state which is 12 volts in this example (Figures 6-4 (a) and 6-4 (c)). The covariance of the estimation decreases noticeably when each measurement is considered in the estimation; it reduces at each time step from the *a priori* estimate to the *a posteriori* one (from around 1.6 to 0.2, Figure 6-4 (b) and 6-4(d)). Figures 6-4 (c) and 6-4 (d) show how the *a priori* and posteriori estimations and the corresponding covariance propagate with time.

For the second simulation, we impose more uncertainty into our model and establish a model with a higher Q value $(Q = 5)$ while $R = 1$. As it can be intuitively concluded, in this case that we are not sure about the system that we have defined, the Kalman filter *a posteriori* estimation would follow the measurements more than the *a priori* estimation (Figures 6-5 (a) and 6-5 (c) , see for example the closeness of the *a posteriori* estimations (squares) to the measurements (stars)). In this case the filter gives more weight to the noisy measurements rather than the *a priori* estimation and, consequently, results in higher estimation variance (Figure 6-5 (b) and 6-5 (d)). Comparison of the values the covariance of the estimations shows that in the second simulation they are higher than in the first simulation (6 vs. 1.6 and 1 vs 0.64).

In the case where one is more confident about the defined system (i.e., $Q = 0.1$ and R = 1), one expects the filter to give more weight to the *a priori* estimations than the noisy measurements in each time step (See Figures 6-6 (a) and 6-6 (c)). We also predict smaller estimation error covariance (P) (Figures 6-6 (b) and 6-6 (d), compare 1 vs 1.6 and 0.3 vs 0.64).

High (low) value of Q results in high (low) *a priori* estimation error P_k^-, that will cause, consequently, high (low) gain value (K) as well as high (low) *a posteriori* estimation error (P_k^+). High (low) gain value means more (less) weight for the measurement of the same iteration rather than the *a priori* estimation and it will illustrate what the new estimation would be.

Example 2

Here I want to discuss the most typical example of the Kalman filter which is discussed in almost every textbook and webpage. The task is studying the performance of the Kalman filter assuming a motion with constant acceleration. The motion of a body is governed by the following law:

$$\begin{cases} d_t = \frac{1}{2}\, a\, t^2 + V_0 t + d_0 & (parabola\ shape) \\ V_t = at + V_0 & (Straight\ line) \end{cases} \qquad a = constant \tag{6-20}$$

where d_t and V_t are the position and the velocity of the body at time t, respectively, d_0 and V_0 are the initial position and velocity of the body, and a is the constant acceleration.

The state of the system, in this case, is the position of the body depends on both vehicle position and velocity.

Mathematically, the state vector is written as

$$x_k = \begin{bmatrix} d_k \\ V_k \end{bmatrix} \tag{6-21}$$

Knowing the position and velocity at time k, they can be calculated at time k+1 as

$$\begin{aligned} d_{k+1} &= \frac{1}{2}\, a\, \Delta t^2 + V_k \Delta t + d_k + \widetilde{d_k} \\ V_{k+1} &= a\Delta t + V_k + \widetilde{V_k} \end{aligned} \tag{6-22}$$

where Δt is the time difference between time step k and $k+1$, $\widetilde{d_k}$ is the position noise, and $\widetilde{V_k}$ is the velocity noise. Thus, in the matrix form, the equations become

$$\begin{bmatrix} d_{k+1} \\ V_{k+1} \end{bmatrix} = \begin{bmatrix} \frac{1}{2}\, a\, \Delta t^2 + V_k \Delta t + d_k + \widetilde{d_k} \\ a\Delta t + V_k + \widetilde{V_k} \end{bmatrix} = \begin{bmatrix} 1 & \Delta t \\ 0 & 1 \end{bmatrix} \begin{bmatrix} d_k \\ V_k \end{bmatrix} + \begin{bmatrix} \frac{1}{2}\, \Delta t^2 \\ \Delta t \end{bmatrix} a + \begin{bmatrix} \widetilde{d_k} \\ \widetilde{V_k} \end{bmatrix}$$

$$x_{k+1} = \begin{bmatrix} 1 & \Delta t \\ 0 & 1 \end{bmatrix} x_k + \begin{bmatrix} \frac{1}{2}\, \Delta t^2 \\ \Delta t \end{bmatrix} a + \begin{bmatrix} \widetilde{d_k} \\ \widetilde{V_k} \end{bmatrix} \tag{6-23}$$

On the other hand, position is the only variable that is measured in this example, so the equation that illustrates how the measurements are related to the state of the system can be written as

$$\begin{aligned} d_k &= [1 \quad 0] \begin{bmatrix} d_k \\ V_k \end{bmatrix} + z_k \\ y_k &= [1 \quad 0]\ x_k + z_k \end{aligned} \tag{6-24}$$

where z_k is the measurement error, and

$$x_{k+1} = F_k x_k + G_k u_k + \omega_k$$

$$y_k = H_k x_k + v_k \qquad 6\text{-}1$$

The steps in the Kalman filter construction in this example are:

i. Comparison of Equations ٦-23 and 6-24 with Equation 6-1, helps us build the model of the system

$$F_k = \begin{bmatrix} 1 & \Delta t \\ 0 & 1 \end{bmatrix}, \quad G_k = \begin{bmatrix} \frac{1}{2}\Delta t^2 \\ \Delta t \end{bmatrix}, \quad x_k = \begin{bmatrix} d_k \\ V_k \end{bmatrix}, \quad u_k = a,$$

$$\omega_k = \begin{bmatrix} \widetilde{d_k} \\ \widetilde{V_k} \end{bmatrix} = \begin{bmatrix} \frac{1}{2}\Delta t^2 \\ \Delta t \end{bmatrix}$$

$$H_k = [1 \quad 0], \quad v_k = z_k \qquad 6\text{-}25$$

ii. To start the filter the initial state estimation and the covariance of that estimation are

$$x_0 = \begin{bmatrix} 0 \\ 0 \end{bmatrix}$$

$$P_0 = (acceleration\ noise)^2 \begin{bmatrix} (\frac{1}{2}\Delta t^2)^2 & (\frac{1}{2}\Delta t^2)(\Delta t) \\ (\frac{1}{2}\Delta t^2)(\Delta t) & (\Delta t)^2 \end{bmatrix} \qquad 6\text{-}26$$

Now we can start to run the filter loop by plugging Equations 6-26 into the measurement update equations in Figure 6-3.

Figure 6-7 simulates the motion of a body moving with an acceleration of 1. How the Kalman tracks the object and reduces the measurement error in its estimations (Figure 6-6 (b)).

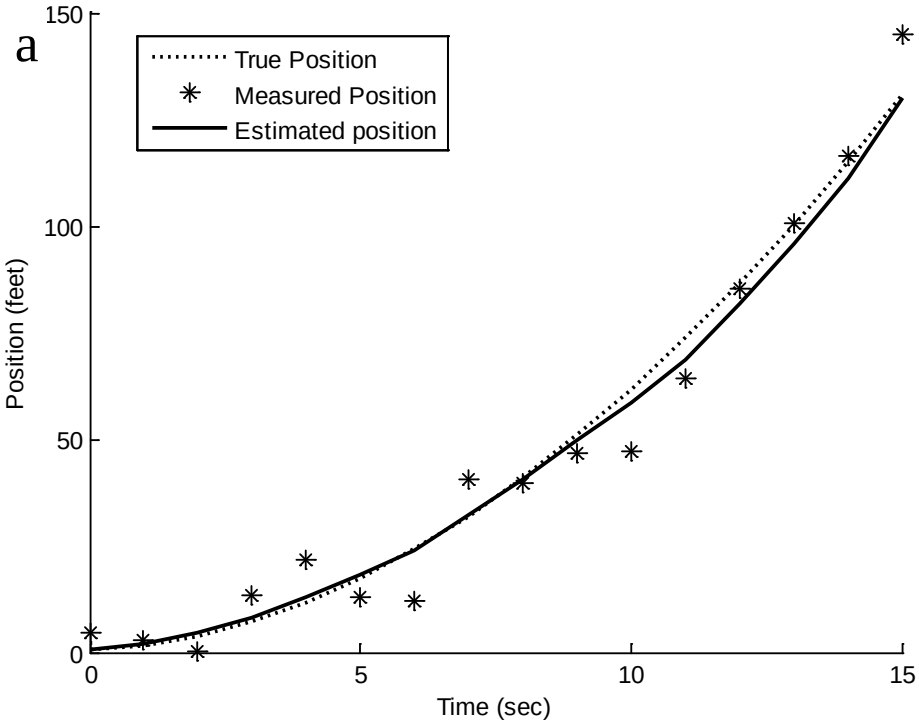
a
True Position
Measured Position
Estimated position
Position (feet)
Time (sec)
150
100
50
0
0
5
10
15

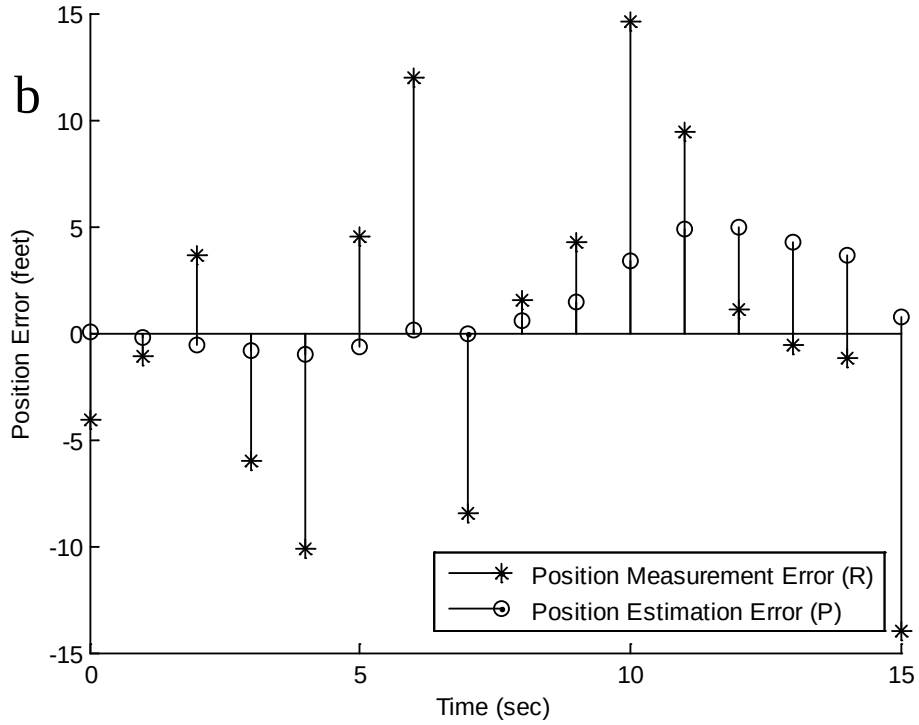
b
Position Error (feet)
Time (sec)
Position Measurement Error (R)
Position Estimation Error (P)
15
10
5
0
-5
-10
-15
0
5
10
15

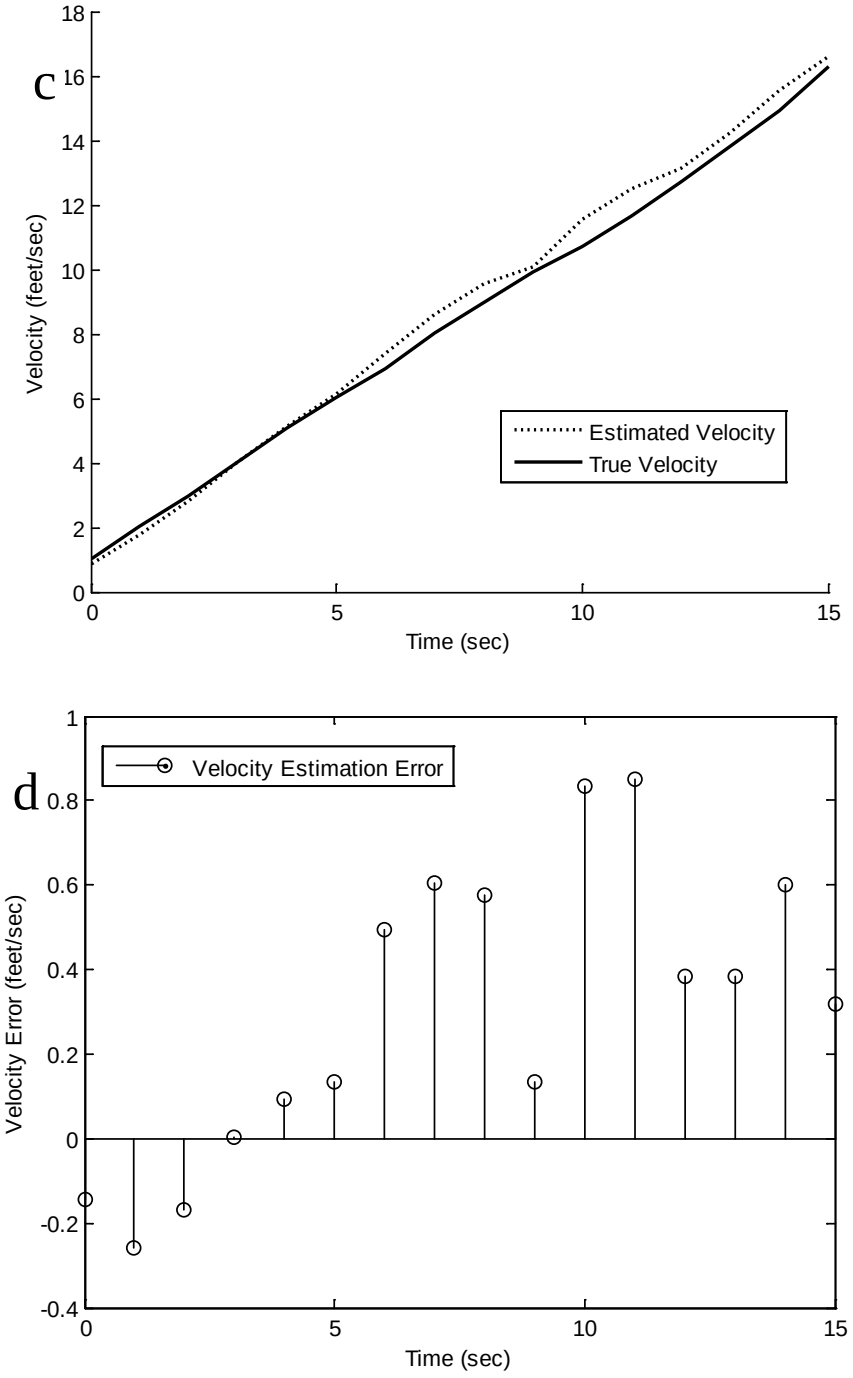

Figure 6-7: Tracking a body with constant acceleration (a) Vehicle Position (True, Measured, and Estimated), (b) Position Measurement Error and Position Estimation Error, (c) Velocity (True and Estimated), and (d) Velocity Estimation Error. The parameters for the example are a=1, $x_0 = \begin{bmatrix} 0 \\ 0 \end{bmatrix}, P_0 = \begin{bmatrix} \frac{1}{4} & \frac{1}{2} \\ \frac{1}{2} & 1 \end{bmatrix}, \Delta t = 1.$

Another popular simple case in the textbooks on the Kalman filter is the motion with constant velocity. Considering that the one-dimensional motion of a body is ruled by the following law:

$$\begin{cases} d_t = (V * t) + d_0 \\ V = constant \end{cases} \quad 6\text{-}27$$

where d_t is the position at time t, d_0 is the position that the body starts moving from and V is the constant velocity.

The state vector in this case is defined as

$$x_k = \begin{bmatrix} d_k \\ V_k \end{bmatrix} \quad 6\text{-}28$$

Knowing the state at time k, it can be calculated at time k+1 as:

$$d_{k+1} = V\Delta t + d_k + \widetilde{d_k}$$
$$V_{k+1} = V_k + \widetilde{V_k} \quad 6\text{-}29$$

and in the matrix form

$$\begin{bmatrix} d_{k+1} \\ V_{k+1} \end{bmatrix} = \begin{bmatrix} V_k\Delta t + d_k + \widetilde{d_k} \\ V_k + \widetilde{V_k} \end{bmatrix} = \begin{bmatrix} 1 & \Delta t \\ 0 & 1 \end{bmatrix} \begin{bmatrix} d_k \\ V_k \end{bmatrix} + \begin{bmatrix} \widetilde{d_k} \\ \widetilde{V_k} \end{bmatrix}$$

$$x_{k+1} = \begin{bmatrix} 1 & \Delta t \\ 0 & 1 \end{bmatrix} x_k + \begin{bmatrix} \widetilde{d_k} \\ \widetilde{V_k} \end{bmatrix} \quad 6\text{-}30$$

The measurements matrix can be written as

$$d_k = [1 \quad 0] \begin{bmatrix} d_k \\ V_k \end{bmatrix} + z_k$$

$$y_k = [1 \quad 0]\ x_k + z_k \quad 6\text{-}31$$

where z_k, Δt, $\widetilde{d_k}$, and $\widetilde{V_k}$ are characterized as before.

Once again, the steps in the Kalman filter construction in this example are:

i. To define the model of the system, we need the following matrices

$$F_k = \begin{bmatrix} 1 & \Delta t \\ 0 & 1 \end{bmatrix}, \quad x_k = \begin{bmatrix} d_k \\ V_k \end{bmatrix}, \quad \omega_k = \begin{bmatrix} \widetilde{d_k} \\ \widetilde{V_k} \end{bmatrix} = \begin{bmatrix} \omega_d \\ \omega_V \end{bmatrix}$$

$$H_k = [1 \quad 0], \quad v_k = z_k \quad 6\text{-}32$$

ii. Initial state estimation and the covariance of that estimations is described as

$$x_0 = \begin{bmatrix} 0 \\ 1 \end{bmatrix} \qquad P_0 = (\omega_V)^2 \quad 6\text{-}33$$

iii. One can begin iterating at this juncture by plugging Equations 6-33 into the measurement update equations in Figure 6-3.

Figure 6-7 shows the Kalman filter behavior.

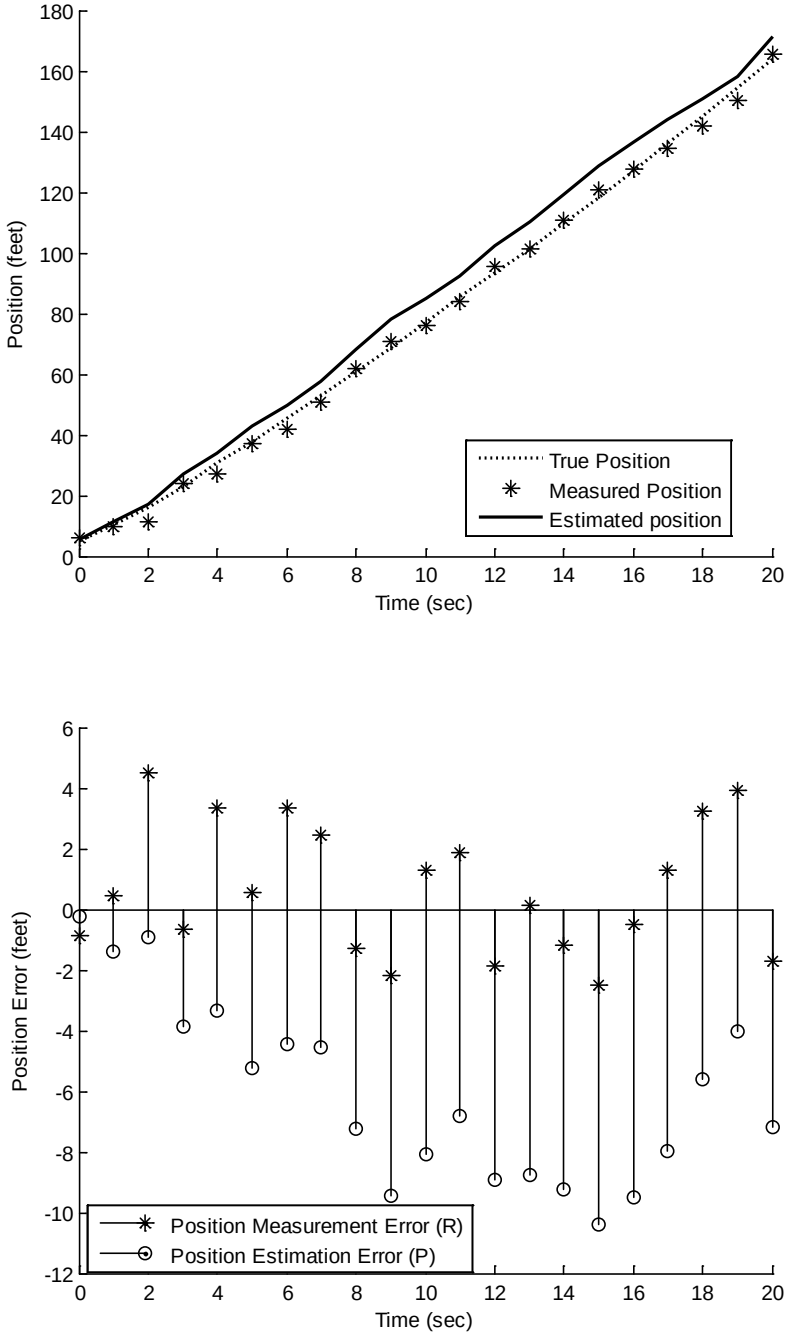

Figure 6-8: Tracking a body with constant velocity (a) Vehicle Position (True, Measured, and Estimated), (b) Position Measurement Error and Position Estimation Error.
$x_0 = \begin{bmatrix} 0 \\ 5 \end{bmatrix}, P_0 = \begin{bmatrix} 0.25 & 0.25 \\ 0.25 & 0.25 \end{bmatrix}, \Delta t = 1.$

Convergence to the Steady-state

Before closing this chapter, an important point should be considered regarding running the Kalman filter. In tuning the filter, a consideration should be given to the convergence of the covariance of the estimation and the gain value to steady-state values after a certain number of time steps. It is possible to test and run the filter to check the convergence but it is more practical to investigate that through some equations instead. Both the *a posteriori* estimation covariance and the Kalman gain value will converge to a steady-state if the *a priori* estimation covariance does also converge (Figure 6-3 and Table 6-2)

On the other hand, it can be proved (Simon, 2006) that the covariance of the *a priori* estimation of a scalar system can be written as

$$P_k^- = \frac{\tau_1\mu_1^{k-1}(2RH^2P_1^- - \tau_2) - \tau_2\mu_2^{k-1}(2H^2P_1^- - \tau_1)}{2H^2\mu_1^{k-1}(2RH^2P_1^- - \tau_2) - 2H^2\mu_2^{k-1}(2H^2P_1^- - \tau_1)}$$

where

$\tau_1 = H^2Q + R(F^2 - 1) + \sigma,$

$\tau_2 = H^2Q + R(F^2 - 1) - \sigma,$

$\mu_1 = H^2Q + R(F^2 + 1) + \sigma,$

$\mu_2 = H^2Q + R(F^2 + 1) - \sigma,$ and

$\sigma = \sqrt{H^2Q + R(F+1)^2}\sqrt{H^2Q + R(F-1)^2}$ 6-34

If we take into account the case where $\mu_2 < \mu_1$, we can easily conclude that as k increases, μ_2^k gets smaller and smaller relative to μ_1^k (Simon, 2006). Therefore, the steady state of the *a priori* estimation covariance can be written as

$$\lim_{k\to\infty} P_k^- = \lim_{k\to\infty} \frac{\tau_1\mu_1^{k-1}(2RH^2P_1^- - \tau_2) - \tau_2\mu_2^{k-1}(2H^2P_1^- - \tau_1)}{2H^2\mu_1^{k-1}(2RH^2P_1^- - \tau_2) - 2H^2\mu_2^{k-1}(2H^2P_1^- - \tau_1)}$$

$$= \lim_{k\to\infty} \frac{\tau_1\mu_1^{k-1}(2RH^2P_1^- - \tau_2)}{2H^2\mu_1^{k-1}(2RH^2P_1^- - \tau_2)}$$

$$= \frac{\tau_1}{2H^2}$$ 6-35

Equations 6-9 and 6-10 can be used to find the steady-state of the *a posteriori* estimation covariance and the Kalman gain value

$$P_k^+ = (I-K_kH_k)P_k^- \quad 5\text{-}9$$

$$K_k = P_k^-H_k{}^T(H_kP_k^-H_k{}^T + R_k)^{-1} \quad 5\text{-}10$$

If we go back to the example 1 where the first simulation was *R=Q=F= H =1*, then the values of parameters of Equation 6-34 are

$$\sigma = \sqrt{H^2Q + R(F+1)^2}\sqrt{H^2Q + R(F-1)^2} =$$

$$\sqrt{1^2 * 1 + 1(1+1)^2}\sqrt{1^2 * 1 + 1(1-1)^2} = \sqrt{5}$$

$$\tau_1 = H^2Q + R(F^2-1) + \sigma = 1^2 * 1 + 1(1^2-1) + \sqrt{5} = 1 + \sqrt{5}$$

$$P_\infty^- = \frac{\tau_1}{2H^2} = \frac{1+\sqrt{5}}{2 * 1^2} = 1.6$$

$$K_\infty = P_\infty^- H_k{}^T\left(H_kP_\infty^-H_k{}^T + R_k\right)^{-1} = 1.6 * 1(1 * 1.6 * 1 + 1)^{-1}$$

$$= \frac{1.6}{2.6} = 0.62$$

$$P_\infty^+ = (I - K_\infty H_k)P_\infty^- = (1 - 0.6 * 1)1.6 = 0.64 \quad 6\text{-}36$$

Figure 6-4 (d) shows the *a priori* and *a posteriori* estimation covariance. The Kalman gain value of this example is plotted in Figure 6-9 and it converges to 0.62.

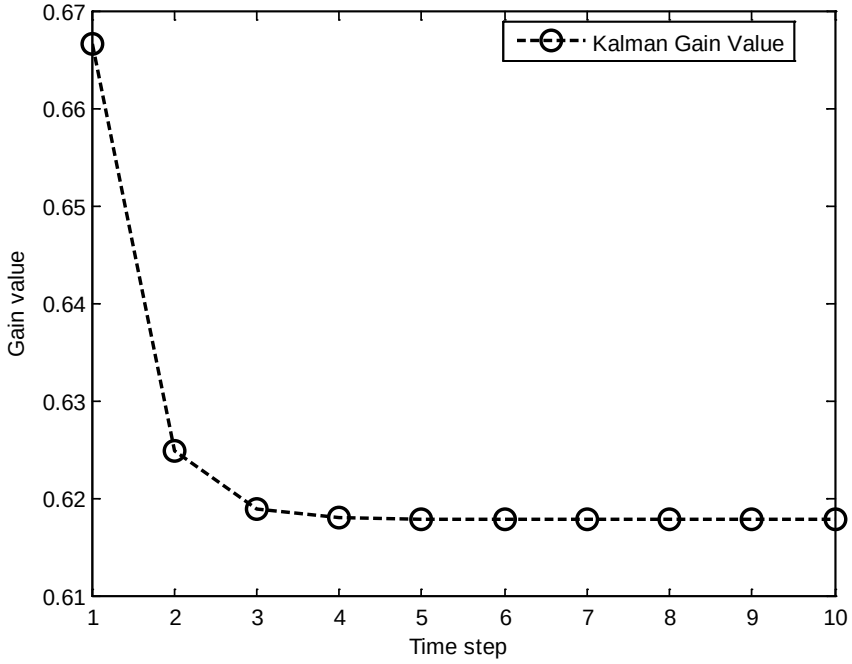

Figure 6-9: Kalman gain value (Example 1, simulation 1 of Chapter 5). The steady-state of the gain value converges to 0.62 (Equation 6-36).

CHAPTER 7. SOME VARIATIONS AND EXTENSIONS OF THE KALMAN FILTER

In this chapter I want to review some generalizations of the Kalman filter. Although there are lots of these generalizations, the purpose of all them is unique and that is to make the filter more flexible and practical for a broader set of problems. In this chapter I will discuss just the ones that I applied to our FTG data in my thesis.

Here are the generalizations that I will cover in this chapter:

- ✓ Kalman filtering with fading memory
- ✓ Constrained Kalman filtering
- ✓ Kalman Smoothers

Fading-memory Kalman filter

As it is discussed in chapter 6, sometimes it is hard to define a model for a system and in case of mismodeling, that happens if our model does not match reality, the Kalman filter might diverge from the true state. One of the solutions for such a case is adding fictitious process noise. It results in giving more weight to the measurements rather than the filter estimations; this way it can reduce the effects of a model that was not defined perfectly. Another way to compensate the effects of mismodeling is using the Kalman filter with fading memory (Schle et all., 1967).

The concept of this version of the Kalman filter is that more emphasis should be given to the recent data. It is achieved by entering an α term in the cost function and consequently, forcing the filter to converge to an estimate that reduces the weight of old measurements while increases the weight of the most recent ones. In standard Kalman filter, this α term is considered to be 1 so equal weight is given to all measurements (regardless of old or new ones) while in fading memory filter it set to be greater than 1 . The solution to such a cost function is the Kalman gain in which R_k is replaced with $\alpha^{-2k}R_k$ and Q_k is replaced with $\alpha^{-2k-2}Q_k$ (Sorenson and Sacks, 1971). The original Kalman filter gain is written as

$$K_k = P_k^- H_k^T (H_k P_k^- H_k^T + R_k)^{-1} = P_k^+ H_k^T R_k^{-1} \qquad 6\text{-}10$$

Replacing R_k and Q_k with their new solutions gives

$$K_k = P_k^- H_k{}^T (H_k P_k^- H_k{}^T + \alpha^{-2k} R_k)^{-1} \quad 7\text{-}1$$
$$= P_k^- H_k{}^T [\alpha^{-2k} \left(H_k \alpha^{2k} P_k^- H_k{}^T + R_k\right)]^{-1}$$
$$= \alpha^{2k} P_k^- H_k{}^T (H_k \alpha^{2k} P_k^- H_k{}^T + R_k)^{-1}$$

Time update equation for estimation error covariance can be calculated replacing Q_k with its new solution in equation 6-7

$$\mathrm{P_k^-} = \mathrm{F_{k\text{-}1} P_{k\text{-}1}^+ F_{k\text{-}1}^T} + \mathrm{Q_{k\text{-}1}} \quad 6\text{-}7$$

$$P_k^- = F_{k-1} P_{k-1}^+ F_{k-1}^T + \alpha^{-2k} Q_{k-1} \quad 7\text{-}2$$

Multiplying both sides of the equation in α^{2k} results

$$\alpha^{2k} P_k^- = F_{k-1} \alpha^{2k} P_{k-1}^+ F_{k-1}^T + Q_{k-1} \quad 7\text{-}3$$

For time update equations, all time steps on the right hand side of the equation should be stated based on $k-1$ while on the right hand side should be stated based on k so

$$\alpha^{2k} P_k^- = \alpha^2 F_{k-1} \alpha^{2(k-1)} P_{k-1}^+ F_{k-1}^T + Q_{k-1} \quad 7\text{-}4$$

On the other hand, measurement update equation for calculating estimation error covariance is stated as

$$P_k^+ = P_k^- - K_k H_k P_k^- \quad 6\text{-}9$$

To make it in accordance with 7-4, both sides of the equation is multiplied by α^{2k}.

$$\alpha^{2k} P_k^+ = \alpha^{2k} P_k^- - K_k H_k \alpha^{2k} P_k^- \quad 7\text{-}5$$

The state update equations remain unchanged since there is no R or Q in them.

$$\mathrm{x_k^-} = \mathrm{F_{k\text{-}1} \hat{x}_{k\text{-}1}^+ + G_{k\text{-}1} u_{k\text{-}1}} \quad \textit{6-6}$$

$$\mathrm{\hat{x}_k^+ = \hat{x}_k^- + K_k \left(y_k\text{-}H_k \hat{x}_k^-\right)} \quad \textit{6-8}$$

Defining two new parameters $\tilde{P}_k^-$ and $\tilde{P}_k^+$ as below can lead to fading memory Kalman filter equation as summarized inTable 7-1.

$$\tilde{P}_k^- = \alpha^{2k} P_k^-$$
$$\tilde{P}_k^+ = \alpha^{2k} P_k^+ \quad 7\text{-}6$$

Table 7-1: The Kalman filter operation loop for fading memory Kalman filter.

Time update (Prediction)	Measurement update (Correction)
1) Priori update $x_k^- = F_{k-1}\hat{x}_{k-1}^+ + G_{k-1}u_{k-1}$	3) Kalman gain $K_k = \tilde{P}_k^- H_k{}^T (H_k \tilde{P}_k^- H_k{}^T + R_k)^{-1}$
2) Priori error covariance $\tilde{P}_k^- = \alpha^2 F_{k-1}\tilde{P}_{k-1}^+ F_{k-1}^T + Q_{k-1}$	4) Posteriori update $\hat{x}_k^+ = \hat{x}_k^- + K_k(y_k - H_k\hat{x}_k^-)$ 5) Posteriori error covariance $\tilde{P}_k^+ = \tilde{P}_k^- - K_k H_k \tilde{P}_k^-$

Running and tuning the filter has the same steps as discussed before in chapter 6:

I. **<u>Building a model:</u>** the system and measurement equations are as stated in equations 6-1 and 6-2.

II. **<u>Initializing the process:</u>** the filter initialized as equations 6-11 and 6-12.

III. **<u>Iterating the procedure:</u>** operation loop summarized in Table 7-1 should be run repeatedly.

Figure 7-1 illustrates how fading memory Kalman filter emphasizes on the recent measurement by giving more weight to it rather than the model suggestion in estimation process. It can be observed comparing 7-1c and 7-1f. Gain value is the parameter determining the importance of the most recent measurement in estimation. The higher the gain value is the more weight is given to the measurement. The effect of α parameter and how it affects the filter operation in fading memory version is clear comparing 7-1 a and 7-1 d. In standard Kalman filter; when process noise estimation covariance (Q) is zero (i.e. when we are 100% confident about our model) the best estimate that can be made is what the model tells us. It means that after some time steps, the Kalman gain value converges to zero and the measurements are neglected completely in estimation process. While, in fading memory Kalman filter, even when Q is zero, some weight will be given to the measurements and the estimation is something between what the model predicts and the measured value. In standard Kalman filter, when the confidence about the model is 100%, there is no doubt in the filter estimation. It means that the output of

the filter, which is the model prediction, is 100% accurate ($P \to 0$)(Figure 7-1 f). While, in fading memory filter, some weight will be given to the measurement, there is always some degree of uncertainty in estimation so $P \neq 0$ (Figure 7-1c).

The following example can be modelled as

$$x_k = x_{k-1}$$
$$y_k = H_k x_k + v_k$$
$$v_k \sim (0, R_k)$$
$$Q_k = 0 \qquad \text{7-7}$$

According to chapter 6, the steady state of the standard Kalman filter is calculated as (Figures 7-1b and 7-1c).

$$\sigma = \sqrt{H^2Q + R(F+1)^2}\sqrt{H^2Q + R(F-1)^2}$$
$$\tau_1 = H^2Q + R(F^2 - 1) + \sigma$$
$$\lim_{k\to\infty} P_k^- = \frac{\tau_1}{2H^2} = 0$$
$$K_\infty = P_\infty^- {H_k}^T \left(H_k P_\infty^- {H_k}^T + R_k\right)^{-1} = 0$$
$$P_\infty^+ = (I - K_\infty H_k) P_\infty^- = 0 \qquad \text{7-8}$$

For fading memory filter, the steady state is determined using equation in Table 7-1.

$$\tilde{P}_k^- = \alpha^2 \tilde{P}_{k-1}^+$$
$$K_k = \tilde{P}_k^- {H_k}^T (H_k \tilde{P}_k^- {H_k}^T + R_k)^{-1} = \frac{\tilde{P}_k^-}{\tilde{P}_k^- + R_k}$$
$$= \frac{\alpha^2 \tilde{P}_{k-1}^+}{\alpha^2 \tilde{P}_{k-1}^+ + R}$$
$$\tilde{P}_k^+ = \tilde{P}_k^- - K_k \tilde{P}_k^-$$
$$= \alpha^2 \tilde{P}_{k-1}^+ - \left(\frac{\alpha^2 \tilde{P}_{k-1}^+}{\alpha^2 \tilde{P}_{k-1}^+ + R}\right) \alpha^2 \tilde{P}_{k-1}^+ \qquad \text{7-9}$$

When steady state of the system is reached, we expect $\tilde{P}_k^+ = \tilde{P}_{k-1}^+$

$$\tilde{P}_\infty^+ = \alpha^2 \tilde{P}_\infty^+ - \left(\frac{\alpha^2 \tilde{P}_\infty^+}{\alpha^2 \tilde{P}_\infty^+ + R}\right) \alpha^2 \tilde{P}_\infty^+$$
$$1 = \alpha^2 - \left(\frac{\alpha^2 \tilde{P}_\infty^+}{\alpha^2 \tilde{P}_\infty^+ + R}\right) \alpha^2$$

$$1 = \frac{\alpha^2 R}{\alpha^2 \tilde{P}_\infty^+ + R}$$

$$\tilde{P}_\infty^+ = \frac{R(\alpha^2-1)}{\alpha^2} \qquad 7\text{-}10$$

Substituting 7-10 in 7-9, the gain value for the steady state can be written as

$$K_\infty = \frac{\alpha^2 \tilde{P}_\infty^+}{\alpha^2 \tilde{P}_\infty^+ + R} = \frac{R(\alpha^2-1)}{R(\alpha^2-1)+R}$$

$$= \frac{(\alpha^2-1)}{(\alpha^2-1)+1}$$

$$= \frac{(\alpha^2-1)}{\alpha^2} \qquad 7\text{-}11$$

In the following example

$R = 0.5 \qquad and \qquad \alpha = 1.1$

Substituting these values in 7-10 and 7-11 gives (Figures 7-1 b and 7-1 c)

$P_\infty = 0.087 \quad and \quad K_\infty = 0.17$

In standard filter ($\alpha = 1$), so equations 7-10 and 7-11 converge to zero as it is expected.

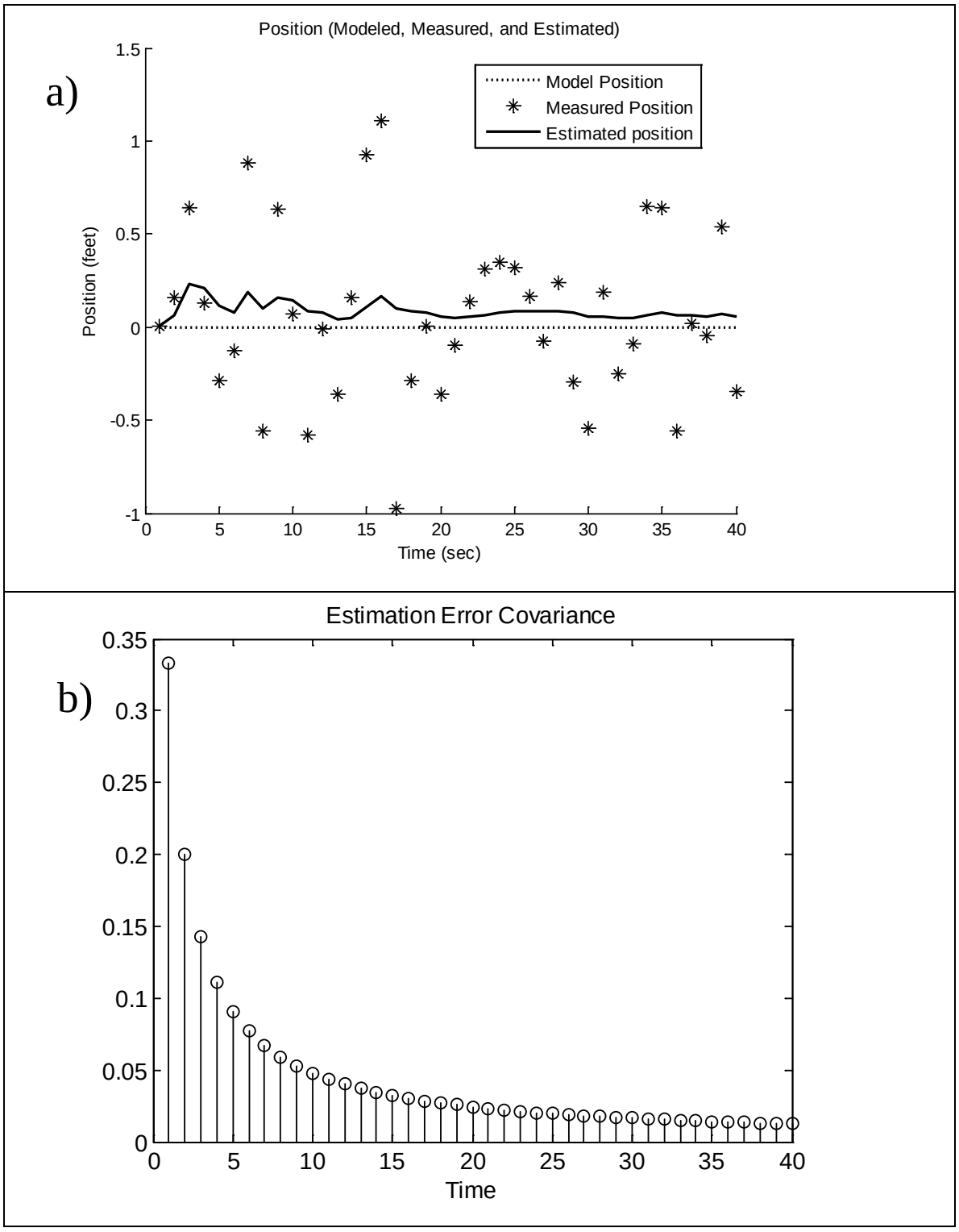
a)
Position (Modeled, Measured, and Estimated)
Model Position
Measured Position
Estimated position
Position (feet)
Time (sec)
b)
Estimation Error Covariance
Time

c)

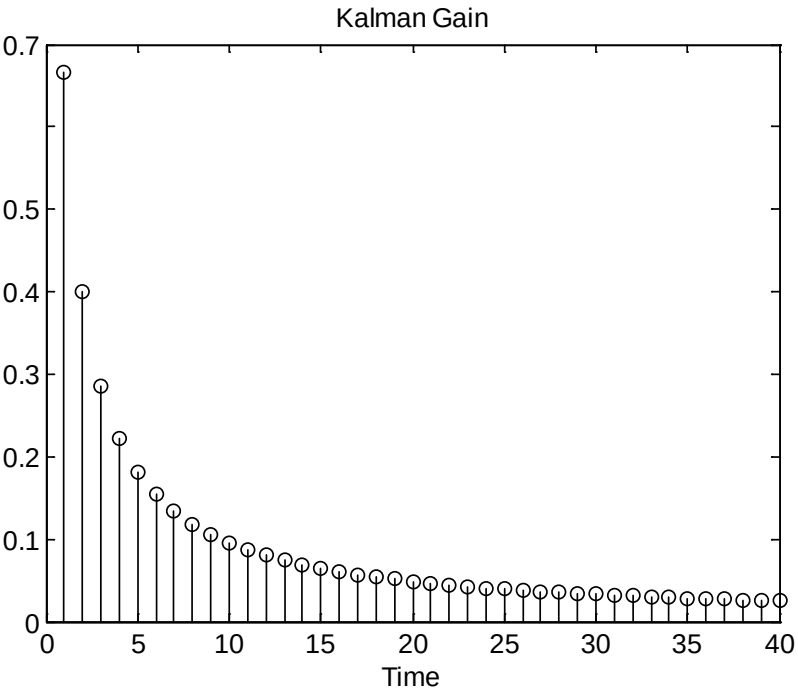
Kalman Gain
0.7
0.5
0.4
0.3
0.2
0.1
0
0
5
10
15
20
25
30
35
40
Time

d)

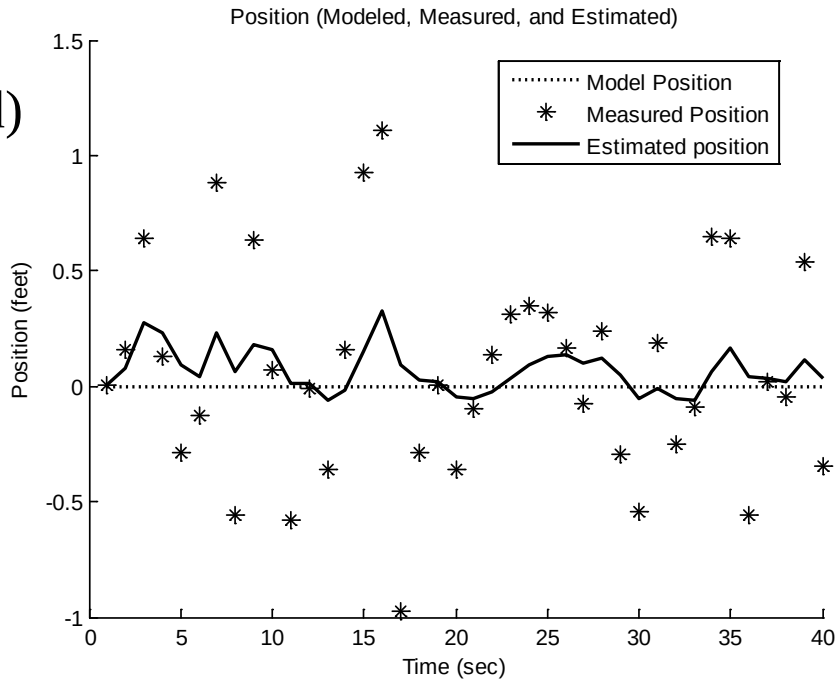
Position (Modeled, Measured, and Estimated)
Model Position
Measured Position
Estimated position
Position (feet)
1.5
1
0.5
0
-0.5
-1
0
5
10
15
20
25
30
35
40
Time (sec)

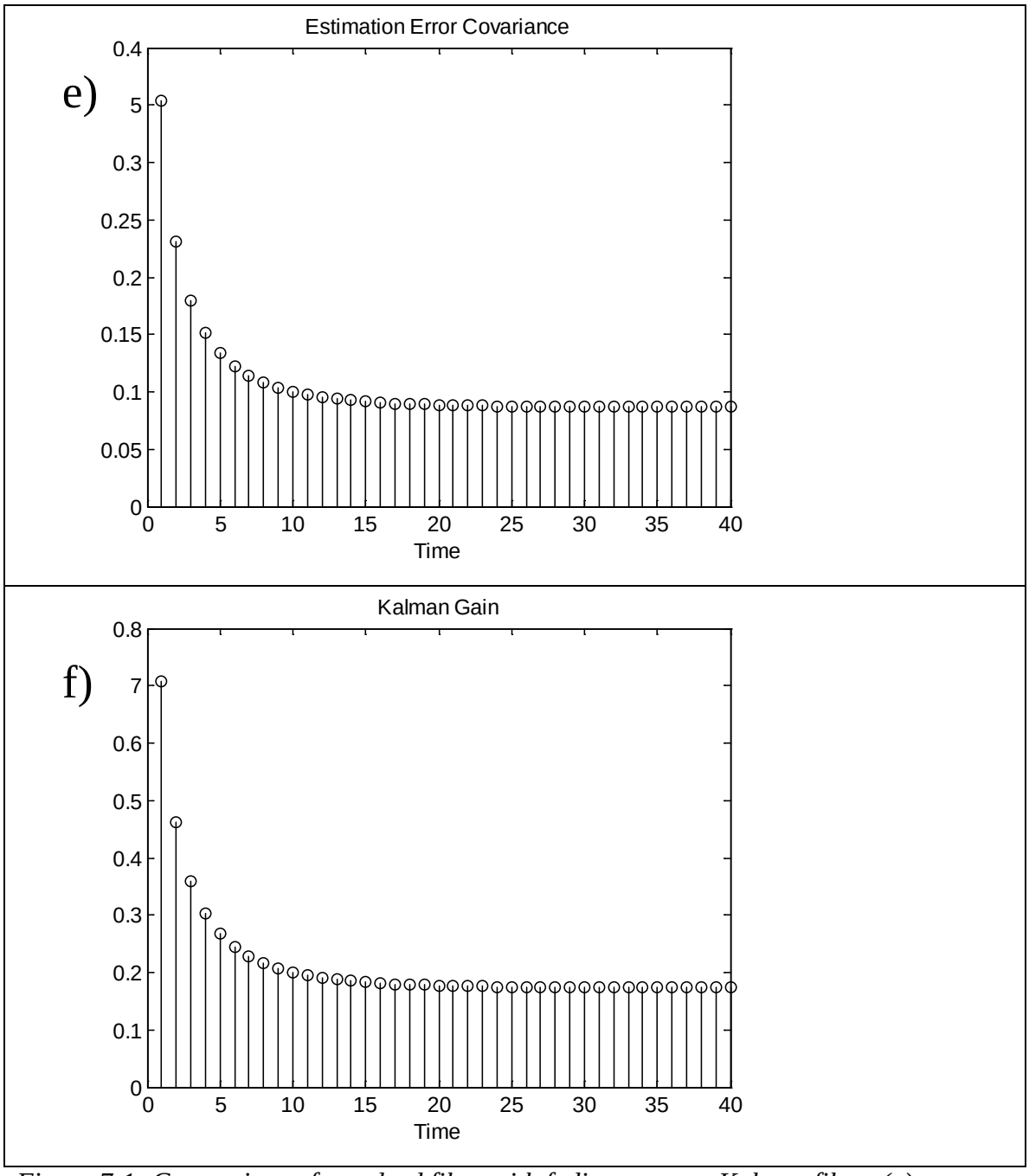

Figure 7-1: Comparison of standard filter with fading memory Kalman filter. (a) modelled, measured and estimated position from a standard Kalman filter (b) the corresponding estimation error covariance converging to zero; the estimation are believed to be 100% accurate (c) the gain value tends to be zero in higher time steps; resulting in neglecting the measurements and giving all weight to the modelled estimate . d) The same system but using the fading memory Kalman filter (alpha is considered 1.1). The filter is more responsive to new measurements. (e) The estimation error covariance. Although the process noise covariance is zero $(Q = 0)$*, the estimations always have a degree of uncertainty so P does not reach zero. (f) Kalman gain for the fading memory filter. It never converges to zero so always some weight is given to the measurements.*

Constrained Kalman filter

Sometimes there is some information about the model that is neglected in running the filter because it is difficult to simply involve them in the structure. On the other hand, we want that information to be incorporated in the filtering procedure to get more accurate estimations. This additional information might be in the form of equality (e.g., fixed speed of a moving object) or inequality constraints (e.g., maximum speed of a motor) (Simon, 2010).

Model reduction (Wen and Durrant-Whyte, 1992), perfect measurements (Porrill, 1988), projection approaches (Hayward, 1998) and A pdf truncation approach (Simon and Chia, 2002; and Simon, 2006) are the different ways that researchers treat the constraints. Here, I will only focus on discussing the first two approaches that mathematically are identical (Simon, 2010). The straightforward model reduction approach that works based on diminishing the parameters of the system usually can be easily implemented. Reducing the dimension of the problem brings up the advantage of the method which is less computational effort. In spite of simplicity of the approach, it has two major disadvantages that sometimes make it undesirable. First, sometimes reducing the dimension of the problem makes the physical meaning of the state lost; it would be difficult to recognize and interpret the state equations. Second, this approach is only applicable for equality equations (i.e. $Dx = d$) and cannot be used directly for inequality constraints (i.e. $Dx \leq d$)(Simon, 2006).

Suppose the system that we are dealing with has 3 variables ($x_1, x_2\ and\ x_3$) and 3 measured parameters ($y_1, y_2\ and\ y_3$). The state, measurement, and observation matrices can be written

$$x_k = \begin{bmatrix} x_1 \\ x_2 \\ x_3 \end{bmatrix} \qquad H = \begin{bmatrix} 1 & 0 & 0 \\ 0 & 1 & 0 \\ 0 & 0 & 1 \end{bmatrix} \qquad y_k = \begin{bmatrix} y_1 \\ y_2 \\ y_3 \end{bmatrix} \tag{7-12}$$

So the system is defined by the following equations as

$$x_{k+1} = \begin{bmatrix} 1 & 0 & 0 \\ 0 & 1 & 0 \\ 0 & 0 & 1 \end{bmatrix} x_k + \begin{bmatrix} \omega_{k1} \\ \omega_{k2} \\ \omega_{k3} \end{bmatrix}$$

$$y_k = \begin{bmatrix} 1 & 0 & 0 \\ 0 & 1 & 0 \\ 0 & 0 & 1 \end{bmatrix} x_k + \begin{bmatrix} v_{k1} \\ v_{k2} \\ v_{k3} \end{bmatrix} \quad 7\text{-}13$$

If from the scientific fact underlying the problem, it is kwon that the following constraint is always satisfied between the states,

$$x_1 + x_2 + x_3 = 0 \quad 7\text{-}14$$

Then the dimension of the problem can be reduced:

$$x_3 = -(x_1 + x_2) \quad 7\text{-}15$$

Substituting this in measurement and transition matrix results in

$$x_{k+1}(1) = x_k(1)$$

$$x_{k+1}(2) = x_k(2)$$

$$y_k = \begin{bmatrix} x_1 \\ x_2 \\ x_3 \end{bmatrix} + \begin{bmatrix} v_1 \\ v_2 \\ v_3 \end{bmatrix}$$

$$y_k = \begin{bmatrix} x_1 \\ x_2 \\ -(x_1 + x_2) \end{bmatrix} + \begin{bmatrix} v_1 \\ v_2 \\ v_3 \end{bmatrix}$$

$$F = H = \begin{bmatrix} 1 & 0 \\ 0 & 1 \end{bmatrix} \quad 7\text{-}16$$

Some researchers involve the state constraints in the Kalman filter operation loop by considering them as perfect measurements (Porrill, 1988). Supposing the constraint is given as $Dx_k = d$, it can be interpreted there are some perfect measurements available that have not been contaminated by any noise $v_k = 0$. The measurement update equation of standard Kalman filter can be augmented by adding this information as

$$\begin{bmatrix} y_k \\ d \end{bmatrix} = \begin{bmatrix} H \\ D \end{bmatrix} x_k + \begin{bmatrix} v_k \\ 0 \end{bmatrix} \quad 7\text{-}17$$

The time update and the estimation error covariance equations are as the standard filter. I used the perfect measurement method to incorporate Laplace's equation in our filtering procedure. Laplace's equation is written as

$$x_1 + x_2 + x_3 = 0 \quad 7\text{-}18$$

The measurement update equation for our case of study is defined as

$$\begin{bmatrix} y_1 \\ y_2 \\ y_3 \\ 0 \end{bmatrix} = \begin{bmatrix} 1 & 0 & 0 \\ 0 & 1 & 0 \\ 0 & 0 & 1 \\ 1 & 1 & 1 \end{bmatrix} x_k + \begin{bmatrix} v_1 \\ v_2 \\ v_3 \\ 0 \end{bmatrix} \quad 7\text{-}19$$

Figure 7-2 compares standard and constrained filter results. It can be seen that constrained filter (perfect measurement) results are closer to the model estimations (true position) and is more successful in determining the position than the standard filter. Table 7-2 illustrates this comparison quantitatively by evaluating RMS (Root Mean Square) errors. The table shows that the root mean square of the difference between modeled and estimated position is less in constrained Kalman filter and it can be seen in Figure 7-2 as well. But the best point about the constrained Kalman filter is that although its estimation are close to the estimations of the standard filter, it can estimate so that the state estimate get close to the constraint (Table 7-2, RMS error based on the $x_1+x_2+x_3=0$ criterion).

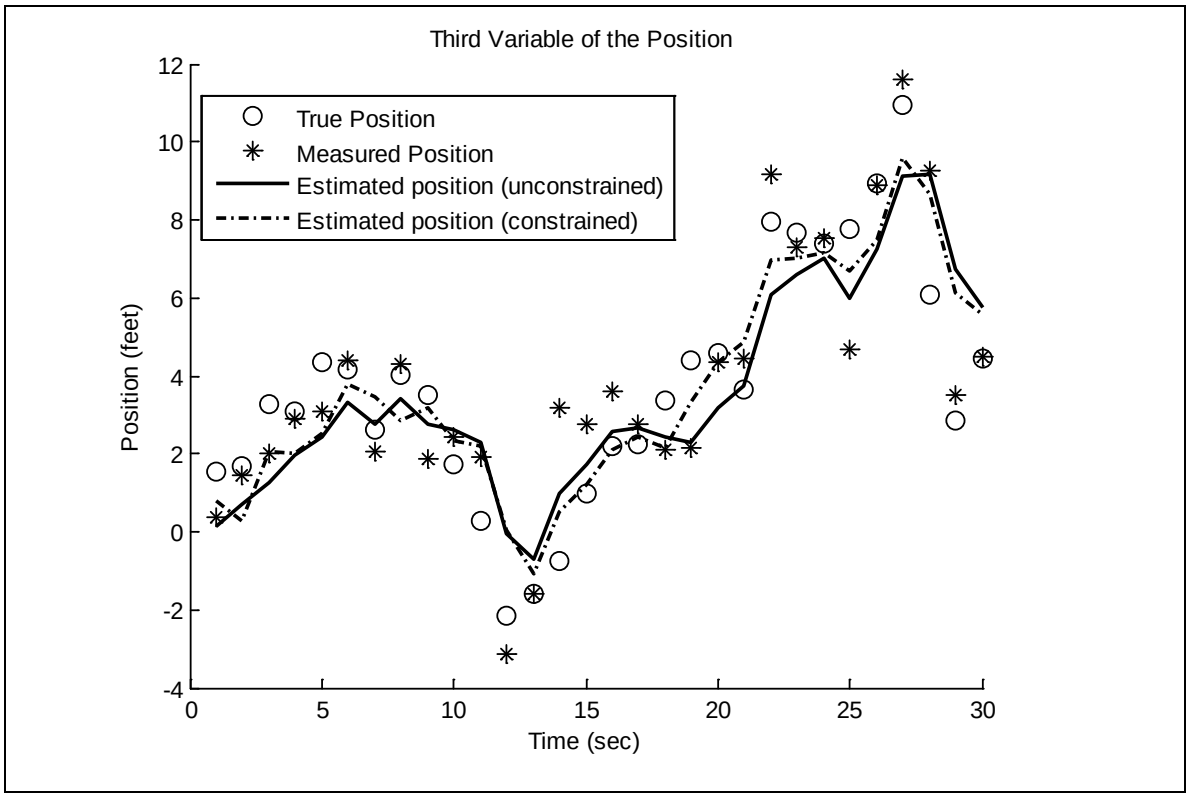

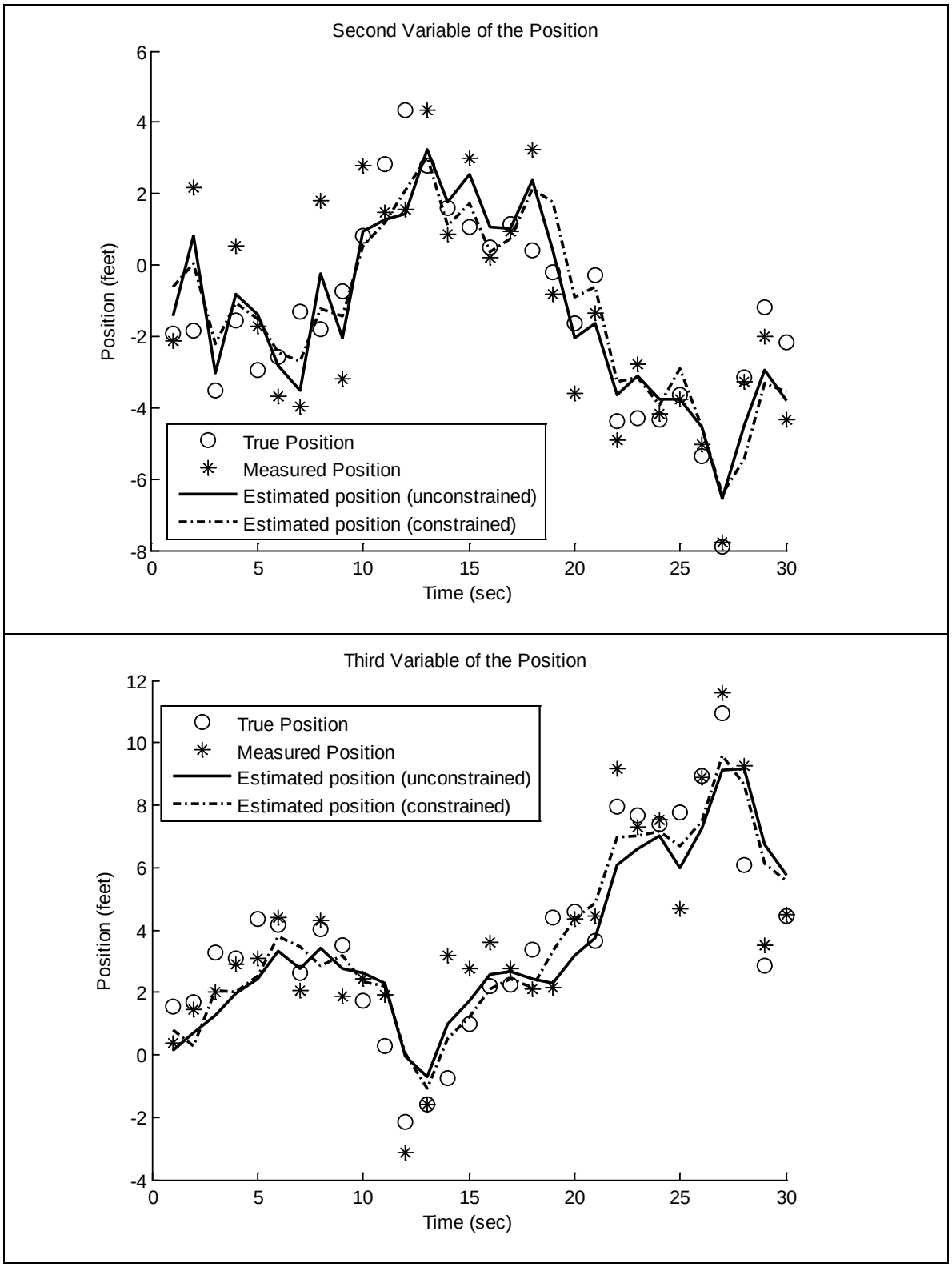

Figure 7-2: Comparison of standard and constrained Kalman filter (solid line versus dashed one).

Table 7-2: Root Mean Square error for the following example analyzing standard and constrained Kalman filter operation.

	Standard Kalman filter	Constrained Kalman filter
RMS error of the state variables (True position – estimated position)	1.983	1.6299
RMS error regarding the criterion ($x_1+x_2+x_3=0$)	1.4419	6.1615e-016

The Perfect measurement approach is easy to understand and incorporate but it also has some disadvantages: it can increase the possibility of numerical problems such as zero determinants that results in a non-invertible matrix plus like model reduction it is applicable for equality constraints directly and not for the inequality problems. Also it increases the size of the matrix that needs to be inverted by adding rows to the measurement equation (equation 7-17) (Simon and Chia, 2002).

Kalman smoothers

Estimations that can be obtained in standard Kalman filters use past and current observations to predict the current state so estimations are limited to *a priori* and *a posteriori* estimations (Figure 6-2). The *a priori* estimate (x_k^-) of a time step which is obtained from the time update equation is based on measurements up to that particular time step while *a posteriori* one (x_k^+), calculated from the measurement update step, is based on measurements up to and including that given time step.

$$\hat{x}_k^+ = E[\, x_k \mid y_1, y_2, \dots y_k] = a\ posteriori\ estimate$$

$$\hat{x}_k^- = E\left[\, x_k \mid y_1, y_2, \dots y_{k-1}\right] = \text{a priori estimate} \qquad 7\text{-}20$$

Although the past and current information is adequate for calculating the system state, it is not optimal; the estimations can be improved by considering all available data to estimate the sequence of states (Nakata and Tonetti, 2010). That is applicable for problems that estimations are made after all measurements are recorded (off-line estimation problems) or for the systems estimations can be made with some delay (on-line estimation problems) (Shimkin, 2009). Suppose the measurements include records up to time step 20 and the best estimate of time 10 is requested. According to chapter 6 and the above definition, estimation based on measurements 1 to 9 is *a priori* ($\hat{x}_{10}^-$) and if

measurement 10 is considered as well the estimation obtained would be *a posteriori* ($\hat{x}_{10}^{+}$). It is clear that availability of measurements up to time 20 might be a help to have an even better estimate of x_{10}. This argument is just a start point to show there are more varieties of estimations than just *a priori* and *a priori* one. The extension of the Kalman filter which improves the standard filter by adding future measurements is known as *Optimal Smoothing.*

Before discussing optimal smoothing, it worth mentioning that there is another common notation used in most text books to indicate the measurements that have been considered for the estimation of a given time. That is, $\hat{x}_{k,j}$ is the best estimate of time step k given all the measurements up to an including time j. With this notation *a priori* and *a posteriori* estimations are defined as

$$\hat{x}_k^- = \hat{x}_{k,k-1}$$
$$\hat{x}_k^+ = \hat{x}_{k,k} \qquad 7\text{-}21$$

According to this notation, the Kalman smoothers that are listed as three main types can be noted as the following (Shimkin, 2009):

- ✓ Fixed-point smoothing: $\hat{x}_{M_0|k} for\ k = M_0, M_0 + 1, \ldots$
- ✓ Fixed-lag smoothing: $\hat{x}_{k|k+l_0} for k = 0,1, \ldots$ 7-22
- ✓ Fixed-interval smoothing: $\hat{x}_{k|P_0} for\ k = 0,1, \ldots P_0$

A common feature among the smoothers is that future measurements are considered in estimations. In fixed point smoothing, the goal is to get the best estimate of a fixed point (N_0) incorporating new additional measurements ($M_0, M_0 + 1, \ldots$). In other words, with this approach, as time progresses, we continue to update the estimate of point (N_0) based on the increasing number of measurements and thus improve the quality of our estimation ($\hat{x}_k$).

Using the fix-lag smoother, we try to obtain an estimate of the state ($\hat{x}_k$) given measurements up to and including time $+l_0$. In this scenario, as new measurements are added to our information, the time index of the estimation point , (k), changes but the lag l_0 remains constant. This way, for each estimation point, l_0 future measurements are taken into account.

For the last type of smoothers, fixed-interval smoothing, a fixed interval of measurements is available $(y_1, y_2, \ldots, y_{P_0})$ and the target is to use all the measurements in the interval for some of the interior points of the interval. Table 7-3 depicts the Kalman smoothers at estimation times *k* and *k+1*. Table 7-4 brings an example for each of them.

Table 7-3: Kalman smoothers at estimation points k and k+1.

	Time step k	Time step k+1
Fixed-point smoother	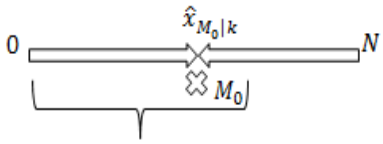	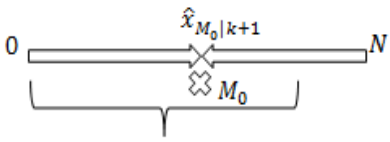
Fixed-lag smoother	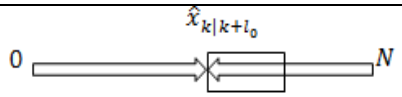	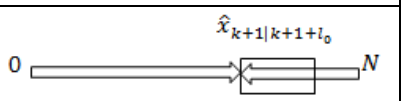
Fixed-interval smoother	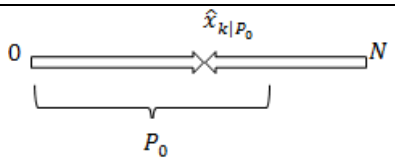	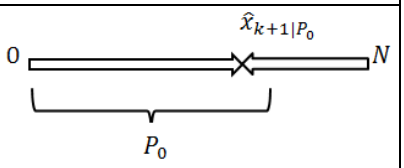

Table 7-4: Kalman smoothers and the corresponding examples taken from Simon 2006.

Fixed-point smoother	A satellite orbits continually and sends photographs to be process and displayed for a particular fixed point.
Fixed-lag smoother	A satellite orbits continually and sends photographs to be shown with a constant delay for each point.
Fixed-interval smoother	During the weekend all data has been recorded and after the weekend, all collected data are going to be used for the estimation of the state for each point

Here, just the fixed-lag smoother is discussed since that is the approach that I used for filtering. I selected this method to reduce the effect of nonlinearity that we had in our data and improve the quality of the estimations.

Before explaining how the fixed-lag Kalman filter works, we need to derive an alternative form for the Kalman filter.

An alternative form for the Kalman filter

As Table 6-2 shows one-step Kalman filter is determined as

$$\begin{cases} K_k = P_k^- H_k^T (H_k P_k^- H_k^T + R_k)^{-1} = P_k^+ H_k^T R_k^{-1} & 6\text{-}10 \\ \hat{x}_{k+1}^- = F_k (I - K_k H_k)\, \hat{x}_k^- + F_k K_k y_k + G_k u_k & 6\text{-}14 \\ P_{k+1}^- = F_k P_k^- F_k^T - F_k P_k^- H_k^T (H_k P_k^- H_k^T + R_k)^{-1} H_k P_k^- F_k^T + Q_k & 6\text{-}16 \end{cases}$$

On the other hand, we define L_k as

$$L_k = F_k K_k \qquad 7\text{-}23$$

where L_k is the redefined Kalman gain, $F_k$is the state transition matrix, and K_k is the standard Kalman gain.

Multiplying both sides of equation 6-10 in F_k results in

$$L_k = F_k P_k^- H_k^T (H_k P_k^- H_k^T + R_k)^{-1} \qquad 7\text{-}24$$

Assuming $G_k = 0$, the state update equation 6-14 can be written as

$$\begin{aligned} \hat{x}_{k+1}^- &= F_k \hat{x}_k^- - F_k K_k H_k \hat{x}_k^- + F_k K_k y_k \\ &= F_k \hat{x}_k^- + F_k K_k (y_k - H_k \hat{x}_k^-) \\ &= F_k \hat{x}_k^- + L_k (y_k - H_k \hat{x}_k^-) \end{aligned} \qquad 7\text{-}25$$

Rearranging the priori estimation error covariance, equation 6-16 gives us

$$\begin{aligned} P_{k+1}^- &= F_k P_k^- \left[F_k^T - H_k^T \left(H_k P_k^- H_k^T + R_k \right)^{-1} H_k P_k^- F_k^T \right] + Q_k \\ &= F_k P_k^- \left[F_k^T - H_k^T K_k^T F_k^T \right] + Q_k \\ &= F_k P_k^- \left[F_k - F_k K_k H_k \right]^T + Q_k \\ &= F_k P_k^- \left[F_k - L_k H_k \right]^T + Q_k \end{aligned} \qquad 7\text{-}26$$

Equations 7-24, 7-25, and 7-26 build another alternative form of the standard Kalman filter.

$$\begin{cases} L_k = F_k P_k^- H_k^T (H_k P_k^- H_k^T + R_k)^{-1} \\ \hat{x}_{k+1}^- = F_k \hat{x}_k^- + L_k (y_k - H_k \hat{x}_k^-) \\ P_{k+1}^- = F_k P_k^- \left[F_k - L_k H_k \right]^T + Q_k \end{cases} \qquad 7\text{-}27$$

Deriving the fixed-lag smoother

As equation 7-22 and Table 7-3 show, in fixed-lag method our goal is to calculate the best estimate of each estimation point based on measurements up to and including N future time steps. That is, our estimation of a state at time t_{k-N} is calculated considering measurements until time t_k. As measurements are obtained, time index k changes while the lag N remains constant. So what the filter determines is $\hat{x}_{k-N|k}$ for $k = N, N+1, \ldots$

The main idea is to define an "augmented state vector", x_{k+1}, and corresponding augmented system equation. A new notation is defined here as $x_{k,m}$ and it refers to the state of x_{k-m} which propagates from time $k-m$ to time k with an identity transition matrix and zero process noise. Following this definition,

$$x_{k+1,1} = x_k$$
$$x_{k+1,2} = x_{k-1} = x_{k,1}$$
$$x_{k+1,3} = x_{k-2} = x_{k,2}$$
$$\vdots \qquad \text{7-28}$$

From equation 7-28 it can be concluded that

$$x_{k+1,N+1} = x_{k,N} = x_{k-1,N-1} = \cdots = x_{k-N} \qquad \text{7-29}$$

Combining above equations and the state update equation (6-19), the augmented system can be delineated as

$$x_{k+1} = F_k x_k + \omega_k \qquad \text{6-19}$$

$$\begin{bmatrix} x_{k+1} \\ x_{k+1,1} \\ \vdots \\ x_{k+1,N+1} \end{bmatrix} = \begin{bmatrix} F_k & 0 & \cdots & 0 \\ I & 0 & \cdots & 0 \\ \vdots & \ddots & \ddots & \vdots \\ 0 & \ldots & I & 0 \end{bmatrix} \begin{bmatrix} x_k \\ x_{k,1} \\ \vdots \\ x_{k,N+1} \end{bmatrix} + \begin{bmatrix} I \\ 0 \\ \vdots \\ 0 \end{bmatrix} \omega_k \qquad \text{7-30}$$

The first row of equation 7-30 composes the dynamic system and the remaining rows form the successive time delays. It helps us to calculate the state of the system; x_k is the state of the system at time t_k and the components of the augmented vector are sequentially delayed states. The last component of the augmented state vector at time t_{k+1} is what we wish to calculate in a smoothed filter. In other words, this last component is $\hat{x}_{k-N|K}$.

Considering the measurement equation (6-19), it can be augmented as

$$y_k = H_k x_k + v_k \qquad \text{6-19}$$

$$y_k = [H_k \quad 0 \quad 0 \quad \dots \quad 0] \begin{bmatrix} x_k \\ x_{k,1} \\ \vdots \\ x_{k,N+1} \end{bmatrix} + v_k \qquad 7\text{-}31$$

where the terms F_k, H_k, ω_k, and $v_k$are the same as those explained in Table 6-1.

Covariance of the augmented state estimate and the augmented Kalman gain matrix are delineated as

$$P_{k+1}^{-} = \begin{bmatrix} P_{k+1}^{0,0} & P_{k+1}^{0,1} & \dots & P_{k+1}^{0,N+1} \\ P_{k+1}^{1,0} & P_{k+1}^{1,1} & \dots & P_{k+1}^{1,N+1} \\ \vdots & \vdots & \dots & \vdots \\ P_{k+1}^{N+1,0} & P_{k+1}^{N+1,1} & \dots & P_{k+1}^{N+1,N+1} \end{bmatrix} \qquad L_k = \begin{bmatrix} L_{k,0} \\ L_{k,1} \\ \vdots \\ L_{k,N+1} \end{bmatrix} \qquad 7\text{-}32$$

<u>State estimation</u>

Substituting state transition matrix from 7-30 into 7-25 yields:

$$\begin{bmatrix} x_{k+1} \\ x_{k+1,1} \\ \vdots \\ x_{k+1,N+1} \end{bmatrix} = \begin{bmatrix} F_k & 0 & \cdots & 0 \\ I & 0 & \cdots & 0 \\ \vdots & \ddots & \ddots & \vdots \\ 0 & \dots & I & 0 \end{bmatrix} \begin{bmatrix} x_k \\ x_{k,1} \\ \vdots \\ x_{k,N+1} \end{bmatrix} + \begin{bmatrix} L_{k,0} \\ L_{k,1} \\ \vdots \\ L_{k,N+1} \end{bmatrix} \left(y_k - [H_k \quad 0 \quad 0 \quad \dots \quad 0] \begin{bmatrix} x_k \\ x_{k,1} \\ \vdots \\ x_{k,N+1} \end{bmatrix} \right) \qquad 7\text{-}33$$

Equation 7-28 states that

$x_{k+1} = x_{k+1|k} = \hat{x}_{k+1}^{-}$

$x_{k+1,1} = x_{k|k} = \hat{x}_k^{+}$

$x_{k+1,2} = \hat{x}_{k-1|k}$

$\vdots$

$x_{k+1,N+1} = \hat{x}_{k-N|k}$ 7-34

Similarly, for the right hand side of the equation:

$x_k = x_{k|k-1} = \hat{x}_k^{-}$

$x_{k+1,1} = \hat{x}_{k-1|k-1}$

$\vdots$

$x_{k,N+1} = \hat{x}_{k-N-1|k-1}$ 7-35

Substituting 7-34 and 7-35 in 7-33 results in state update equation as

$$\begin{bmatrix} \hat{x}_{k+1}^{-} \\ \hat{x}_{k|k} \\ \vdots \\ \hat{x}_{k-N|k} \end{bmatrix} = \begin{bmatrix} F_k & 0 & \cdots & 0 \\ I & 0 & \cdots & 0 \\ \vdots & \ddots & \ddots & \vdots \\ 0 & \ldots & I & 0 \end{bmatrix} \begin{bmatrix} \hat{x}_{k}^{-} \\ \hat{x}_{k-1|k-1} \\ \vdots \\ \hat{x}_{k-N-1|k-1} \end{bmatrix} +$$

$$\begin{bmatrix} L_{k,0} \\ L_{k,1} \\ \vdots \\ L_{k,N+1} \end{bmatrix} \left(y_k - \begin{bmatrix} H_k & 0 & 0 & \ldots & 0 \end{bmatrix} \begin{bmatrix} \hat{x}_{k}^{-} \\ \hat{x}_{k-1|k-1} \\ \vdots \\ \hat{x}_{k-N-1|k-1} \end{bmatrix} \right) \qquad 7\text{-}36$$

The first component of the state vector on the left hand side of the equation 7-36, $\hat{x}_{k+1}^{-}$, is the *a priori* estimate of state at time k+1 taking into account measurements up to and including time k. The second component is estimation of point k having the same data set. Consequently, the last component of the vector, $\hat{x}_{k-N,k}$, is our estimation of point $k-N$, considering measurements up to and including time k and that is the state estimate we want to obtain from fixed-lag smoother. Mathematically, the rows of this equation determine each of the augmented state components.

$$\hat{x}_{k+1}^{-} = F_k \hat{x}_{k}^{-} + L_{k,0}(y_k - H_k \hat{x}_{k}^{-})$$

$$\vdots$$

$$\hat{x}_{k-i|k} = \hat{x}_{k-i|k-1} + L_{k,i+1}(y_k - H_k \hat{x}_{k}^{-})$$

$$\vdots$$

$$\hat{x}_{k-N|k} = \hat{x}_{k-N|k-1} + L_{k,N+1}(y_k - H_k \hat{x}_{k}^{-}) \qquad 7\text{-}37$$

<u>Gain matrices</u>

Taking state transition matrix from 7-30 and substituting it in 7-24 yields:

$$\begin{bmatrix} L_{k,0} \\ L_{k,1} \\ \vdots \\ L_{k,N+1} \end{bmatrix} = \begin{bmatrix} F_k & 0 & \cdots & 0 \\ I & 0 & \cdots & 0 \\ \vdots & \ddots & \ddots & \vdots \\ 0 & \ldots & I & 0 \end{bmatrix} \begin{bmatrix} P_k^{0,0} & P_k^{0,1} & \ldots & P_k^{0,N+1} \\ P_k^{1,0} & P_k^{1,1} & \ldots & P_k^{1,N+1} \\ \vdots & \vdots & \cdots & \vdots \\ P_k^{N+1,0} & P_k^{N+1,1} & \cdots & P_k^{N+1,N+1} \end{bmatrix} \begin{bmatrix} H_k^T \\ 0 \\ \vdots \\ 0 \end{bmatrix} \times$$

$$\left(\begin{bmatrix} H_k & 0 & 0 & \ldots & 0 \end{bmatrix} \begin{bmatrix} P_k^{0,0} & P_k^{0,1} & \ldots & P_k^{0,N+1} \\ P_k^{1,0} & P_k^{1,1} & \ldots & P_k^{1,N+1} \\ \vdots & \vdots & \cdots & \vdots \\ P_k^{N+1,0} & P_k^{N+1,1} & \cdots & P_k^{N+1,N+1} \end{bmatrix} \begin{bmatrix} H_k^T \\ 0 \\ \vdots \\ 0 \end{bmatrix} + R_k \right)^{-1}$$

$$\begin{bmatrix} L_{k,0} \\ L_{k,1} \\ \vdots \\ L_{k,N+1} \end{bmatrix} = \begin{bmatrix} F_k P_k^{0,0} H_k^T \\ P_k^{0,0} H_k^T \\ \vdots \\ P_k^{0,N} H_k^T \end{bmatrix} (H_k P_k^{0,0} H_k^T + R_k)^{-1} \quad 7\text{-}38$$

In the above equation $L_{k,0}$ is the standard Kalman filter gain matrix. From the above equation

$$L_{k,0} = F_k P_k^{0,0} H_k^T (H_k P_k^{0,0} H_k^T + R_k)^{-1} \quad 7\text{-}39$$

Considering that $P_k^{0,0}$ is the *a priori* estimation error covariance, P_k^-,

$$L_{k,0} = F_k P_k^- H_k^T (H_k P_k^- H_k^T + R_k)^{-1} \quad 7\text{-}40$$

That is exactly what we expect (equation 6-10). $L_{k,N+1}$ is the Kalman gain we want to obtain in fixed-lag smoother and is calculated as

$$L_{k,i} = P_k^{0,i-1} H_k^T (H_k P_k^{0,0} H_k^T + R_k)^{-1}$$

$$L_{k,N+1} = P_k^{0,N} H_k^T (H_k P_k^- H_k^T + R_k)^{-1} \quad 7\text{-}41$$

<u>Estimation error covariance</u>

Starting from equations 7-26 and substituting 7-30 in that, the covariance update equation for the augmented system can be written as

$$\begin{aligned} P_{k+1}^- &= F_k P_k^- [F_k - L_k H_k]^T + Q_k \\ &= F_k P_k^- (F_k^T - H_k^T L_k^T) + Q_k \end{aligned} \quad 7\text{-}42$$

$$\begin{bmatrix} P_{k+1}^{0,0} & P_{k+1}^{0,1} & \cdots & P_{k+1}^{0,N+1} \\ P_{k+1}^{1,0} & P_{k+1}^{1,1} & \cdots & P_{k+1}^{1,N+1} \\ \vdots & \vdots & \cdots & \vdots \\ P_{k+1}^{N+1,0} & P_{k+1}^{N+1,1} & \cdots & P_{k+1}^{N+1,N+1} \end{bmatrix} = \begin{bmatrix} F_k & 0 & \cdots & 0 \\ I & 0 & \cdots & 0 \\ \vdots & \ddots & \ddots & \vdots \\ 0 & \cdots & I & 0 \end{bmatrix} \begin{bmatrix} P_k^{0,0} & P_k^{0,1} & \cdots & P_k^{0,N+1} \\ P_k^{1,0} & P_k^{1,1} & \cdots & P_k^{1,N+1} \\ \vdots & \vdots & \cdots & \vdots \\ P_k^{N+1,0} & P_k^{N+1,1} & \cdots & P_k^{N+1,N+1} \end{bmatrix} \times$$

$$\left(\begin{bmatrix} F_k^T & I & \cdots & 0 \\ 0 & \cdots & \ddots & \vdots \\ \vdots & \ddots & \ddots & I \\ 0 & \cdots & \cdots & 0 \end{bmatrix} - \begin{bmatrix} H_k^T \\ 0 \\ \vdots \\ 0 \end{bmatrix} L_k^T \right) + \begin{bmatrix} Q_k & 0 & \cdots & 0 \\ 0 & 0 & \cdots & 0 \\ \vdots & \ddots & \ddots & \vdots \\ 0 & \cdots & 0 & 0 \end{bmatrix}$$

$$= \begin{bmatrix} F_k P_k^{0,0} & F_k P_k^{0,1} & \cdots & F_k P_k^{0,N+1} \\ P_k^{0,0} & P_k^{0,1} & \cdots & P_k^{0,N+1} \\ \vdots & \vdots & \cdots & \vdots \\ P_k^{N,0} & P_k^{N,1} & \cdots & P_k^{N,N+1} \end{bmatrix} \times$$

$$\left(\begin{bmatrix} F_k^T & I & \cdots & 0 \\ 0 & \cdots & \ddots & \vdots \\ \vdots & \ddots & \ddots & I \\ 0 & \cdots & \cdots & 0 \end{bmatrix} - H_k^T (H_k P_k^{0,0} H_k^T + R_k)^{-1} H_k \times \begin{bmatrix} P_k^{0,0} F_k^T P_k^{0,0} \cdots P_k^{0,N} \\ 0 & 0 & \cdots & 0 \\ \vdots & \ddots & \ddots & \vdots \\ 0 & 0 & \cdots & 0 \end{bmatrix}\right) + \begin{bmatrix} Q_k & 0 & \cdots & 0 \\ 0 & 0 & \cdots & 0 \\ \vdots & \ddots & \ddots & \vdots \\ 0 & \cdots & 0 & 0 \end{bmatrix} \quad 7\text{-}43$$

This is important to notice that estimation error covariance matrix is a symmetric matrix. So, $P_k^{i,0} = P_k^{0,i}$ and $P_k^{i,0} = (P_k^{i,0})^T$.The state estimate that we expect from this smoother is $\hat{x}_{k-N|k}$. The corresponding estimation error covariance is $P_k^{N+1,0}$. It can be obtained as

$$\begin{aligned} P_{k+1}^{0,0} &= F_k P_k^{0,0} \left[F_k^T - H_k^T \left(H_k P_k^{0,0} H_k^T + R_k\right)^{-1} H_k P_k^{0,0} F_k^T\right] + Q_k \\ &= F_k P_k^{0,0} \left(F_k^T - H_k^T L_{k,0}^T\right) + Q_k \\ &= F_k P_k^{0,0} (F_k - L_{k,0} H_k)^T + Q_k \\ P_{k+1}^{0,1} &= P_k^{0,0} [F_k^T - H_k^T \left(H_k P_k^{0,0} H_k^T + R_k\right)^{-1} H_k P_k^{0,0} F_k^T] \\ &= P_k^{0,0} (F_k - L_{k,0} H_k)^T \\ &\vdots \\ P_{k+1}^{0,N+1} &= P_k^{0,N} \left[F_k^T - H_k^T \left(H_k P_k^{0,0} H_k^T + R_k\right)^{-1} H_k P_k^{0,0} F_k^T\right] \\ &= P_k^{0,N} (F_k - L_{k,0} H_k)^T \end{aligned} \quad 7\text{-}44$$

Equations 7-37, 7-41, and 7-44 establish the main body of the fixed-lag smoother and lead to get to the final result for each point as (Simon, 2006)

$$\begin{cases} \hat{x}_{k-N|k} = \hat{x}_{k-N|k-1} + L_{k,N+1} (y_k - H_k \hat{x}_k^-) \\ L_{k,N+1} = P_k^{0,N} H_k^T (H_k P_k^- H_k^T + R_k)^{-1} \\ P_{k+1}^{0,N+1} = P_k^{0,N} \left(F_k - L_{k,0} H_k\right)^T \end{cases} \quad 7\text{-}45$$

Running the fixed-lag smoother

To get to the point stated in equation 7-45, each point needs to get through a procedure. The smother starts with equation 7-37, 7-39, and 7-44 as (Sage and Melsa (1971; Crassidis and Junkins, 2004)

$$\begin{cases} \hat{x}_{k+1}^- = F_k \hat{x}_k^- + L_{k,0} (y_k - H_k \hat{x}_k^-) \\ L_{k,0} = F_k P_k^{0,0} H_k^T \left(H_k P_k^{0,0} H_k^T + R_k\right)^{-1} \\ P_{k+1}^{0,0} = F_k P_k^{0,0} (F_k - L_{k,0} H_k)^T + Q_k \end{cases} \quad 7\text{-}46$$

Taking into account that

$$L_{k,0} = F_k K_k \quad , \; P_k^{0,0} = P_k^- \quad , \; \hat{x}_{k+1|k} = \hat{x}_{k+1}^- \tag{7-47}$$

Equations 7-46 are the standard one-step Kalman filter (compare with equation 7-27). The outputs obtained from the standard one-step Kalman filter, are fed to the smoother part of the filter as the inputs. Then for each successive time step, k, the following loop would be run for $i = 1, \dots, N+1$.

$$\begin{cases} \hat{x}_{k-i+1|k} = \hat{x}_{k-i+1|k-1} + L_{k,i}(y_k - H_k \hat{x}_k^-) \\ L_{k,i} = P_k^{0,i-1} H_k^T \left(H_k P_k^{0,0} H_k^T + R_k\right)^{-1} \\ P_{k+1}^{0,i} = P_k^{0,i-1} \left(F_k - L_{k,0} H_k\right)^T \end{cases} \tag{7-48}$$

The following steps that should be run for each successive k, summarize the fixed-lag smoother:

I. ***<u>Initializing the states of the fixed-lag smoother:</u>*** It is achieved by running the standard Kalman filter (Equations 7-46)

II. ***<u>Updating the fixed-lag smoother:</u>*** reached by sequentially running the loop in 7-48 for $i = 1, \dots, N+1$ to get to the final result as 7-45.

Table 7-5: Fixed-lag smoother and its steps.

Running the standard Kalman filter	• ***Building a model:*** $$x_k = F_{k-1}x_{k-1} + G_{k-1}u_{k-1} + \omega_k$$ $$y_k = H_k x_k + v_k$$ • ***Initializing the process*** $$\hat{x}_0^+ = E(x_0)$$ $$P_0^+ = E[(x_0 - \hat{x}_0^+)(x_0 - \hat{x}_0^+)^T]$$ • ***Iterating the procedure*** $$\hat{x}_{k+1}^- = F_k\hat{x}_k^- + L_{k,0}(y_k - H_k\hat{x}_k^-)$$ $$L_{k,0} = F_k P_k^{0,0} H_k^T \left(H_k P_k^{0,0} H_k^T + R_k\right)^{-1}$$ $$P_{k+1}^{0,0} = F_k P_k^{0,0}(F_k - L_{k,0}H_k)^T + Q_k$$
Running the smoother part	• ***Initializing the process*** $L_{k,0} = L_k$, $P_k^{0,0} = P_k^-$, $\hat{x}_{k+1\|k} = \hat{x}_{k+1}^-$ • ***Iterating the procedure*** *For* $i = 1, \dots, N+1$. $$\hat{x}_{k-i+1\|k} = \hat{x}_{k-i+1\|k-1} + L_{k,i}(y_k - H_k\hat{x}_k^-)$$ $$L_{k,i} = P_k^{0,i-1} H_k^T \left(H_k P_k^{0,0} H_k^T + R_k\right)^{-1}$$ $$P_{k+1}^{0,i} = P_k^{0,i-1}\left(F_k - L_{k,0}H_k\right)^T$$

<u>Calculating improvement</u>

To figure out how much this extension of the Kalman filter has smoothed the data, a parameter which is known as *percent improvement* have been defined (Simon, 2006):

$$percent\ improvement = \frac{100\ Tr(P_k^{0,0} - P_k^{N+1,N+1})}{Tr(P_k^{0,0})} \qquad 7\text{-}49$$

To calculate $P_k^{N+1,N+1}$ which is the $\mathrm{N}+1, \mathrm{N}+1$th element of the covariance matrix, the diagonal components of the matrix $\mathrm{P_{k+1}}$should be calculated.

$$P_{k+1}^{1,1} = P_k^{0,0}\left[I - H_k^T\left(H_k P_k^{0,0} H_k^T + R_k\right)^{-1} H_k P_k^{0,0}\right]$$
$$= P_k^{0,0} - P_k^{0,0} H_k^T L_{k,1}^T$$
$$P_{k+1}^{2,2} = P_k^{0,1}\left[-H_k^T L_{k,2}^T\right] + P_k^{1,1}$$
$$= P_k^{1,1} - P_k^{0,1} H_k^T L_{k,2}^T$$

$$\vdots$$

$$P_{k+1}^{i,i} = P_k^{i-1,i-1} - P_k^{0,i-1} H_k^T L_{k,i}^T$$

$$\vdots$$

$$P_{k+1}^{N+1,N+1} = P_k^{N,N} - P_k^{0,N} H_k^T L_{k,N+1}^T \qquad 7\text{-}50$$

Figure 7-3 shows Kalman filter operation versus the fixed-lag Kalman filter. The measurements are T_{zz} component of full tensor gravity data set (tie line T110). This is the data set that Kalman filter will be applied to in the next chapters. Here, the lag is considered 20.

Standard Kalman filter reduces noise to an acceptable degree but a delay can be seen in peak area. Fixed-lag smoother is more successful in reaching the peak comparing with the standard filter but on the side areas standard filter still performs better and results in more even estimations (Figure 7-3 a).

Percent Improvement (Figure ٣-٧ b) illustrates that as an average, the estimation error covariance has been improved using the fixed-lag smoother and literally, we are more confident about the estimations obtained from the smoother.

Fixed-lag approach is strong in catching the peak but it does that at the expense of more noisy estimations on the side areas. Looking at Figure 7-3 a and the standard filter that has moved to the left brings this to mind that there is even an easier way to reach the peak and having less noisy estimation at the sides with compensating the lag and having estimation that are moved to right. On the other hand, having future measurements available, means the filter can be run from the last measurement to the first instead of first to the last. Mathematically, there is no priority in measurements based on the order they have been collected. When it comes to estimation, it does not really matter when they have been recorded. It is just important that they are accessible.

Having smoother estimations and being able to process the data regardless of their order of collection, are two reasons that forward-backward smoothing is considered applicable. This extension of the Kalman filter has been discussed in next section.

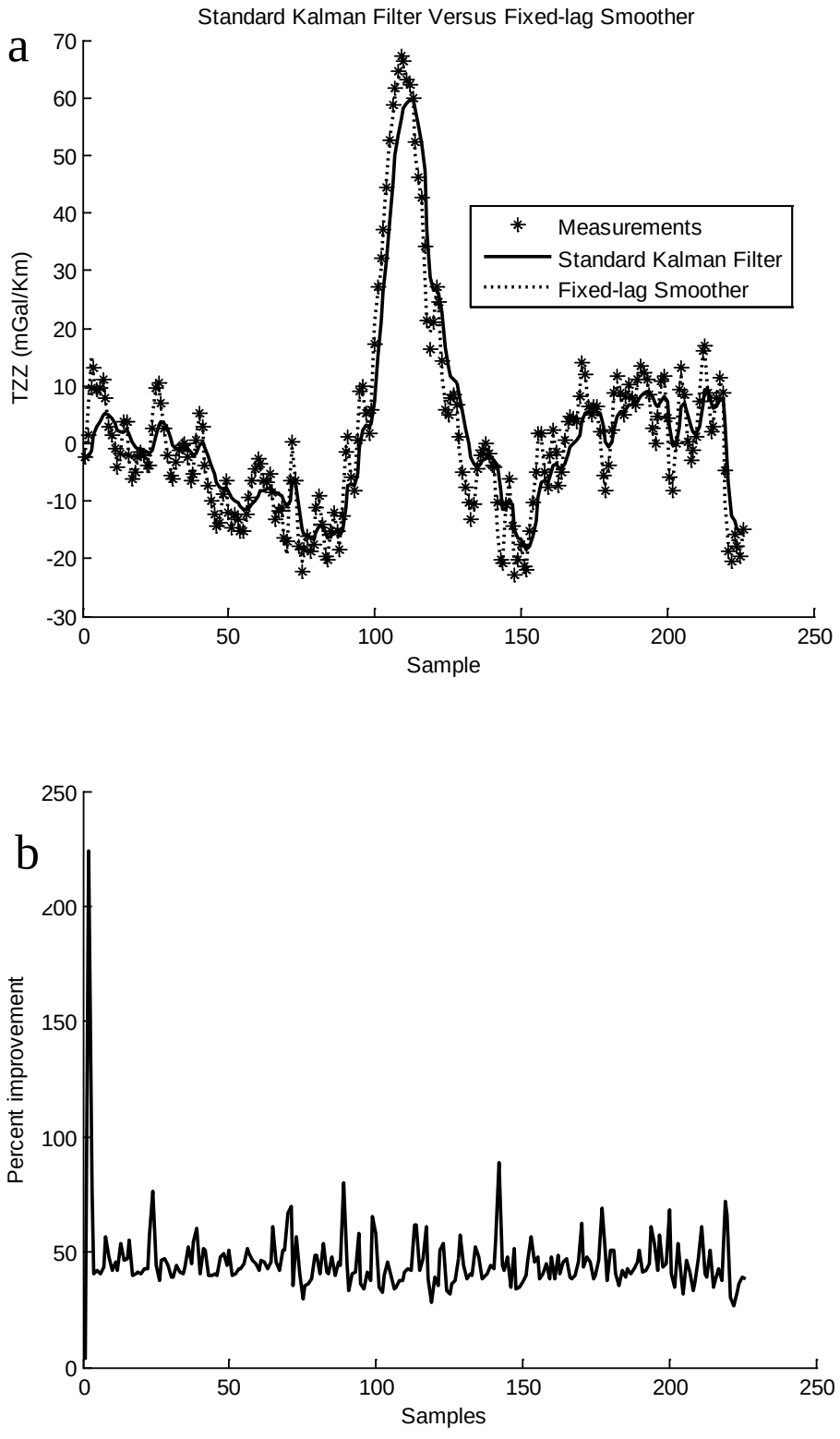

Figure 7-3: Comparison of standard and Fixed-lag smoother (solid line versus dashed one) and percent improvement.

Forward-backward smoother

Standard Kalman filter calculates the best estimate of point m based on measurements up to $(\hat{x}_f)$. But how measurements $K = m\ to\ K = N$ can be included in the filter to obtain a better estimation? Another estimation of point m can be made based on measurements $K = N\ to\ K = m$ $(\hat{x}_b)$. This time the filter runs backward in time. Two estimations are then combined and the forward-backward estimation is formed (Fraser and Potter, 1969). To incorporate both forward and backward to get the best estimate of point m, weighted mean of them should be calculated.

$$\hat{x} = K_f\hat{x}_f + K_b\hat{x}_b \qquad 7\text{-}51$$

K_f and K_b should be determined. It is clear that if more weight is given to any of the estimations, less weight should be given to the other one. In other words, they should satisfy in equation 7-52:

$$K_f + K_b = I \qquad 7\text{-}52$$

$$\hat{x} = K_f\hat{x}_f + (I - K_f)\hat{x}_b \qquad 7\text{-}53$$

Equation 7-53 tells that parameters K_f, $\hat{x}_f$, and $\hat{x}_b$ should be determined. $\hat{x}_f$ is the best estimate of point $k = m$ running the filter forward while $\hat{x}_b$ is the best estimate of the same point running the filter backward.

Steps to calculate the optimal estimation from forward-backward smoother are:

I. ***Running the standard Kalman filter:*** from $k = 1\ to\ k = m$

II. ***Running the Kalman filter backward:*** from $k = N\ to\ k = m + 1$ when N is the last available measurement.

III. ***Running the smoother:*** assigning weight to forward and backward estimations.

Table 7-6 summarizes the forward-backward optimal filter and its equations (Simon, 2006).

Figure 7-4 shows the forward-backward (FB) smoother applied on the same data set in Figure 7-3. The measurements are a line from full tensor gravity data set (tie T110). It can be observed that FB filter has located the peak accurately and compared with each of the individual filters gives smoother estimations. It also provides more reliable results by

having lower estimation error covariance which is intuitively expected that the estimation based on two is more accurate than each of the estimations.

Table 7-6: Backward-forward smoother and its steps.

Running the standard Kalman filter	• ***Building a model:*** $x_k = F_{k-1}x_{k-1} + \omega_k$ $y_k = H_k x_k + v_k$ $\omega_k \sim (0, Q_k)$ $v_k \sim (0, R_k)$ • ***Initializing the process*** $\hat{x}_{f0}^{+} = E(x_0)$ $P_{f0}^{+} = E[(x_0 - \hat{x}_0^{+})(x_0 - \hat{x}_0^{+})^T]$ • ***Iterating the procedure (For k=1,. . .,m)*** $P_{fk}^{-} = F_{k-1}P_{k-1}^{+}F_{k-1}^{T} + Q_{k-1}$ $K_{fk} = P_{fk}^{-}H_k{}^T(H_k P_{fk}^{-} H_k{}^T + R_k)^{-1}$ $x_{fk}^{-} = F_{k-1}\hat{x}_{f,k-1}^{+}$ $\hat{x}_{fk}^{+} = \hat{x}_{fk}^{-} + K_{fk}(y_k - H_k\hat{x}_{fk}^{-})$ $P_{fk}^{+} = (I - K_{fk}H_k)P_{fk}^{-}$
Running the backward filter	• ***Initializing the process*** $\hat{x}_{bN}^{-} = E(x_N)$ $I_{bN}^{-}=0$ • ***Iterating the procedure*** *For* $k = N, N-1, \ldots m+1.$ $I_{bk}^{+} = I_{bk}^{-} + H_k{}^T R_k{}^{-1} H_k$ $K_{bk} = (I_{bk}^{+})^{-1} H_k{}^T R_k{}^{-1}$ $\hat{x}_{bk}^{+} = \hat{x}_{bk}^{-} + K_{bk}(y_k - H_k\hat{x}_{fk}^{-})$ $I_{b,k-1}^{-} = F_{k-1}^{T}[(I_{bk}^{+})^{-1} + Q_{k-1}]^{-1}F_{k-1}$ $\hat{x}_{b,k-1}^{-} = F_{k-1}^{-1}\hat{x}_{bk}^{+}$
Running the smoother	$P_{bm}^{-} = (I_{bm}^{-})^{-1}$ $K_k = P_{bm}^{-}(P_{fm}^{+} + P_{bm}^{-})^{-1}$ $\hat{x}_m = K_f\hat{x}_{fk}^{+} + (I - K_f)\hat{x}_{bm}^{-}$ $P_m = [(P_{fm}^{+})^{-1} + (P_{bm}^{-})^{-1}]^{-1}$

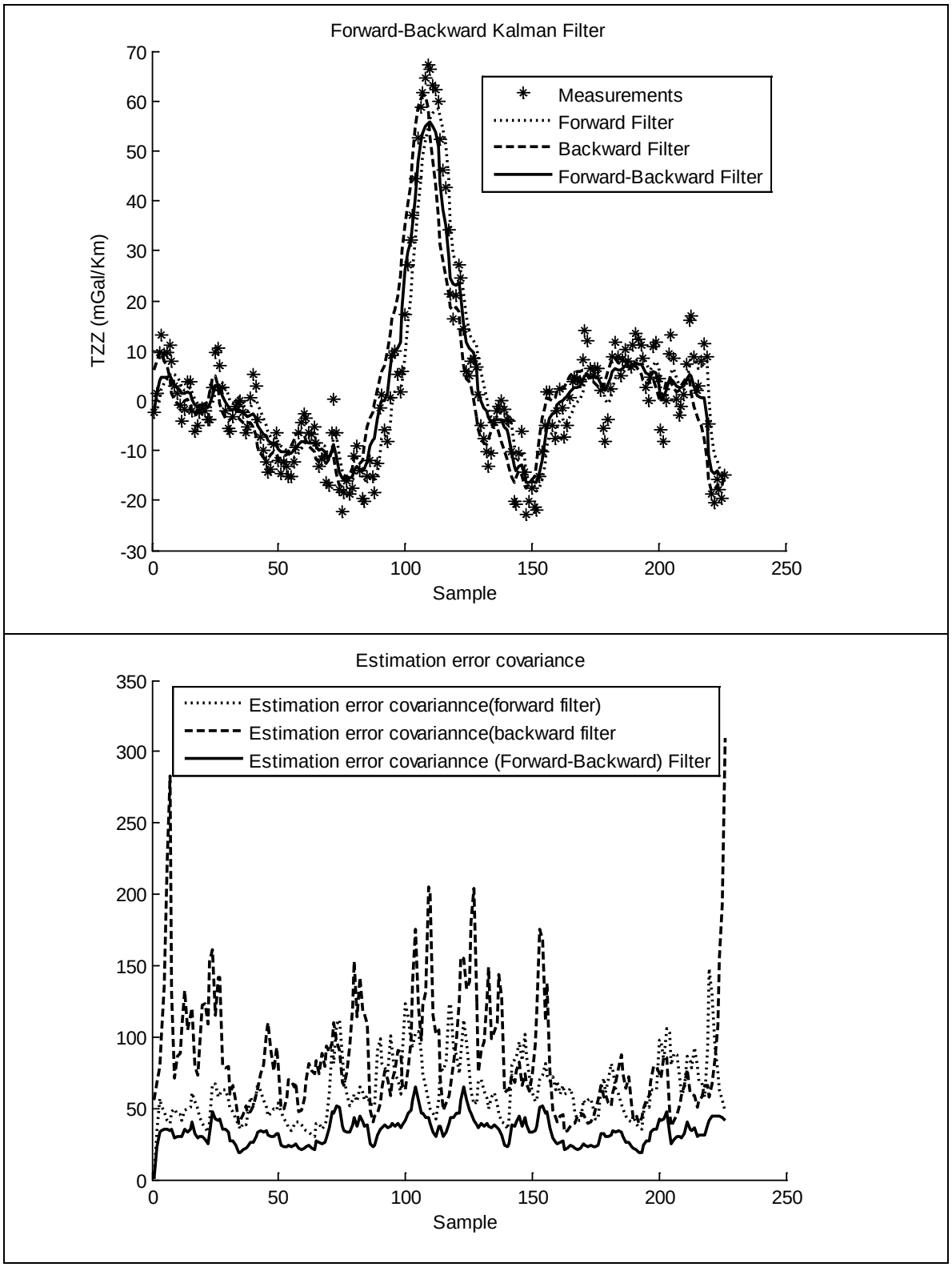

Figure 7-4: the FB Kalman filter. a) Comparing forward, backward, and FB smoother. The input is T_{zz} component of line T110 and b) Comparing estimation error covariance of the filters.

CHAPTER 8. APPLYING THE KALMAN FILTER ON FTG DATA OF VINTON SALT DOME

In this chapter, the results of applying the Kalman filter on FTG data of the Vinton salt Dome are discussed. The details of equations and the concepts of the filters are discussed in chapters 5 through 7.

The application of the Kalman filter started with the standard Kalman filter. Then fading memory Kalman filter, constrained Kalman filter, fixed-lag smoother, forward-backward smoother, and eventually the most meaningful filter for us which is forward-backward constrained Kalman filter are applied respectively.

What is important to take into account is that in our filtering all components of FTG data are processes at the same time. So except in one of the approaches of constrained Kalman filter, six components are filtered simultaneously.

In chapter 8, it was discussed that gradiometry data have 9 different components as:

$$T_{ij} = \begin{bmatrix} T_{xx} & T_{xy} & T_{xz} \\ T_{yx} & T_{yy} & T_{yz} \\ T_{zx} & T_{zy} & T_{zz} \end{bmatrix} \qquad 8\text{-}1$$

While

$$T_{yz} = T_{zy}$$
$$T_{xy} = T_{yx}$$
$$T_{xz} = T_{zx}$$

Considering this characteristic, only six components should be processed. To show how the Kalman filters work, the filter's behavior on two profiles is examined; T110, a tie line which goes through the dome anomaly and also L471 (Figure 8-1).

As it was discussed in chapter 6, determining process noise covariance (Q), is very critical. The filter is tuned by trying different values of Q. High (low) process noise covariance results in high (low) gain value (K) which consequently brings about more (less) weight for the measurement of the same iteration rather than the *a priori* estimation. In our filter Q is determined by the filter length. Higher (lower) filter length involves more (less) points in calculating Q which generally engenders higher (lower) value of Q (Figure 8-2). Tie line 110 has a clear peak in T_{zz} component and it was

investigated in most cases as a checking point in determining the filter parameters. shows how one can determine the optimum value of process noise covariance (Q).

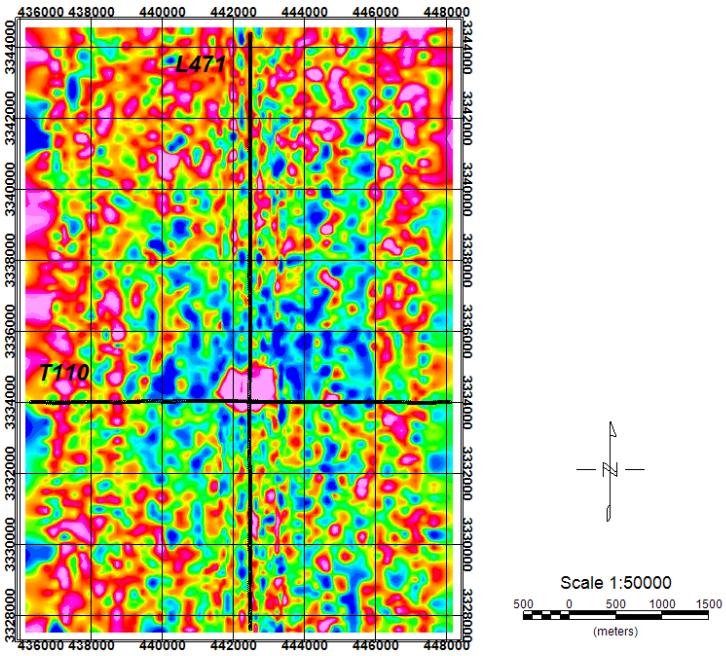

Figure 8-1: The position of L471 and T110 the profile and tie line which go through the salt dome anomaly and we selected for tuning the filter.

What is critical in determining Q is that if it is assigned a low value the filter can remove the noise in the side area but it cannot reach the peak properly also the direction of filtering can introduce bias which is relatively considerable. On the other hand, higher value of Q results in reaching the peak but is not very effective in reducing noise (Figure 8-3 (a) versus (b)). Our solution for this issue is applying the filter successively (Figure 8-3(c) and (d)). As it is clear, applying the filter repeatedly (3 times) can cause over filtering.

The pit of bias that seems dominantly in low process noise covariance case, can be treated by running the filter in both directions along a profile, forward and backward (Figure 8-4).

The question that arises here is that is whether the filter can give an acceptable result without having to run the filter repeatedly? To address this concern, fading-memory Kalman filter is applied. As it was discussed in chapter 7, this filter gives more weight to the most recent estimation. In this extension, more emphasis should be given to the recent data. It is achieved by entering an α term in the cost function and consequently, forcing the filter to converge to an estimate that reduces the weight of old measurements while increases the weight of the most recent ones. In standard Kalman filter, this α term is considered to be 1 so equal weight is given to all measurements (regardless of old or new ones) while in fading memory filter it set to be greater than 1.

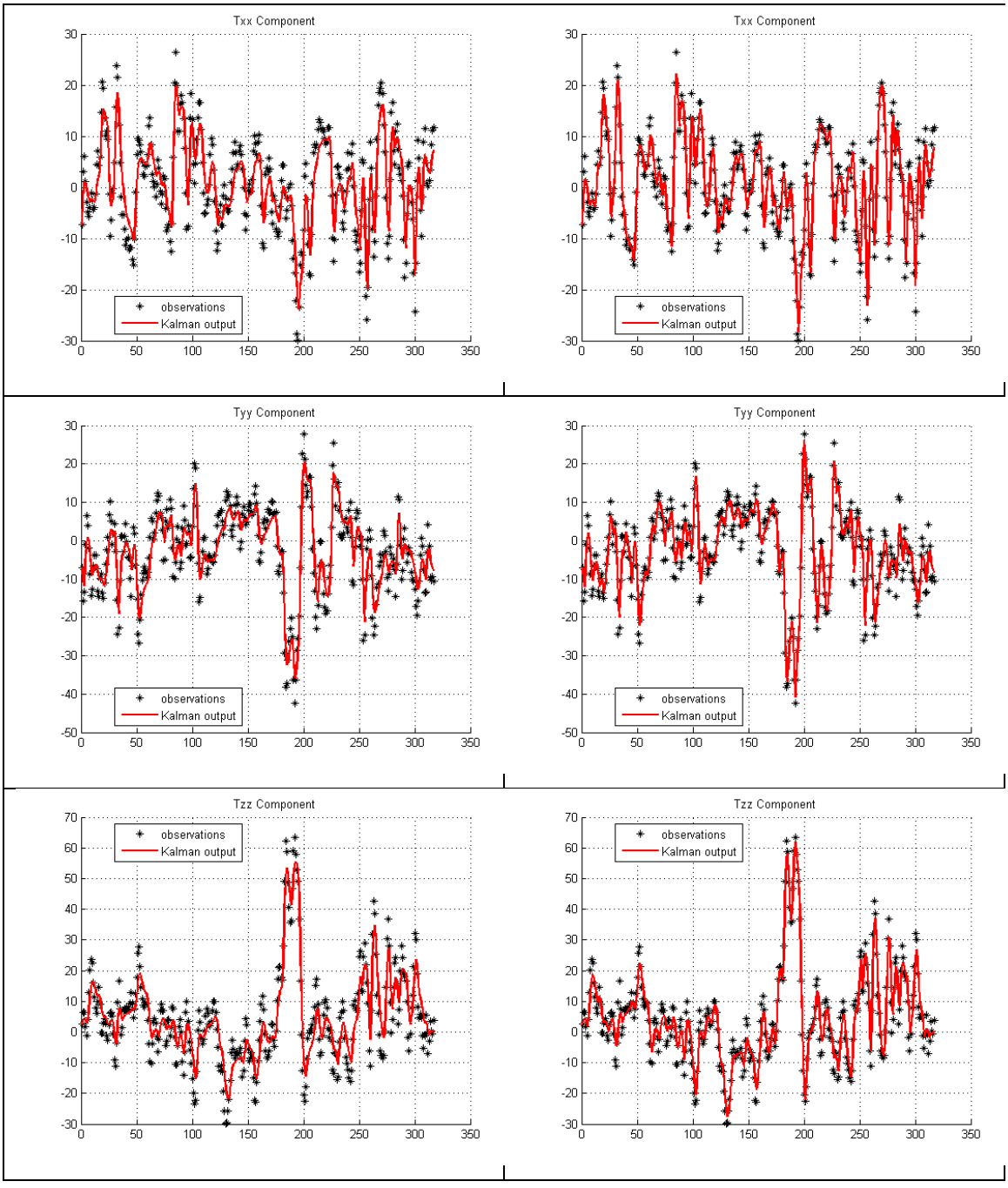
Txx Component
observations
Kalman output
Txx Component
observations
Kalman output
Tyy Component
observations
Kalman output
Tyy Component
observations
Kalman output
Tzz Component
observations
Kalman output
Tzz Component
observations
Kalman output

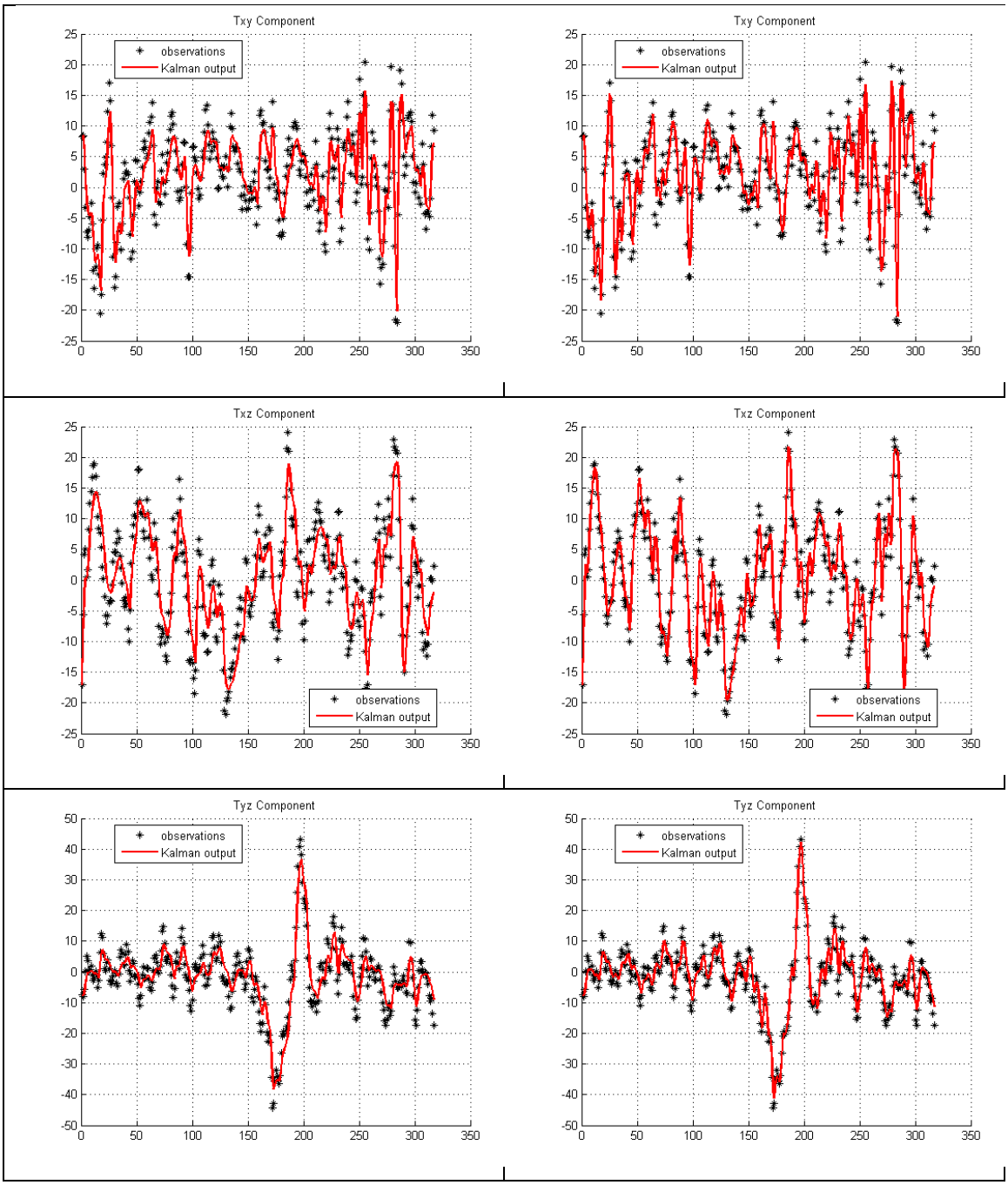

Figure 8-2: Importance of Q in filter operation; Standard Kalman filter applied on profile L471. Left hand side figures show the six FTG filtered data with lower assigned process noise covariance while the right hand side ones illustrate the filter behavior with higher process noise covariance. As it is predictable higher value for Q results in more weight given to the noisy measurements and the filter gives estimations closer to the measurements.

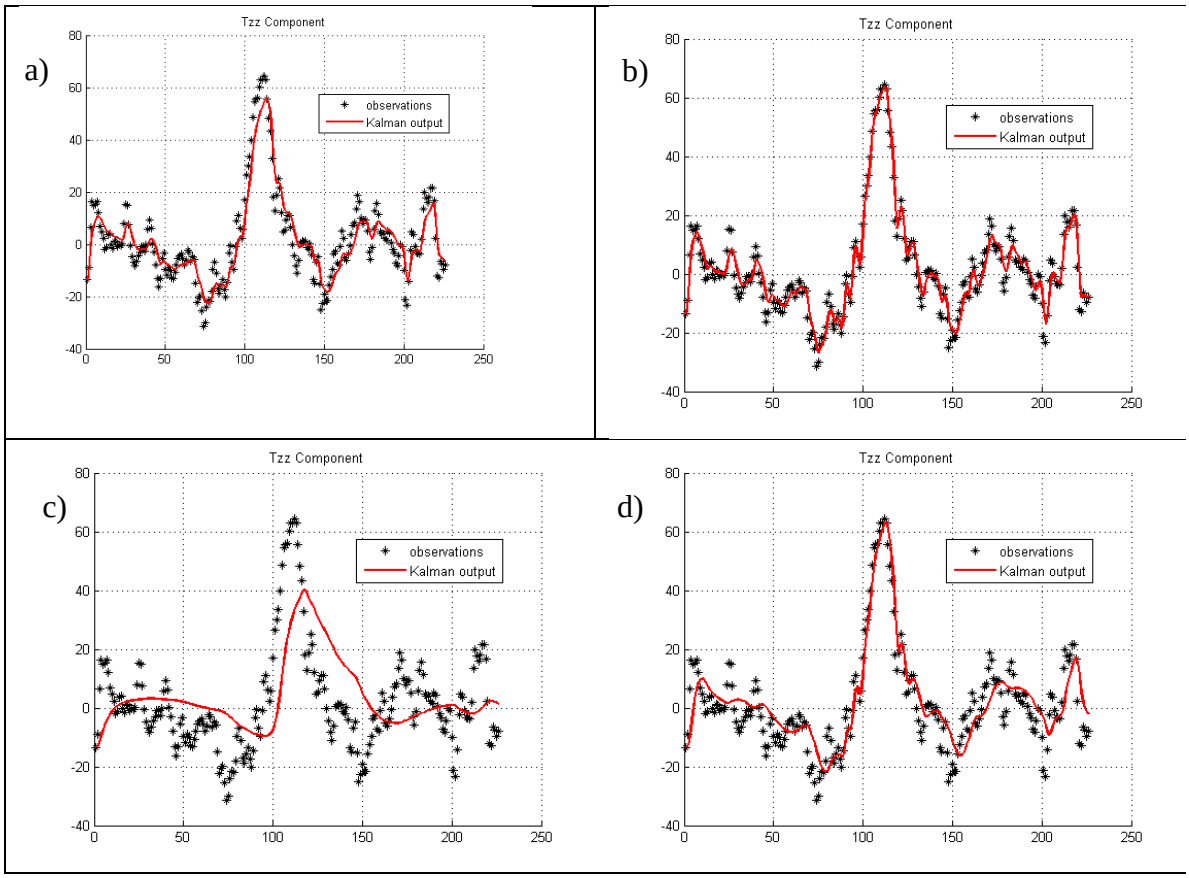

Figure 8-3: A trade-off between smoother filtering and reaching peaks; (a) and (c) have low process noise covariance while (b) and (d) are filtered given high process noise covariance. Low Q results in smoother filtering while producing more biased and missing reaching the peak properly. (a) and (b) are the first iteration of the standard Kalman filter while (c) and (d) are the third iterations. The data is T_{zz} component of T110.

Figure 8-5 shows how fading-memory Kalman filter works. The behavior of the filter is so that it can get the peak properly but in side areas it cannot perform as well as the standard Kalman filter with low process noise covariance.

The next extension that was applied on our FTG data is constrained Kalman filter. The constraint that is most meaningful for potential field data is Laplace's equation. Laplace's constraint is stated as

$$\boldsymbol{T_{xx} + T_{yy} + T_{zz} = 0} \qquad 8\text{-}2$$

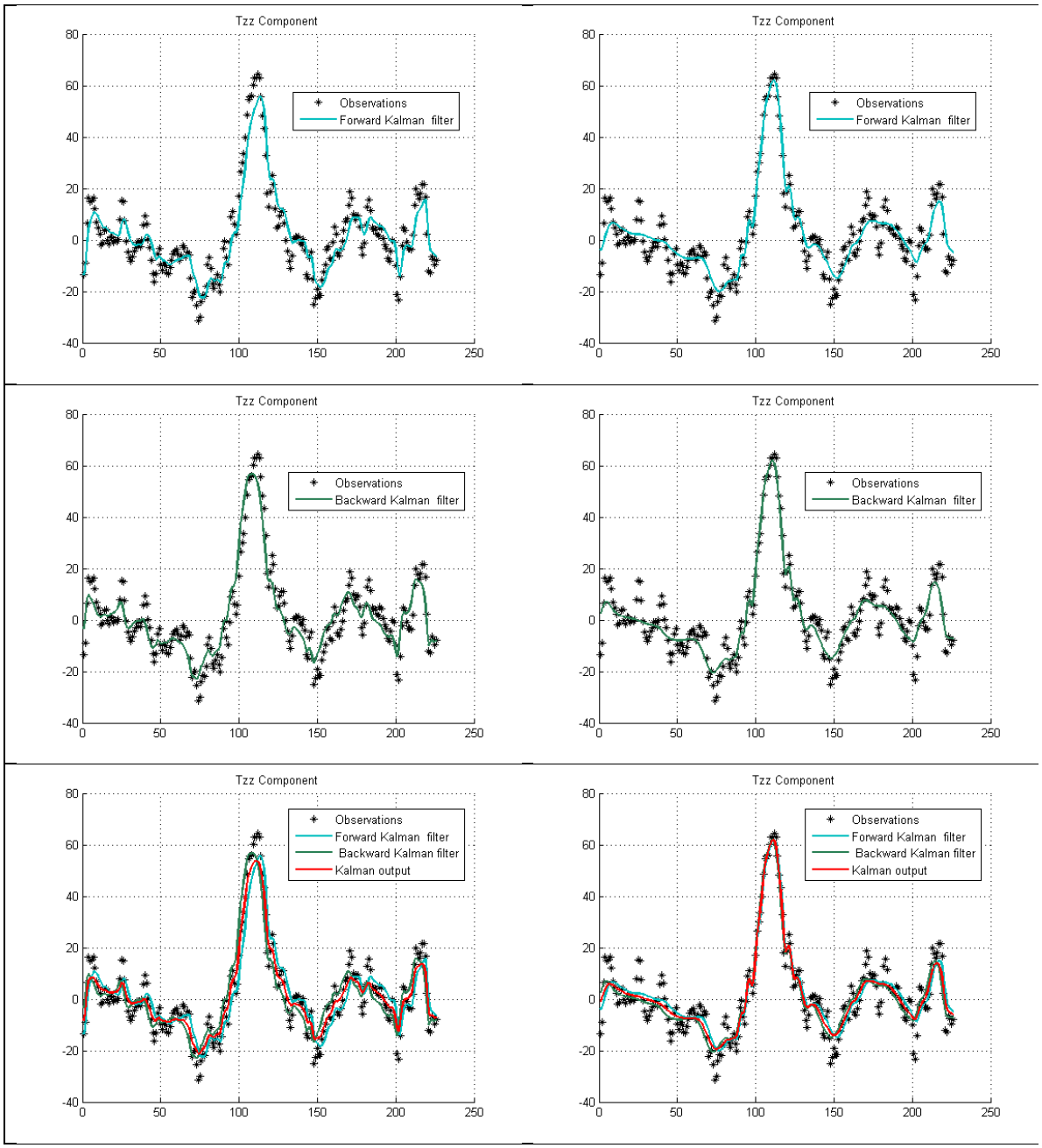

Figure 8-4:Running the filter in both directions along the profile; right figures correspond to the first iteration of low process noise covariance while left ones are results of third iteration of running the filter with high process noise covariance.

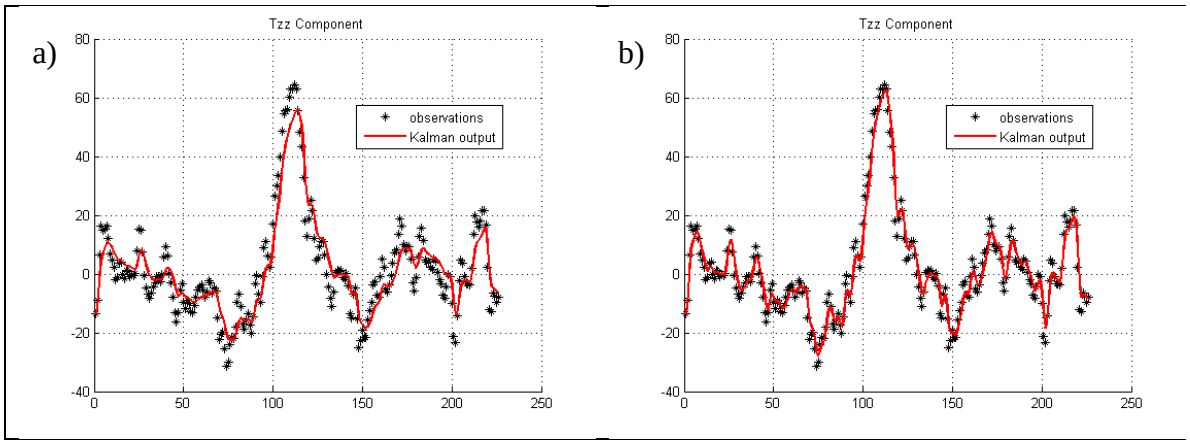

Figure 8-5: Standard Kalman filter (a) and fading-meory Kalman filter with $\alpha = 1.3$(b).

In order to incorporate the constraint of Laplace's equation, we used two strategies: Model Reduction (Wen & Durrant-Whyte, 1992) and Perfect Constraint (also called Perfect Measurement, Porrill, 1988). These two strategies are discussed in detail in chapter 7.

Model Reduction approach reduces the parameter space of the system and processes five independent components of the FTG (the remaining diagonal component is computed from the other two). Again to maintain symmetry, the filter is applied in both directions forward and backward (FB). The forward-backward approach which is assembled with Model Reduction approach is the forward-backward smoother explained in chapter 7. As it is discussed there, the weights of forward and backward estimations could be different depending on their estimation error covariances (Fraser and Potter, 1969).

Perfect Constraint (Perfect Measurement) approach is the other strategy used to incorporate Laplace's equation in the Kalman filter. The Laplace's equation constraint is incorporated in the Kalman filter operation loop such that measurements have noise but the constraint equation does not. The measurement update equation of the standard Kalman filter is augmented by adding this perfect constraint. Having zeros in the right hand side of the equation 8-3, makes using the forward-backward smoother impossible.

$$\begin{bmatrix} y_k \\ d \end{bmatrix} = \begin{bmatrix} H \\ D \end{bmatrix} x_k + \begin{bmatrix} v_k \\ 0 \end{bmatrix} \qquad 8\text{-}3$$

In the backward run, inverse of measurement error covariance is needed to be calculated and thoese zeros making the matrix invertible (Table 7-6, Running the

backward filter). So to remove the offset caused by directional filtering, the filter is applied in the forward and backward (FB) sense and the mean of the two estimations at each data point is the final estimate of that data point.

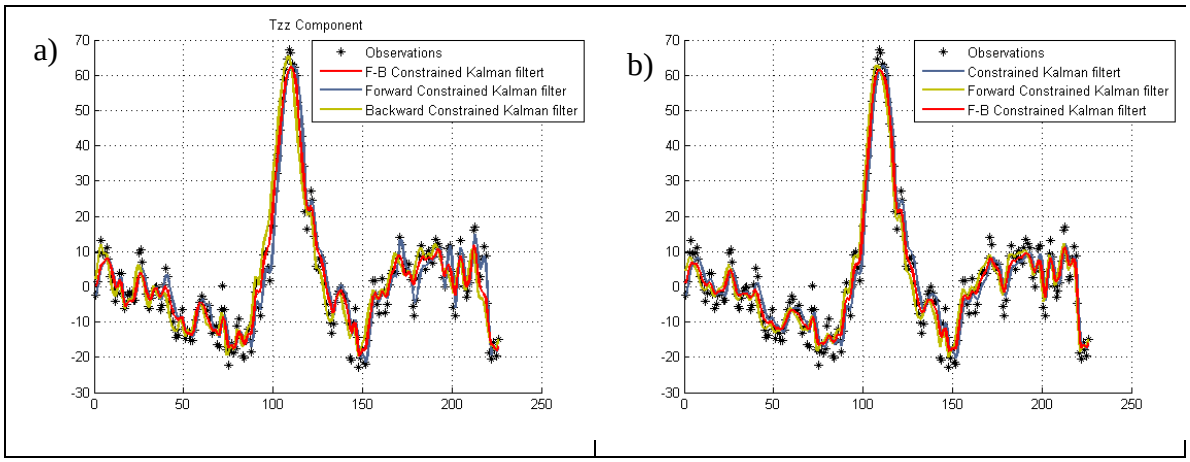

Figure 8-6: Laplace's equation constrained Kalman filter; Model Reduction (a) and Perfect Constraint (b).

The filtered output of the two Kalman filters is nearly identical in most cases. It worth to mention that the backward run causes different estimations.

The last extension that was applied on FTG data set is fixed-lag smoother.

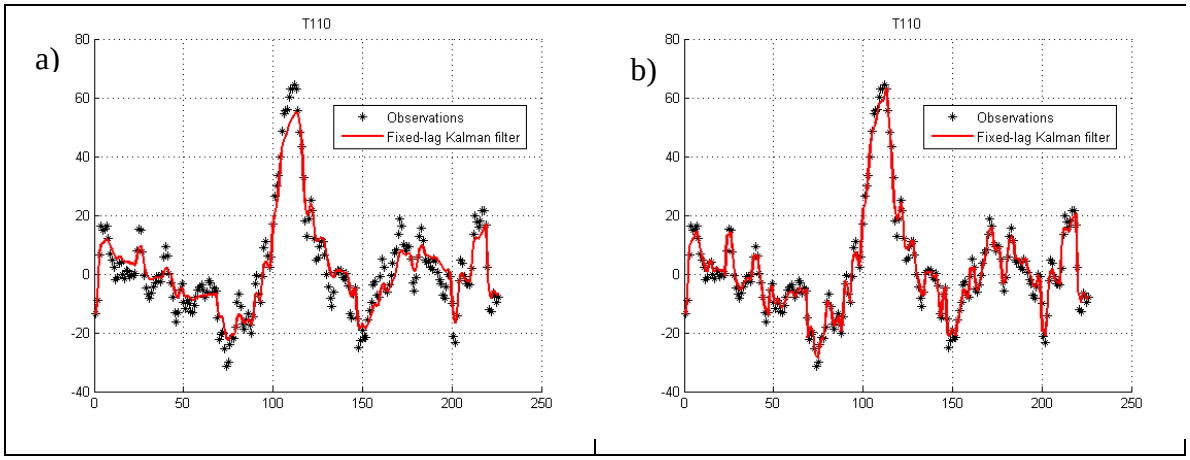

Figure 8-7: Fixed-lag Kalman filter: Lag is given three (a) and 11 (b).

Comparing Figures 8-2 through 8-7 shows that selecting the appropriate parameters like lag and the acceptable α for fading memory Kalman filter enable us to extract signal from noisy measurement. In our case study, Laplace's equation constrained Kalman filter is considered the most reliable result since it assures us our filtered data satisfy the most

meaningful constraint in potential field while it improves the signal-to-noise ratio of gravity gradiometry components.

Our workflow includes simple leveling and decorrugation, both necessary for data processed along profiles to produce 2-D maps.

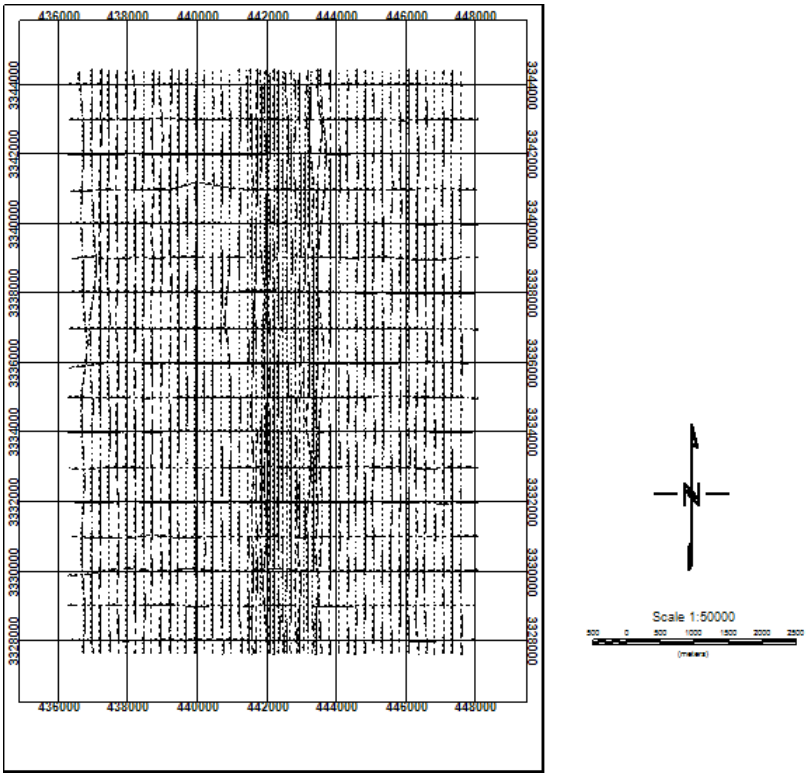

Figure 8-8: Profiles and tie lines.

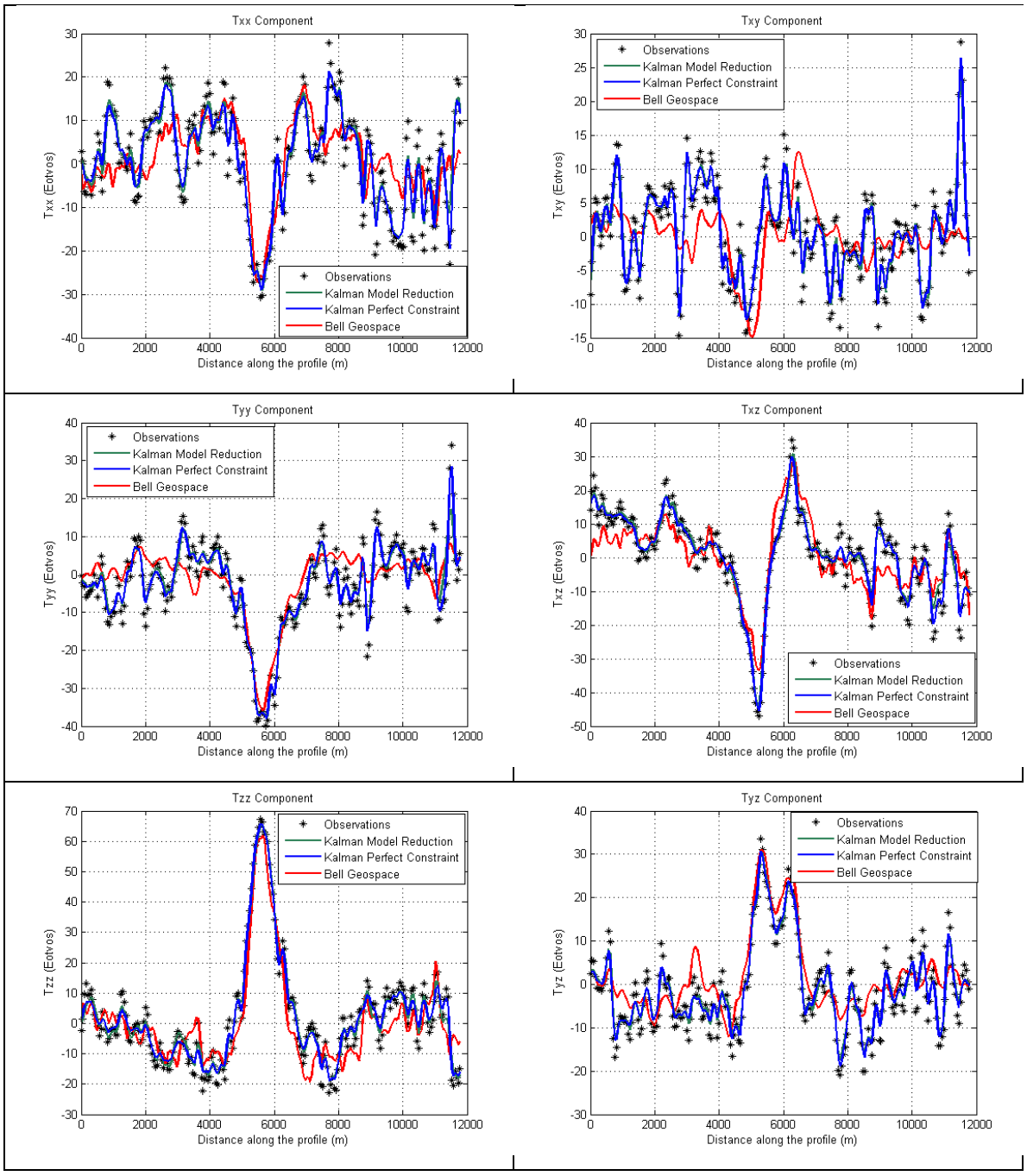

Figure 8-9: FTG components. Leveled Free-air observations - black stars; Laplace's equation constrained Kalman filtered data using two different approaches: Perfect Constraint (blue line, which is mostly indistinguishable from the green line) and Model Reduction (green line); and Bell Geospace leveled and FTNR filtered data (red line).

Comparing our constrained Kalman filter applied on FTG data with advanced Bell Geospace filtered results, illustrates that Kalman filtered data extract signal from noisy data more effectively and Kalman filtered data have greater dynamic range (Figure 8-9).

We compared our filter with the sophisticated Full Tensor Noise Reduction (FTNR) filter of Bell Geospace (Figure 8-10, Figure 8-11, and Figure 8-12).

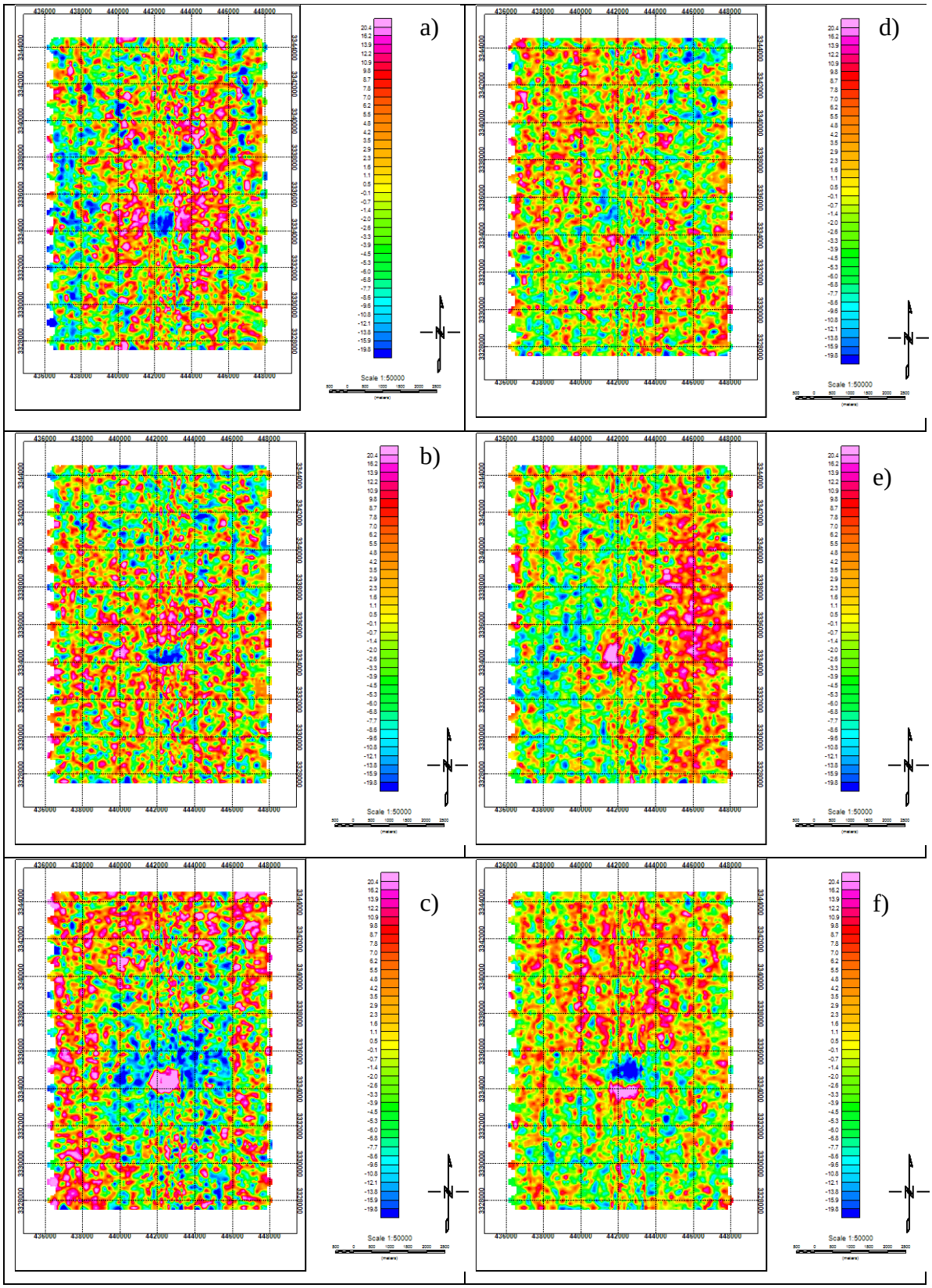

Figure 8-10: Components of Leveled Free-air observations: ; T_{xx} (a), T_{yy} (b), T_{zz} (c), T_{xy} (d), T_{xz} (e), and T_{yz} (f).

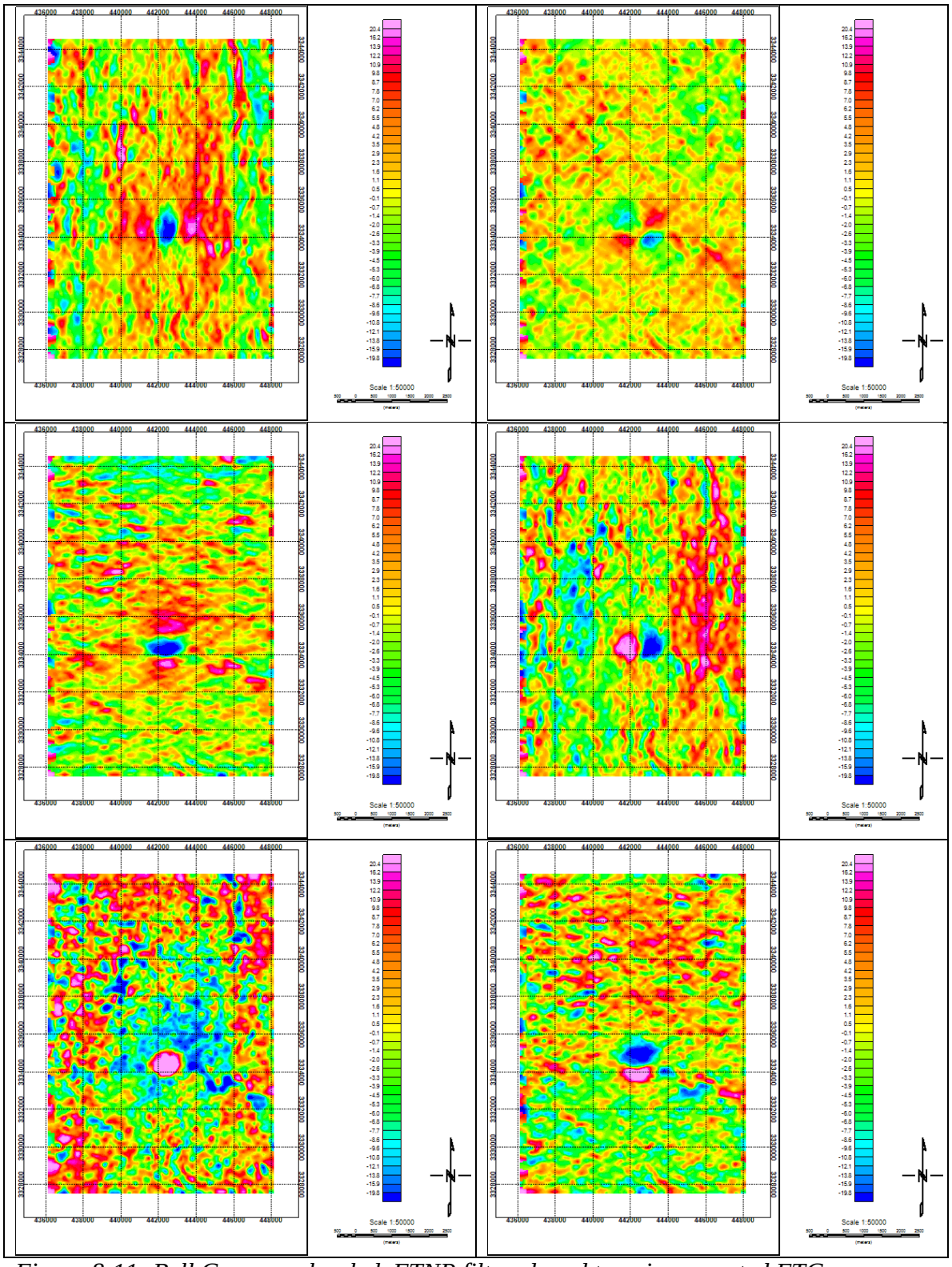

Figure 8-11: Bell Geospace leveled, FTNR filtered, and terrain corrected FTG components (the order is the same as figure 8-10)

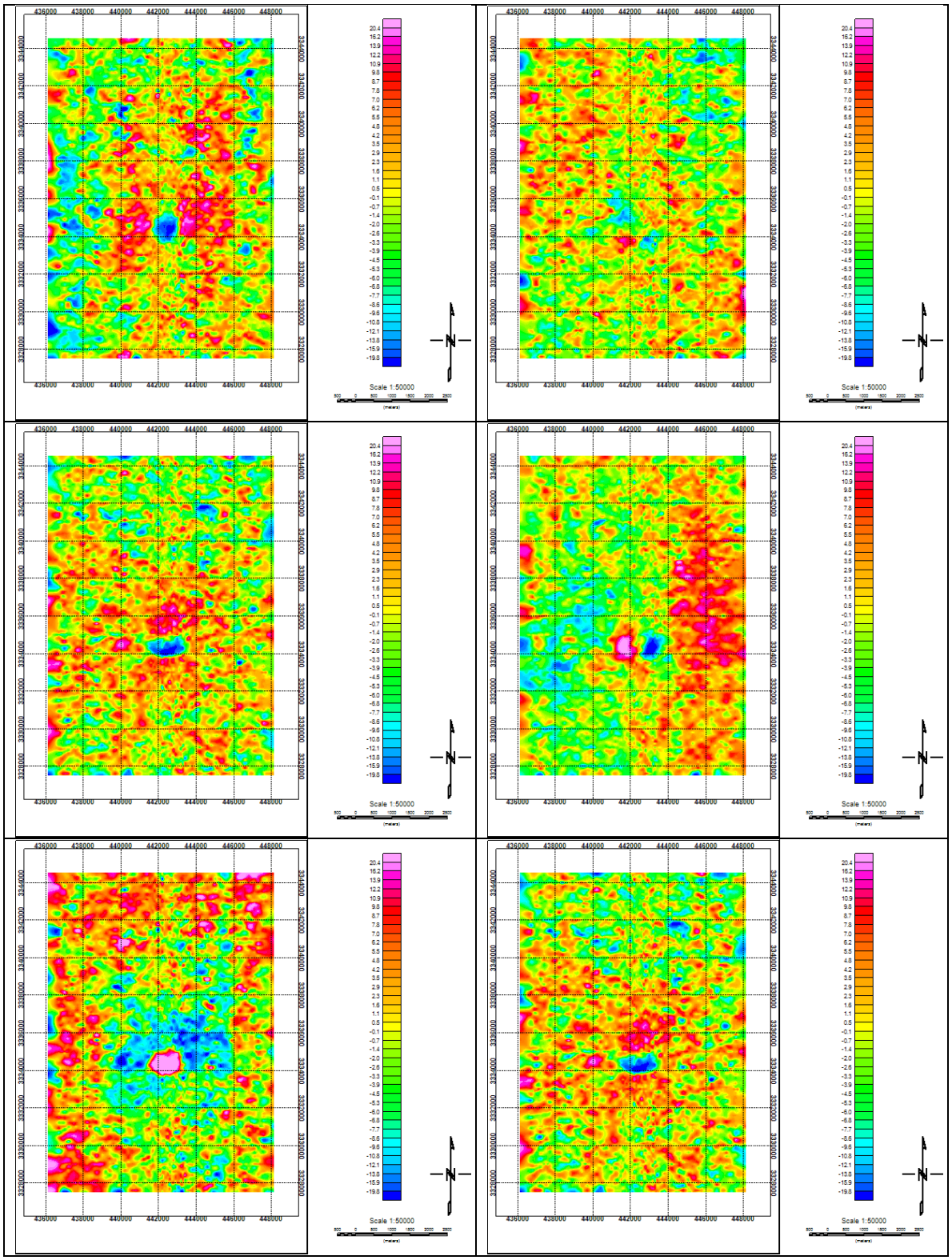

Figure 8-12: Terrain corrected FTG components processed by Kalman filter incorporating Laplace's equation constraint in the Perfect Constraint approach (the order is the same as figure 10-3)

CHAPTER 9. DISCUSSION OF RESULTS AND CONCLUSIONS

We have applied several extensions and optimal smoothing approaches of the Kalman filter, one of the best known recursive data processing techniques, on the Full Tensor Gradiometry (FTG) data acquired by Bell Geospace over the Vinton salt dome located in southwest Louisiana. We used the filter to improve the signal-to-noise ratio of gravity gradiometry components. We tested the standard Kalman filter and Fading memory and Constrained Kalman filter extensions with Fixed-lag and Forward-Backward smoothing methods to maintain symmetry.

Our most meaningful results were obtained through the Kalman filter with the constraint of Laplace's equation combined with the Forward-Backward filter operations. Laplace's equation constraint was incorporated using two separate strategies: Model reduction and Perfect constraint (or Perfect measurement). In general, the data processed using the Kalman filter have greater dynamic range than previously filtered data and also have the ability to extract a signal from noisy data without having to remove a band of wavenumbers. In addition, our constrained Kalman filter also has the ability to force the Laplace's equation constraint. These characteristics enable the Kalman filter to investigate short wavelength signals associated with near-surface lateral density variations. In analyzing two dimensional maps for geologic variations, our workflow includes leveling and decorrugation, both procedures necessary for data processed along profiles (Figure 9-1 and Figure 9-2).

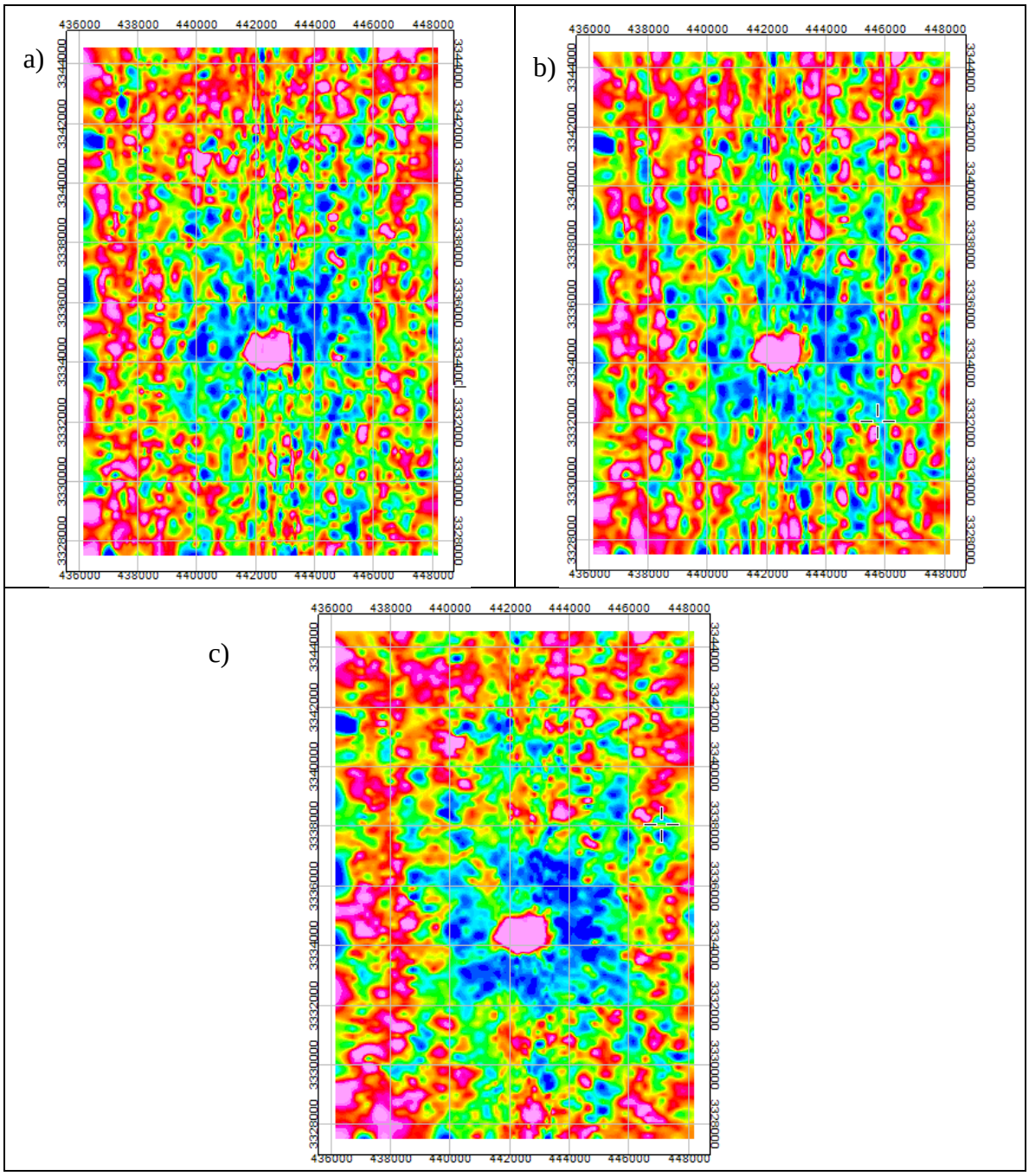

Figure 9-1: The Laplace's equation constrained Kalman filtered data (a), after levelling (b), and after levelling and decorrugation (c).

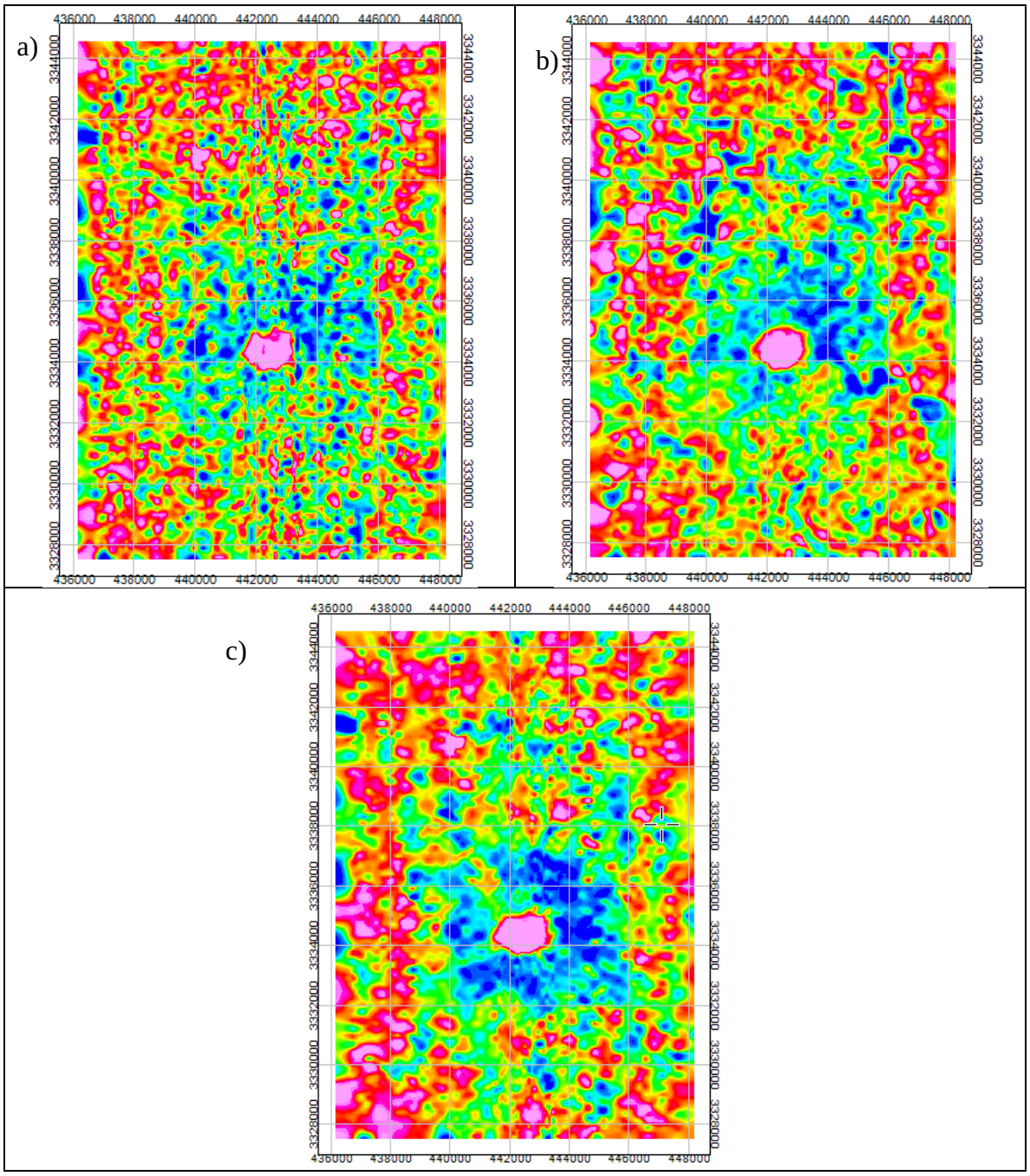

Figure 9-2: Raw (a), FTNT processed data (b), and the Laplace's equation constrained Kalman filtered data (c).

Kalman filtered processed data presented a more continuous image of the caprock and deep salt than available from Full Tensor Noise Reduction (FTNR) filter.

There is extensive faulting around the Vinton dome. Many faults were mapped and detected by Coker (2006) and Ennen (2012). The radial fault sets around the dome can be easily seen in the data processed using the Kalman filter (Figure 9-3)

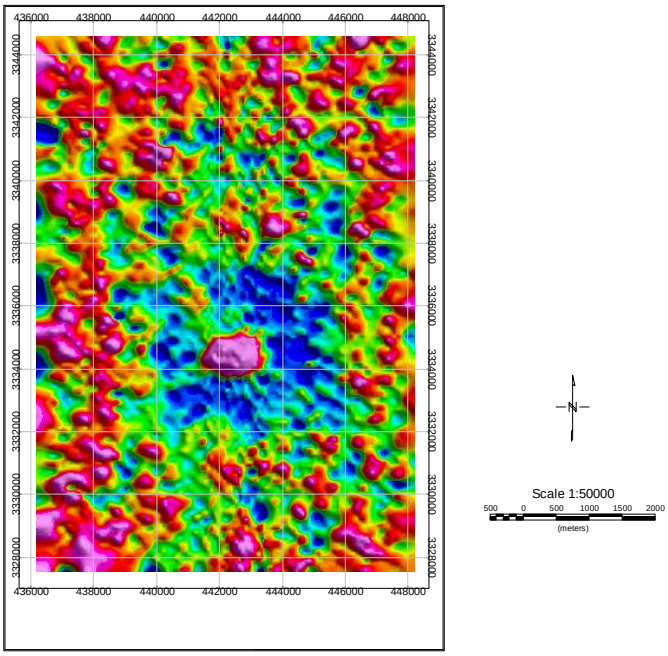

Figure 9-3: Color shaded leveled decorrugated Tzz compont.

Figure 9-4 shows Coker's fault interpretation from seismic and Ennen's from modelling.

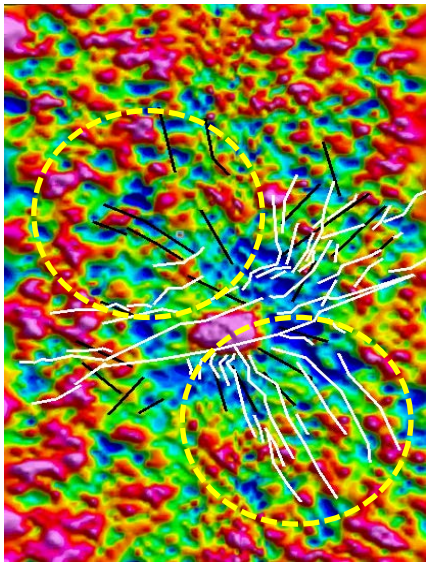

Figure 9-4: Color-shaded leveled decorrugated data with Ennen's (2012) interpreted faults overlaid in black and Coker's (2006) faults in white.

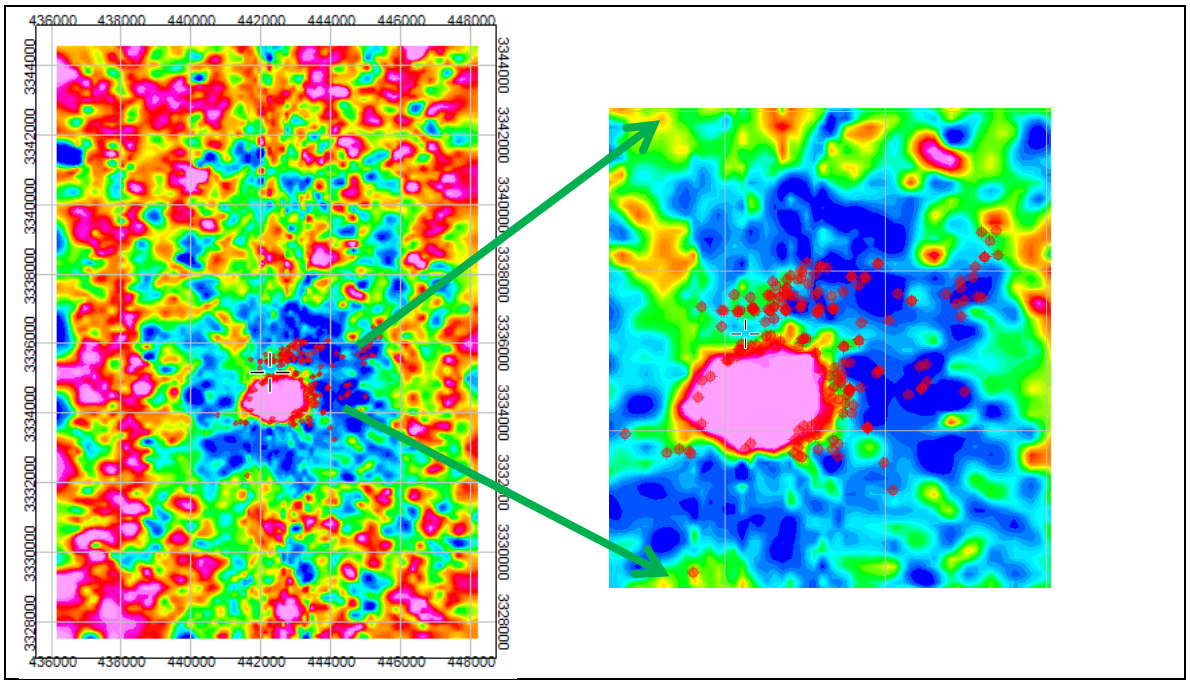

Figure 9-5: Operation oil wells overlaid on Tzz component on Kalman filtered data.

Several previously mapped near-subsurface geologic features (faults and fractures) and their continuity are more readily apparent in our Kalman filter processed components (Figure 9-4 and Figure 9-5). Since the processed data generally agree with the previously mapped and interpreted structures (faults in southeast and northwest of the area), the interpretation of faults and fractures could be extended to previously unmapped areas where features show continuity not seen prior to the use of the Kalman filters. These structures and the associated gravity highs and lows could be useful in determining more precisely the locations and nature of petroleum traps.

Advantages and disadvantages of the Kalman filter

Kalman filter has been shown to be the optimal solution of a linear problem in the sense that no nonlinear filter designed so far can perform better than it, and even when the noise components are not Gaussian, it is the optimal filter among the entire family of linear filters. The most significant advantage of the Kalman filter is that it can process multiple components simultaneously. One of the pros of the Kalman filter is that it

provides estimation error for the estimations. It also provides us with formulas for advancing the error covariance matrix in time.

The most important disadvantage of applying the Kalman filter is its computational complexity. There are multiple parameters that need to be defined and tuned to run the filter effectively. The other dawnback of this filter are the assumptions made in deriving the filter. The system that can go through the Kalman filter is a linear contaminated by white Gaussian noise which is not true in some problems. Plus, the use of Kalman filter equations for large dimensional systems requires us to handle matrices with large dimension.

REFERENCES

Barnes, G. J., and Lumley, J. M., 2010, Noise analysis and reduction in full tensor gravity gradiometry data: ASEG-PESA Airborne Gravity 2010 Workshop, 21-27.

Barton, D.C., 1933, Mechanic of formation salt domes with special reference to Gulf Coast salt domes of Texas and Louisiana: American Association of Petroleum Geologists, 17(9), 1025-1083.

Bell Geospace, Inc., 2008, Processing and Acquisition of air-FTG data, Vinton dome, Vinton, Lousiana.

Bell, R. E., Anderson, R., and Pratson, L. F. , 1997, Gravity gradiometry resurfaces: The Leading Edge, 16, no. 1, 55–59, doi:10.1190/1.1437431.

Blakely, R.J., 1995, Potential Theory in Gravity and Magnetic Applications: Cambridge University Press.

Branson, R.B., 1991, Productive trends and production history, south Louisiana and adjacent offshore, in: Goldthwaite, D., ed., An introduction to Central Gulf Coast Geology, New Orleans Geological Society, 61-70.

Breard, S.Q., Callender, D. A., and Nault, M. J., 1996, Local Foraminiferal Faunas: The Key to Enhanced Stratigraphic Resolution of Expanded Cenozoic Sections in the Gulf Coast Basin: Gulf Coast Association of Geological Societies Transactions, 46, 55-62.

Canizares, R., and Madsen, H., 1998, Data assimilation and nested hydrodynamic modeling in storm surge forecasting: Proceedings of the International Conference on Coastal Engineering, 1(26), 1378-1391.

Coburn, G.W., 2002, A methodology for defining the base and geometry of salt bodies in the deepwater Gulf of Mexico, Gulf Coast Association of Geological Societies Transactions, 52, 123-133.

Coker, M. O., 2006, Aquitanian (Lower Miocene) depositional system: Vinton dome, onshore Gulf of Mexico, southwest Louisiana: M.S. thesis, University of Houston.

Constance, P. E., Holland, M. B., Roche, S. L., Bicquart, P., Bryans, B., Gelinsky, S., Ralph, J. G., and Bloor, R. I., 1999, Simultaneous acquisition of 3D surface

seismic data and 3C, 3D VSP data: 69th Annual International Meeting, SEG, Expanded Abstracts, 104-107.

Cossey, S.P.J., and R.E. Jacobs, 1992, Oligocene Hackberry Formation of southwest Louisiana: Sequence stratigraphy, sedimontology, and hydrocarbon potential. The American Association of Petroleum Geologists Bulletin, 76, 589-606.

Crassidis, J., and Junkins, J., 2004, Optimal Estimation of Dynamic Systems, CRC Press, New York.

Dampeney, C., N., G., 1969, The equivalent source technique: Geophysics , 34(1), 1969.

Dickinson, J.L., Brewster, J., R., Robinson, J.W., and Murphy, C. A., and 2009, Imaging techniques for full tensor gravity gradiometry data: 11th SAGA Biennial Technical Meeting and Exhibition, 84-86.

DiFrancesco, D., Meyer, T., Christensen, A., and FitzGerald, D., 2009, gravity gradiometry-today and tomorrow: 11th Biennial Technical Meeting and Exhibition, SAGA, Extended abstract, 80-83.

Domenico, N., 1994, The SEG Museum's torsion balance: The Leading Edge, 13, 683-686.

Dransfield, M., Le Roux, T., and Burrows, D., 2010, Airborne gravimetry and gravity gradiometry at Fugro Airborne Surveys: In R. J. L. Lane (editor), Airborne Gravity 2010 - Abstracts from the ASEG-PESA Airborne Gravity 2010 Workshop: Published jointly by Geoscience Australia and the Geological Survey of New South Wales, Geoscience Australia Record 2010/23 and GSNSW File GS2010/0457.

Dransfield, M., Roux, T., and Burrows, D., 2010, Airborne gravimetry and gravity gradiometry at Fugro Airborne Surveys: Airborne Gravity, ASEG-PESA Workshop, Extended abstracts, 49-57.

Drécourt, J. P., and Madsen, H. 2001, Role of domain knowledge in data-driven modeling, 4th DHI Software Conference, Scanticon Conference Cetre, Denmark.

Duncan, W. S., 2005, A deterministic evaluation of seismic fidelity using velocity modeling and attribute analysis to improve surface seismic imaging around Vinton Dome Louisiana: M. Sc. Thesis, The University of Houston.

Ennen, C. 2012, Mapping gas-charged fautl blocks around the Vinton salt Dome, Louisiana using gravity gradiometry data: M.S. thesis, University of Houston.

Eti, R.P., 2004, An integrated geophysical study of the Vinton salt dome, Calcasieu Parish, Louisiana: M.Sc Thesis, University of Houston.

Fails, T.G., 1995, Exploration and exploitation of coastal salt basin diapiric structures in the lower Pliocene through Eocene trends: Geology and techniques, New Orleans Geological Society.

Fenneman, N., M., 1906, Oil fields of the Texas – Louisiana gulf coastal plain, Unites States Geological Survey Bulletin, Issue 282, 112-113.

Fraser, D., and Potter, J.,1969, The optimum linear smoother as a combination of two optimum linear filters, Automatic Control, IEEE Transactions, 14(4), 387-390.

Fraser. D., and Potter, J., 1969, The optimum linear smoother as a combination of two optimum linear filters: IEEE Transactions on Automatic Control, 14(4) 387-390.

Fullagar, P., and Pears, G., From gravity gradients to density gradients, 2010: ASEG-PESA Airborne Gravity 2010 Workshop, 79-86.

Galloway, W. E., Ganey-Curry, P., Li, X., and Buffler, R. T., 2000, Cenozoic depositional evolution of the Gulf of Mexico Basin: American Association of Petroleum Geologists, 84, 1743-1774.

Gauss, C. F., 2004, Theory of the Motion of the Heavenly Bodies Moving about the Sun in Conic Sections, Dover, New York, 2004.

Greg Welch, G., and Bishop, G, 1997, SCAAT: Incremental Tracking with Incomplete Information , In Proceedings of SIGGRAPH 97,Los Angeles, CA, August 3–8 1997, In Computer Graphics Proceedings Annual Conference Series, ACM SIGGRAPH, 333–344.

Grewal, M. S., & Andrews, A. P., 2011, Kalman filtering: theory and practice using MATLAB. John Wiley & Sons.

Grewal, M. S., and Andrews, A. P., 2008, Kalman filtering: Theory and practice using MATLAB: Hoboken, N.J. Wiley.

Hammond, S., and Murphy, C., 2003, Air-FTG: Bell Geospace's airborne gravity gradiometer- A description and case study: Preview, 24-26.

Harris, G., D., 1910, Oil and gas in Louisiana with a brief summary of their occurrence in adjacent states: Unites States Geological Survey Bulletin, Issue 429, 103.

Harrison, F.W. Jr., Jones, R.K., and L.C. Searles, eds. 1970, Typical oil and gas fields of southwestern Louisiana, 2, Lafayette Geological Society.

Hatch, D., 2004, Evaluation of a full tensor gravity gradiometer for kimberlite exploration: Airborne Gravity, ASEG-PESA Workshop, Extended abstracts, 73-79.

Haykin, S., 2001, Kalman Filtering and Neural Networks, New York: Wiley.

Hayward, S. D. ,1998, Constrained Kalman filter for least-squares estimation of time-varying beamforming weights, INSTITUTE OF MATHEMATICS AND ITS APPLICATIONS CONFERENCE SERIES , 67, 113-126, OXFORD UNIVERSITY PRESS.

Heinrich, P. V., 2005, Distribution and origin of fault-line scarps of southwest Louisiana, USA: Gulf Coast Association of Geological Societies Transactions, 55, 284-293.

Hoeve, J.A.V., and W.S. Borowski, 1988, Oil and gas developments in Louisiana Gulf Coast onshore in 1987, The American Association of Petroleum Geologists Bulletin, 72, 75-81.

Houtekamer, P. L. , Mitchell, H., L., Pellerin, G., Buehner, M., Charron, M., Spacek, L., and Hansen, B., 2005. Atmospheric data assimilation with an ensemble Kalman Filter: Results with Real Observations: Monthly Weather Review, 133(3), 604-620.

Houtekamer, P. L., Mitchell, H. L., Pellerin, G., Buehner, M., Charron, M., Spacek, L. and Hansen, B., 2005, Atmospheric data assimilation with an ensemble Kalman filter: Results with real observations. Monthly Weather Review, 133, 604–620.

Ingram, R.J., 1991, Salt Tectonics, in: Goldthwaite, D., ed., An introduction to Central Gulf Coast Geology, New Orleans Geological Society, 31-60.

Johnson L., and Sakoulis G., 2003. Maximizing equity market sector predictability in a Bayesian time-varying parameter model: Computational Statistics & Data Analysis 52, 3083-3106.

Johnson, D., L., and Sakoulis,G., 2003, Maximizing Equity Market Sector Predictability in a Bayesian Time Varying Parameter Model, SSRN: http://ssrn.com/abstract=396642 or http://dx.doi.org/10.2139/ssrn.396642.

Joost, V., L., V., P., and Krekel, P., F., 1997, Multisensor data fusion of points, line segments, and surface segments in 3D space: Sensor Fusion VI, 2059. 1, 190-201.

Judson, S.A., and R.A. Stamey, 1933, Overhanging salt on domes of Texas and Louisiana, The American Association of Petroleum Geologists Bulletin, 17, 1492-1520.

Kisin, S., 2003, Tomographic velocity model building: application to Vinton dome VSP data: M.Sc. Thesis, University of Houston.

Kolmogorov, A., Interpolation and extrapolation of stationary random sequences, Selected Works of A . N. Kolmogorov, Volume 11, V. Tikhomirov(Ed.), Kluwer Academic Publishers, Dordrecht, The Netherlands, 272-280.

Kybic, J., 1998, Kalman filtering and speech enhancement, Diploma w0rk, Ecole polytechnique federale De Lausanne.

Kybic, J., 1998. Kalman Filtering and Speech Enhancement, http://cmp.felk.cvut.cz/~kybic/old/dipl/index.html, accessed 3 July 2012.

Lee, J., Li, Y., and Lane R., 2005, Effects of data filtering on inversion of gravity gradient data, SEG Expanded Abstracts 24, 627-630.

Lumley, J., M., White, J., P., Barnes, G., Huang, D., and Paik, H., J., 2010, A superconducting gravity gradiometer tool for exploration: Airborne Gravity, ASEG-PESA Workshop, Extended abstracts, 21-39.

Madsen, H., and Cañizares, R., 1999, Comparison of extended and ensemble Kalman filters for data assimilation in coastal area modelling, International Journal for Numerical Methods in Fluids, 31(6), 961–981.

Maybeck, P., S., 1979, Stochastic models, estimation, and control, v. 1: Academic Press, Inc.

McGee, L., and Schmidt, S., Discovery of the Kalman filter as a practical tool for aerospace and industry, NASA Technical Memo 86847, November 1985.

Moriya, N., 2010, Primer to Kalman filtering, A physicist's perspective: Nova Science Publishers, Inc.

Munroe, M., Hench, T., and Timmons, M., 2009. Sales Rate and Cumulative Sales Forecasting Using Kalman Filtering Techniques, http://www.cs.unc.edu/~welch/kalman/media/pdf/Munroe2009.pdf, accessed 3 July 2012.

Murphy, C. A. and Brewster, J., 2007, Target delineation using Full Tensor Gravity Gradiometry data: ASEG-PESA 19th International Geophysical Conference and Exhibition, Extended Abstract, 1-3.

Murphy, C. A., 2004, The Air-FTG airborne gravity gradiometer system: ASEG-PESA Airborne Gravity 2004 Workshop, 7-14.

Murphy, C. A., 2010, Recent developments with Air-FTG: ASEG-PESA Airborne Gravity 2010 Workshop, 142-151.

Murphy, C., A., and Dickson, J., L., 2009, Exploring exploration play models with FTG gravity data: 11th SAGA Biennial Technical Meeting and Exhibition, 89-91.

Nakata, T., and Tonetti, C., 2010, Kalman Filter and Kalman Smoother, New York University.

Norwest Energy, http://www.norwestenergy.com.au/index.php/projects/ftg-full-tensor-gravity-gradiometry/, accessed 3 July 2012.

O'Brien, J., Rodriguez, A., Sixta, D., Davies, M.A., and P. Houghton, 2005, Resolving the K-2 salt structure in the Gulf of Mexico: An integrated approach using prestack depth imaging and full tensor gravity Gradiometry: The Leading Edge, 24, 404-409.

Owen, E.W., 1975. Trek of the oil finders: A History of Exploration for Petroleum: American Association of Petroleum Geologists Memoir 6, 191-215.

Paine, W.R., Spillers, J.P., Waters, K.M., Andrews, D.I., Baysinger, E.M., Borland, A.M., Cotton, J., Christina Jr. S.T., Hall Jr., J.P., Kimmey, B.W., McDougall, J.E., Meyerhoff, A.A., Munchrath, M.A., Paffett, D.L., Paspberry, F.L., Rockwood, D.N., Roederer Jr., E.P., Stipe, J.C., and H.O. Woodbury, 1968, Geology of Natural Gas in South Louisiana Lafayette and New Orleans Geological Socities: Part 1, Natural Gases of North America, in: Beebe, B.W., and B.F. Curtis, eds., Natural Gases of North America: American Association of Petroleum Geologists Memoir 9(1), 376-434.

Porrill, J., 1988, Optimal combination and constraints for geometrical sensor data, The International Journal of Robotics Research, 7(6), 66-77.

Porrill, J., Optimal combination and constraints for geometrical sensor data: International Journal of Robotics Research, 7(6), 66-77

Prutzman, J.M., 1998, Subsalt imaging using full tensor gradient and 3D seismic data, Mississippi Canyon, Gulf of Mexico, Society of Petroleum Engineers, SPE 49145.

Sage, A. P., and Melsa, J. L., 1971, Estimation theory with applications to communications and control, McGraw-Hill, New York.

Schlee, F. H., Standish, C. J., and Toda, N. F, 1967, Divergence in the Kalman filter, AIAA Journal, 5(6), 1114-1120.

Schmidt, S., F., 1981. The Kalman Filter: Its Recognition and Development for Aerospace Applications: Journal of Guidance and Control, 4(1), 4.

Seni, S. J., and Jackson M.P., 1983, Evolution of Salt Structures, East Texas Diapir Province; Part 1, Sedimentary Record of Halokinesis: American Association of Petroleum Geologists, 67(8), 1219-1244.

Shimkin, N., 2009, Derivations of the discrete-time Kalman filter, Estimation and identification in dynamical systems.

Simon, D. , Reduced order Kalman filtering without model reduction, Controland Intelligent Systems, 2006.

Simon, D., 2006, Optimal State Estimation: Kalman, H-infinity, and Nonlinear Approaches, John Wiley & Sons.

Simon, D., 2010, Kalman filtering with state constraints: a survey of linear and nonlinear algorithms. IET Control Theory & Applications, 4(8), 1303-1318.

Simon, D., and Chia, T. L. ,2002, Kalman filtering with state equality constraints, Aerospace and Electronic Systems, IEEE Transactions on, 38(1), 128-136.

Sorenson, H. W., & Sacks, J. E, 1971, Recursive fading memory filtering. Information Sciences, 3(2), 101-119.

Sorenson, H.W, 1970, Least-squares estimation: from Gauss to Kalman, IEEE Spectrum, 7(7), 63-68.

Stasinowsky, W., 2010, The advantages of the full tensor over Gz: ASEG-PESA Airborne Gravity 2004 Workshop, 178-182.

Swanson, S.M., and A.W. Karlsen, 2009, USGS assessment of undiscovered oil and gas resources for the Oligocene Frio and Anahuac formations, onshore Gulf of Mexico basin, USA, Search and Discovery #101078.

Swanson, S.M., Karlsen, A.W., and Valentine B.J., 2013, Geologic assessment of undiscovered oil and gas resources—Oligocene Frio and Anahuac Formations, United States Gulf of Mexico coastal plain and State waters: U.S. Geological Survey Open-File Report 2013–1257, 66 p., http://dx.doi.org/10.3133/ofr20131257.

Thompson, S. A., and Eichelberger, O. H., 1928, Vinton Salt Dome, Calcasieu Parish, Louisiana: American Association of Petroleum Geologists, 12. 4, 385-394.

Thompson, S.A., and Eichelberger, O.H., 1928, Vinton salt dome, Calcasieu Parish, Louisiana: American Association of Petroleum Geologists Bulletin., 12, 385-394.

Van Leeuwen, E. H., 2000, BHP Develops Airborne Gravity Gradiometer for Mineral Exploration: The Leading Edge, 19, 1296-1297.

Welch, W., and Bishop, G., 1997, SCAAT: Incremental Tracking with Incomplete Information, 25th annual conference on Computer graphics and interactive techniques, http://www.cs.unc.edu/~welch/media/pdf/scaat.pdf, accessed 3 July 2012.

Welch, W., and Bishop, G., 2001, An Introduction to the Kalman Filter, SIGGRAPH 2001, Course 8, http://www.cs.unc.edu/~{welch, gb}, accessed 3 July 2012.

Welch, W., and Bishop, G., 2006, An Introduction to the Kalman Filter, TR 95- 041, http://www.cs.unc.edu/~welch/media/pdf/kalman_intro.pdf, accessed 3 July 2012.

Wen W., and Durrant-Whyte, H., 1992, Model-based multi-sensor data fusion: Proceedings of the IEEE International Conference on Robotics and Automation, Nice, France, May 1992, 1720-1726.

Wen, W., & Durrant-Whyte, H. F.,1992, Model-based multi-sensor data fusion, Robotics and Automation, Proceedings., 1992 IEEE International Conference, 1720-1726.

Wiener, N., Extrapolation, Interpolation, and Smoothing of Stationary TimeSeries, MIT Press, Cambridge, Massachusetts.

Wilson, F., and J.A. Noel, 1983, A gravity analysis of west-central Calcasieu Parish, Louisiana. Gulf Coast Association of Geological Societies Transactions, 33, 243-250.

Zarchan, P. and Musoff, H., 2000. Fundamentals of Kalman filtering: A practical approach: American Institute of Aeronautics and Astronautics, Inc.

Zhang, Z., 1997, Parameter Estimation Techniques: A Tutorial with Application to Conic Fitting: Image and Vision Computing Journal, 15(1), 59-76.

Zhou, H., 2006, First-break vertical seismic profiling tomography for Vinton Salt Dome: Geophysics, 71. 3, 29-36.

Zuidweg, K., and Muamaw, G., R., no date, Airborne Gravity Gradiometry for Exploration Geophysics – The First 5 Years: Bell Geospace report, http://www.hgk.msb.gov.tr/dergi/makaleler/OZEL18/ozel18_46.pdf, accessed 3 July 2012.

MAHNAZ SEPEHRMANESH

mahnaz.sepehrmanesh@uky.edu (859) 684-2730

Education:

- **Master of Science in Geophysics**, University of Kentucky, Lexington, KY
  GPA: 3.72/4.0 **Graduated: Dec 2014**
  Master of Science in Geophysics, University of Tehran, Tehran, Iran
  GPA: 3.4/4.0 **Graduated: Aug 2008**
- **Masters Studies in Geophysics - Seismic Track**, University of Science and Research, Tehran, Iran
  GPA: 3.9/4.0 (24 credit hours tak **Attended: May 2004 – Aug 2005**
- **Bachelor of Science in Mining Exploration Engineering**, University of Tehran, Tehran, Iran **Graduated: Aug 2003**

Computer Skills:

- **Programming:** Matlab, FORTRAN and C ++.
- **Software:** IPI2win, Res2dinv, WinGlink, Mag3D, MagPick, ArcGIS, Geosoft, ENVI, Geomatica, Surfer, and SPSS.

Professional Experiences:

- **University of Kentucky, Lexington** **May 2013 – Sep 2014**
  ✓ Research Assistant, Earth and Environmental Sciences Department
  University of Kentucky, Lexington, KY **Jan 2011 – May 2013**
  ✓ Teaching Assistant, Earth and Environmental Sciences Department
  University of Tehran, Tehran, Iran **2006 - 2008**
  ✓ Data Analyst
  Tehran Padir Consulting Engineers Company, Tehran, Iran **2005 – 2011**
  ✓ Contractor, Multiple Projects
  Safir Danesh, Tehran, Iran **2005 – 2009**
  ✓ Physics and Mathematics Tutor
- **Mahab Ghods Consulting Company, Tehran, Iran** **Summer 2007**
  ✓ Intern
- **Iran Mineral Production and Supply Company, Tehran, Iran** **Summer 2005**
  ✓ Intern
- **Zarmehr Gold Company, Mashad, Iran** **Summer 2004**
  ✓ Intern

Honors and awards:

- Rank first among all applicants (about 300) in "Geophysics Test" and was admitted to Azad University of Science and Research of Tehran **2004**
- Full Scholarship from University of Kentucky, Earth and Environmental Sciences Department, Geophysics Program, full tuition and stipend (about 37,000 per year) **2011-2014**
- National Scholarship for graduate studies, full tuition – Philosophy of Science **2010**
- National Scholarship for undergraduate studies, full tuition – Mining Exploration Engineering **1998-2003**

Publications and Presentations:

- **Sepehrmanesh, M.,** Ravat, D., 2014, Kalman Filters in Improving the Signal to Noise Ratio of Full Tensor Gravity Gradiometry Data, AGU Fall Meeting, San Francisco, CA.
- **Sepehrmanesh, M.**, Ravat, D., 2014, Formulation of Two Kalman Filters Constrained by Laplace's Equation in Extracting Signal from Vinton Salt Dome Gravity Gradiometry Tensor Data, SEG Annual Meeting, Denver, CO.
- **Sepehrmanesh, M.**, Ravat, D., 2014, Constrained Kalman Filter for Improving Processing and Interpretation of the Gravity Gradiometry Tensor Components: An Example of Bell Geospace Vinton Salt Dome Data, Southwest Louisiana, AAPG-SEG Student Expo, 8-9 September, Houston, TX.
- Ravat, D., **Sepehrmanesh, M.**, Salem, A., and Lowry, A., 2013, A new method of constraining geotherms deep in the crust: The utility of the Curie-depth incorporated solution of the heat flow conduction equation, Geol. Soc. Am. Penrose Conference/Workshop on Induced Flow Paths for Geothermal Fluids in Deep Sedimentary Basins, 19-23 October, Park City, UT, Abstract #46.
- **Sepehrmanesh, M.**, Oskooii, B., 2008, Source fault structure of the 2003 Bam earthquake in Iran, inferred from the Magnetotelluric and Aeromagnetic studies presented at 19th EM Workshop, Beijing, China.
- **Sepehrmanesh, M.**, Oskooii, B., 2008, Preliminary results of Magnetotelluric investigation in Bam area, Iran, in comparison with seismogenetic studies , EMSEV-DEMETER Joint Workshop, Sinaia, Romania.
- **Sepehrmanesh, M.**, Oskooii, B., 2008, Recognition of Bam fault zone using magnetotelluric method, Second conference of Iranian mining engineering.